

NASA Contractor Report 3704

NASA
CR
3704
c.1

DC-10 Winglet Flight Evaluation

Staff of Douglas Aircraft Company

CONTRACT NAS1-15327
JUNE 1983



25th Anniversary
1958-1983



FOR EARLY DOMESTIC DISSEMINATION

Because of possible commercial value, these data developed under U.S. Government Contract NAS1-15327 are being disseminated within the U.S. in advance of general publication. These data may be duplicated and used by the recipient with the expressed limitations that the data will not be published nor will they be released to foreign parties without prior permission of the Douglas Aircraft Company. Release of these data to other domestic parties by the recipient shall only be made subject to review after May 1985. The limitations contained in this legend will be subject to review after May 1985. This legend shall be marked on any reproduction of these data in whole or in part.

LOAN COPY
AFWL TECHNICAL
KIRTLAND AFB

0062317



TECH LIBRARY KAFB, NM



NASA Contractor Report 3704

DC-10 Winglet Flight Evaluation

Staff of Douglas Aircraft Company
McDonnell Douglas Corporation
Long Beach, California

Prepared for
Langley Research Center
under Contract NAS1-15327



National Aeronautics
and Space Administration

Scientific and Technical
Information Branch

1983

FOREWORD

This document is the final report of the DC-10 Winglet Flight Evaluation, which was conducted as one task of Contract NAS1-15327 under the NASA Energy Efficient Transport (EET) project. The evaluation program also contained Douglas-sponsored work.

The NASA Technical Monitor for this contract was Mr. T. G. Gainer of Langley Research Center. The on-site NASA representative was Mr. J. R. Tulinius. Acknowledgment is also given to the Director and staff of the Dryden Flight Test Center for their assistance during the program.

The work was conducted by Douglas Aircraft Company, Long Beach, at its facilities at Long Beach and Yuma, and at Edwards Air Force Base. The key personnel were:

M. Klotzsche	Aircraft Energy Efficiency (ACEE) Program Manager
A. B. Taylor	EET Project Manager
P. T. Sumida	Task Manager (also Detail Design subtask)
W. H. Perks	Manufacturing subtask
W. B. Jones	Aircraft Preparation subtask
C. H. Fritz	Laboratory Test subtask
V. A. Clare	Flight Test subtask
D. J. Thomas	Loads Measurement Program
J. T. Callaghan	Aerodynamics
J. E. Donelson	Aerodynamics

The principal authors of this report were:

J. R. Agar	E. G. Salamacha
J. T. Callaghan	C. A. Shollenberger
J. E. Donelson	P. T. Sumida
C. A. Felton	A. B. Taylor
F. S. Heiberger	D. J. Thomas
J. W. Humphreys	

SUMMARY

This report presents the results of a flight evaluation of winglets on a DC-10 Series 10 transport aircraft. The objectives of the program were to determine the effects of winglets on aerodynamic performance and flying qualities by back-to-back tests with and without winglets, to determine flutter-related data, and to determine the effect of winglets on flight loads.

The program consisted of detail design, winglet manufacture, aircraft preparation (including modification of the wing structure and installation of the winglets), and ground and flight testing. The basic winglet configuration used initially in the tests was directly related to the designs developed by Dr. R. T. Whitcomb of NASA Langley. These had a large upper winglet with a small lower winglet. A truncated version of the upper winglet was also tested to evaluate the effect of reducing the span.

During the initial flight tests of the basic winglet, low-speed buffet was encountered. To resolve this problem, a number of configurations were developed and tested, several of which achieved acceptable low-speed buffet characteristics. The greatest low-speed-drag reduction was achieved using leading edge devices on the upper and lower winglets. Lower winglets were required for maximum drag reduction in both cruise and low-speed flight regimes. The addition of outboard aileron droop to the reduced-span winglet configuration enhanced the cruise benefit of winglets.

It was found during the flight tests that winglets had no significant impact on stall speeds, high-speed buffet boundaries, or stability and control characteristics. The flutter tests did not reveal any unforeseen behavior, as the test results agreed with the analytical predictions and ground vibration data. Data from the loads measurement program, which were provided for a concurrent Douglas task, were also in agreement with predictions.

It was estimated from the test results that the application of the reduced-span winglet and aileron droop to a production version of the current DC-10 Series 10 aircraft would yield a 3-percent reduction in fuel burned at the range for capacity loads of passengers and baggage, a 2-percent greater range at this payload, and a 5-percent reduction in takeoff distance at maximum takeoff weight.

CONTENTS

Section	Page
INTRODUCTION	1
SYMBOLS	7
PROGRAM SUMMARY	15
WINGLET INSTALLATION DESIGN AND ANALYSIS	17
Winglet Configuration	17
Structural Design Criteria	21
Prediction of Flight Loads	23
Structural Description	24
Stress Analysis	27
Flutter Analysis	27
WINGLET MANUFACTURE	31
AIRCRAFT PREPARATION AND WINGLET INSTALLATION	37
FLIGHT PROGRAM	39
Test Approach	39
Test Conditions	39
Aerodynamics	39
Structural and Aerodynamic Damping (Flutter)	43
Loads Measurement	44
Flight Instrumentation	46
Aerodynamics Data	46
Flutter	47
Loads	47
Flight Data System	48
Preflight Ground Testing	48
Ground Vibration Test (GVT)	48
Strain Gauge Calibration Tests	49
Flight Test Program	49
RESULTS AND DISCUSSION	53
Baseline Phase	53
Flight Test Program	53
Aerodynamics	53
Loads Measurement	53
Basic Winglet Phase	53
Ground Vibration Test	53
Flight Test Program	54
Flutter	64
Low-Speed Buffet	65
Low-Speed Drag	75
Stall Speeds and Characteristics	76
Cruise Performance	77

CONTENTS

(Continued)

Section	Page
Cruise Buffet	89
Longitudinal Static Stability	90
Longitudinal Maneuvering Stability	92
Longitudinal Trim Characteristics	92
Static Directional Stability	92
Dynamic Lateral Stability (Dutch Roll)	94
Loads Measurement	94
Reduced-Span Winglet Phase	95
Flight Test Program	95
Low-Speed Buffet	99
Low-Speed Drag	102
Cruise Performance	103
IMPACT OF FLIGHT EVALUATION RESULTS ON OPERATIONAL PERFORMANCE	109
CONCLUSIONS	115
REFERENCES	117
APPENDIX A, FLIGHT TEST MEASUREMENT INDEX	119
APPENDIX B, PRESSURE ORIFICE LOCATIONS	141

ILLUSTRATIONS

Figure		Page
1	Winglet Model Under Development in NASA Langley 8-Foot Wind Tunnel ...	2
2	Key Events in the DC-10 Winglet Development Program	3
3	Task Relationships in the DC-10 Winglet Development Program	3
4	Test Aircraft with Basic Winglet	4
5	Test Aircraft with Reduced-Span Winglet	5
6	Flow of Tasks	15
7	Flight Evaluation Program Schedule	16
8	Winglet Geometry Variations from Wind Tunnel Model	17
9	Winglet Rigging to Account for Elastic Deflections	18
10	Principal Winglet Configurations from Application Studies	19
11	Planned Winglet Geometry	20
12	Contingency Configurations	20
13	Envelope Limitations	22
14	Maneuvering Envelope	22
15	Alternatives for Selection of Winglet Design Loads	23
16	Typical Estimated Spanwise Wing Lift Distribution	24
17	Winglet Installation Components	25
18	Basic Winglet Structural Configuration	25
19	Wing Reinforcement — Upper Surface	26
20	Predicted Flutter Speed Versus Wing Fuel — Basic Winglet	29
21	Winglet Spar Machining	31
22	Trailing Edge Assemblies	32
23	Winglet — Start of Assembly	32
24	Upper Winglet Substructure	33
25	Upper Winglet Assembly	33
26	Winglet and Wing Box Extension Juncture	34
27	Lower Winglets	34
28	Winglet and Wing Box Extension Assembly	35
29	Winglet Installation in Progress	37
30	Winglet Installation Complete	38
31	Flight Test Program	39
32	High Speed Performance Test Conditions	41
33	Low Speed Performance Test Conditions	42
34	Stability and Control Test Conditions	43

ILLUSTRATIONS (Continued)

Figure		Page
35	Flutter Test Conditions	44
36	Flutter Test Speeds and Altitudes	45
37	Loads Test Parameters	45
38	Wing and Winglet Pressure and Deflection Instrumentation	47
39	Accelerometer Locations	48
40	Flight Tests Performed during Evaluation of Basic Winglet	50
41	Flight Tests Performed during Evaluation of Reduced Span Winglet	52
42	Ground Vibration Test Results	53
43	GVT First Wing Bending Modes	55
44	GVT Wing Engine Pitch Mode with Winglet in Phase	56
45	GVT Wing Engine Pitch Mode with Winglet Out of Phase	57
46	Configuration Identification for Basic Winglet Flight Program	59
47	Basic Winglet Configuration Features	61
48	Basic Winglet Configurations with Vortilets	62
49	Leading Edge Krueger Flap Geometry for Basic Upper Winglet	63
50	Frequency and Damping Characteristics — 3-Hz Mode (Determined from Wing Tip Normal Acceleration)	64
51	Frequency and Damping Characteristics — 4.5-Hz Mode (Determined from Winglet Longitudinal Acceleration)	65
52	Winglet Flow at Low Speed in the Ames 12-Foot Wind Tunnel	66
53	Winglet Flow in Low-Speed Flight — Inboard (Suction) Side, $C_L = 0.96$, $V/V_{S_{MIN}} = 1.5$	67
54	Winglet Flow in Low-Speed Flight — Inboard (Suction) Side, $C_L = 1.5$, $V/V_{S_{MIN}} = 1.2$	68
55	Winglet Flow in Low-Speed Flight — Outboard (Pressure) Side, $C_L = 1.5$, $V/V_{S_{MIN}} = 1.2$	69
56	Summary of Low-Speed Buffet Characteristics — Basic Winglet	71
57	Winglet Low-Speed Buffet — Acceptability Criteria	73
58	Effect of Winglet Krueger Flap on Winglet Section Loading ($\eta = 57\%$)	74
59	Low-Speed Drag Improvement — Basic Winglet	75
60	Effect of Winglet on Minimum Stall Speed	76
61	Correlation of Measured Range Factor and Drag Improvements for the BWL and RSWL ($0.80 \leq M \leq 0.85$)	78
62	Cruise Drag Improvement — Basic Winglet	79
63	Upper Winglet Flow in Cruise Flight — Inboard (Suction) Side	80

ILLUSTRATIONS

(Continued)

Figure		Page
64	Upper Winglet Flow in Cruise Flight — Outboard (Pressure) Side, $M = 0.82$	81
65	Lower Winglet Flow in Cruise Flight — Outboard (Suction) Side	82
66	Basic Winglet Pressure Distribution at Cruise	83
67	Effect of Lift Coefficient on Basic Winglet Pressure Distribution at Cruise — 12.5-Percent Span	84
68	Effect of Lift Coefficient on Basic Winglet Pressure Distribution at Cruise — 80-Percent Span	85
69	Effect of Lift Coefficient on Basic Winglet Pressure Distribution at Cruise — 95-Percent Span	86
70	Effect of Lower Winglet on Basic Upper Winglet/Wing Tip Pressure Distribution at Cruise	87
71	Basic Winglet Span Load at Cruise	88
72	Basic Winglet and Wing Tip Loading at Cruise	88
73	Effect of Basic Winglet on Wing Span Load — Flight and Wind Tunnel	89
74	Effect of Basic Winglet on High-Speed Buffet Boundary	90
75	Effect of Basic Winglet on Longitudinal Static Stability	91
76	Effect of Basic Winglet on Longitudinal Maneuvering Stability	91
77	Effect of Basic Winglet on Cruise Longitudinal Trim Characteristics	93
78	Effect of Basic and Reduced-Span Winglets on Takeoff Static Directional Stability	93
79	Effect of Basic and Reduced-Span Winglets on Landing Static Directional Stability	94
80	Configuration Identification for Reduced-Span Winglet Flight Program	97
81	Reduced-Span Winglet Configurations	98
82	Leading-Edge Krueger Flap Geometry for Reduced-Span Upper Winglet and Extended-Chord Lower Winglet	99
83	Summary of Low-Speed Buffet Characteristics — Reduced-Span Winglet	100
84	Buffet Response Acceleration Power Spectra	101
85	Low-Speed Drag Improvement — Reduced-Span Winglet	103
86	Cruise Drag Improvement — Reduced-Span Winglet	104
87	Reduced-Span Winglet Pressure Distribution at Cruise	105
88	Effect of Configuration Variables on Cruise Drag Improvement — Reduced-Span Winglet	106
89	Effect of Outboard Aileron Droop on Reduced-Span Winglet/Wing Tip Pressure Distribution at Cruise	107

ILLUSTRATIONS
(Continued)

Figure		Page
90	Increases in Operator's Empty Weight	109
91	Effect of Winglets on DC-10 Series 10 Performance Characteristics	110
92	Effect of Winglet Configurations on Payload Range	111
93	Effect of Winglet Configurations on Takeoff Field Length	112
94	Effect of Winglet Configuration on Fuel Burned	113

INTRODUCTION

One of the technological advances to be considered for energy savings for transport application is the winglet concept developed by Dr. R. T. Whitcomb of the National Aeronautics and Space Administration (NASA), Reference 1. The winglet is an airfoil surface mounted almost vertically at the wingtip. It is intended to reduce lift-induced drag which accounts for as much as 40 percent of the total drag at cruise speed. Historically, one of the primary ways of reducing this drag has been to increase the wing span, but this results in a heavier wing structure and so dilutes the performance gain. The concept of the winglet is to achieve the same drag reduction as the wing tip extension but with less wing bending moment penalty.

A substantial amount of wind tunnel and flight development has been conducted on winglets since the original NASA experiments. Significant performance gains have been demonstrated in the NASA/USAF flight program using the KC-135, which is representative of a large first-generation jet transport aircraft, and other, smaller aircraft. However, the need for additional investigation of winglet application to a representative second-generation jet transport, such as the DC-10, was recognized, primarily due to the differences in wing designs.

Second-generation jet transport wings tend to be less tip-loaded (more twisted) than a wing with a more elliptical loading, such as the typical first-generation design, and therefore do not offer as much potential for induced drag reduction (provided by a wing-tip device). Also, the newer wings incorporate advanced high-lift devices resulting in significantly higher lift coefficients in the low-speed regime. Such high loadings afford greater potential for low-speed-drag reduction but introduce the possibility of adverse viscous effects on winglet performance. The distinction of high loading also separates the typical large transport application from some current production corporate aircraft (e.g., Gulfstream III, Learjet 55, and Westwind 2) which do not achieve such lift at low speeds.

Under the NASA Energy Efficient Transport (EET) project, investigations were therefore conducted to build the technology for the DC-10-type aircraft. The initial EET high-speed wind tunnel test (Reference 2) was used to develop a satisfactory configuration and identify the cruise performance benefit. The development work was performed on a DC-10 Series 10 model, and established a configuration having a large upper winglet and a smaller lower winglet, as shown in Figure 1. Additional evaluations were then made with the larger wing-span Series 30 model. Subsequent model tests were conducted (Reference 3) in which the Series 30 was used as a basis; the general results were applicable to the Series 10 also.

In low-speed wind tunnel tests, it was evident that flow separation on the upper winglet occurred at high incidence near the critical climb condition. With a winglet leading edge slat added, the separation was delayed, but without any apparent effect on the drag reduction. This test program, together with an associated high-speed test program, also investigated the

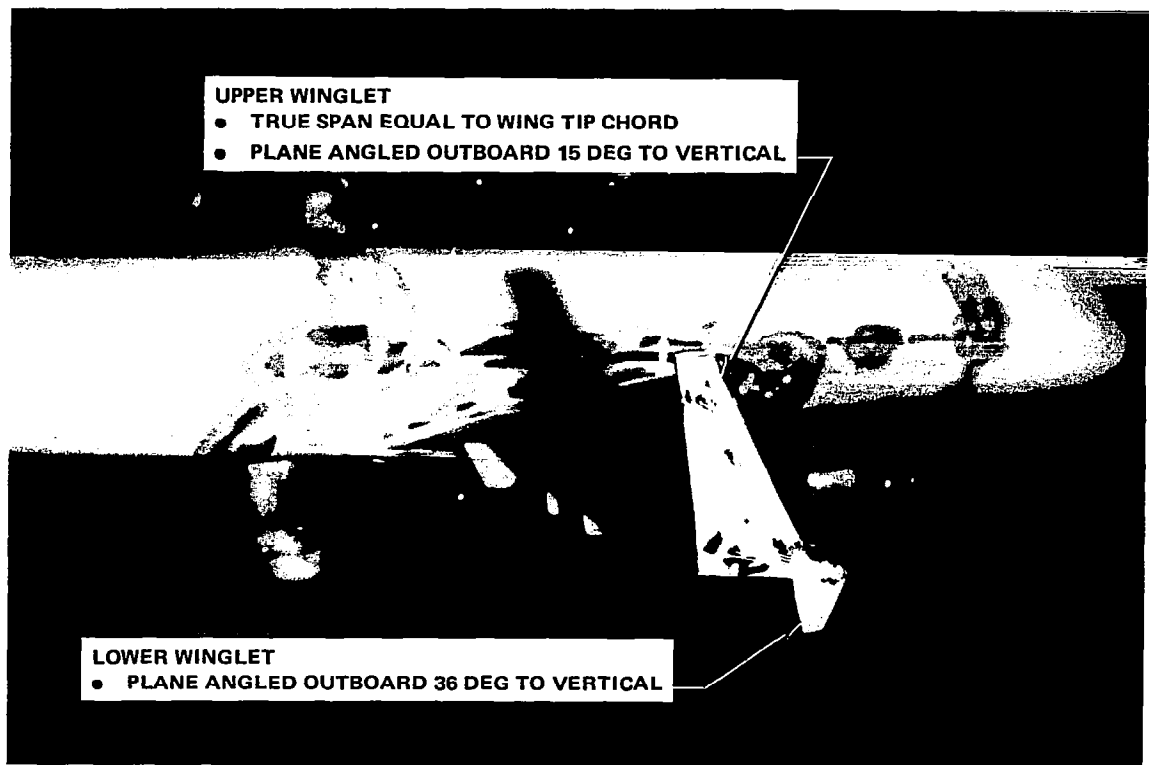


FIGURE 1. WINGLET MODEL UNDER DEVELOPMENT IN NASA LANGLEY 8-FOOT WIND TUNNEL

aerodynamic stability and control characteristics of the aircraft and found them to be affected very little by the winglets. In parallel, the dynamic behavior of this winglet aircraft was investigated. Concern as to the effects of winglets on flutter was somewhat alleviated by a low-speed model test in which good correlation was shown with analyses using modern methods.

The configuration data resulting from these investigations and parallel Douglas work were based on model experiments and analyses. It was considered therefore that the logical next step in development was full-scale flight evaluation. The key events in the development tasks are shown in Figure 2 and the interrelationship of the tasks in Figure 3.

The objectives of the flight evaluation were to determine:

- The effects of winglets on performance and flying qualities of a modern jet transport aircraft, represented by the DC-10. These effects would be determined by back-to-back flights with and without winglets.
- The effects of winglets on aircraft flutter.
- The effects of winglets on flight loads through back-to-back measurements (this portion of the program was sponsored by Douglas).

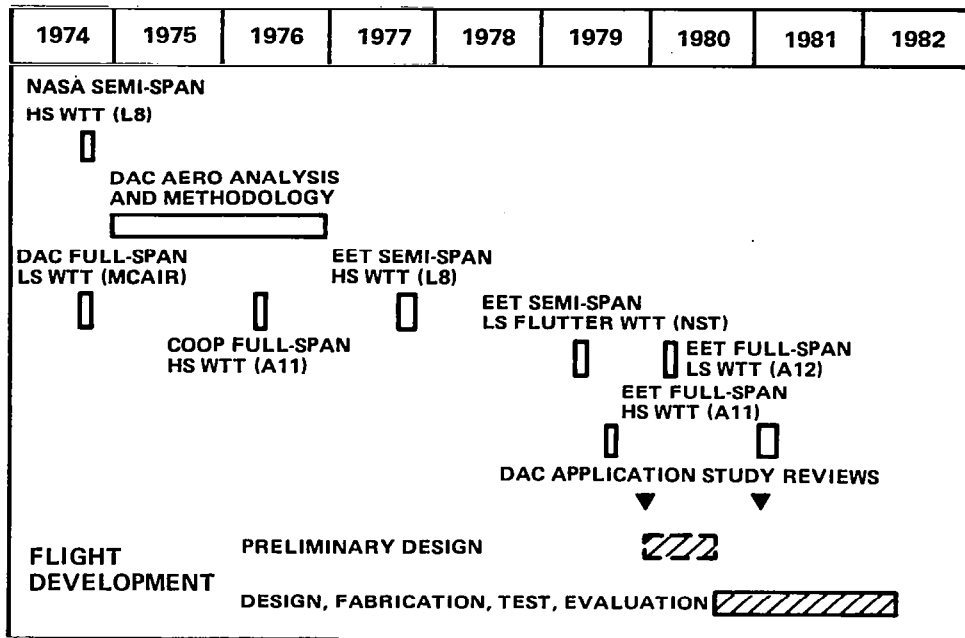


FIGURE 2. KEY EVENTS IN THE DC-10 WINGLET DEVELOPMENT PROGRAM

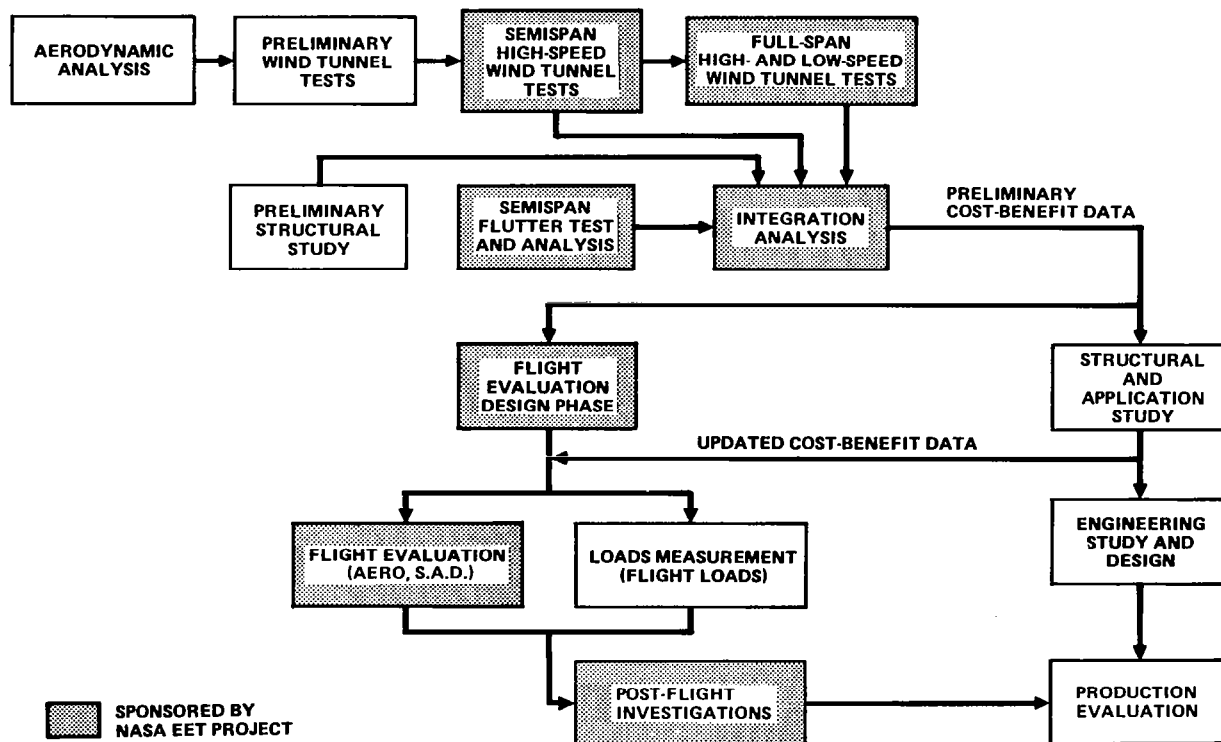


FIGURE 3. TASK RELATIONSHIPS IN THE DC-10 WINGLET DEVELOPMENT PROGRAM

In addition to the basic winglet (BWL) derived from the wind tunnel tests, the program tested a reduced-span winglet (RSWL) so that the effects of upper winglet span could be studied.

The program, from inception of design through manufacture, test, and refurbishment of the test aircraft, was accomplished in 16 months. The test aircraft was leased by Douglas from Continental Airlines in April 1981, and was returned to service at the end of November. The baseline (without winglets) flight test program involved 12 flights and the winglet tests 49 flights. The baseline flights and the winglet first flight were made from the Douglas Long Beach facility. The winglet flutter testing was conducted in flights from Edwards Air Force Base. Subsequent winglet test flights were made from the Douglas facility at Yuma, Arizona.

The predominant activities of the flight test program were performance measurement to determine the drag reduction due to winglets, and development of configurations with satisfactory low-speed characteristics.

The test aircraft equipped with the BWL is shown in flight in Figure 4. The aircraft with the RSWL is shown in Figure 5.



FIGURE 4. TEST AIRCRAFT WITH BASIC WINGLET

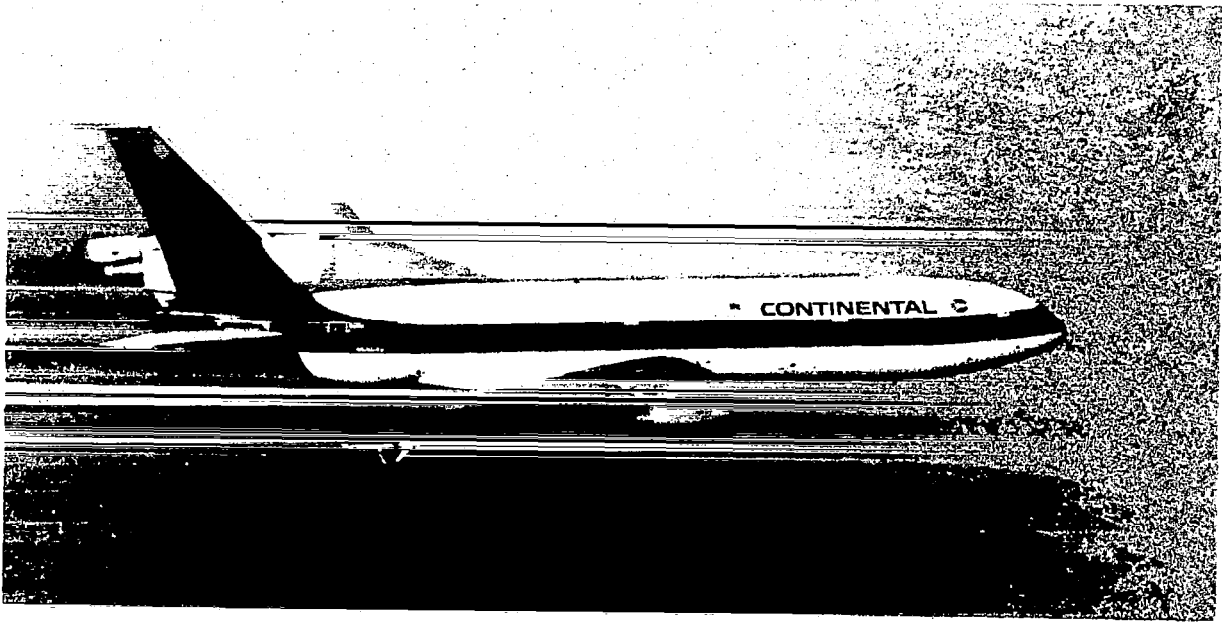


FIGURE 5. TEST AIRCRAFT WITH REDUCED-SPAN WINGLET

SYMBOLS

Measurements were taken and calculations were made during project testing using customary U.S. units. These units have been converted to the International System of Units (SI) for the main body of this report. Units of measure used in the instrumentation activities of this project, described in Appendix A, are retained in customary units.

Symbols for Report

A	point on maneuvering envelope where stall speed intersects +2.5g load factor limit
A11	NASA Ames 11-foot wind tunnel
A12	NASA Ames 12-foot wind tunnel
A13 through 61	identification of test flights performed during winglet phases
A/C	aircraft
AIC	aerodynamic influence coefficient
ALT	altitude
AND	aircraft nose down
ANL	aircraft nose left
ANR	aircraft nose right
ANU	aircraft nose up
AVG	average
a_n	cg normal acceleration
a_z	vertical acceleration (measured at pilot seat)
BWL	baseline winglet
C/C_c	damping ratio (where C_c is the critical damping)
C_D	drag coefficient
C_L	lift coefficient
$C_{L_A}, C_{L_{A/C}}$	aircraft lift coefficient
$C_{L_{\text{Buffet}}}$	buffet lift coefficient
C_ℓ	section lift coefficient
$C_\ell \cdot \frac{c}{\bar{c}}$	section load, defined as section lift coefficient times the ratio of local chord c divided by the MAC \bar{c}

Symbols for Report (Continued)

$\frac{C_l \cdot c}{2b}$	span loading coefficient, defined as section lift coefficient times the local chord c divided by the wing span $2b$.
C_{NFW}	winglet normal force coefficient (for structural load analysis)
C_n	winglet normal force coefficient (for aerodynamic analysis)
C_p	pressure coefficient
CG, cg	center of gravity
CDR	Critical Design Review
C of A	certificate of airworthiness
CONFIG	configuration
D_1	point on maneuvering envelope where V_D coincides with +2.5g load factor
DAC	Douglas Aircraft Company
E	point on maneuvering envelope where V_D coincides with zero load factor
EET	Energy Efficient Transport project, a number of tasks sponsored by NASA under the Aircraft Energy Efficiency program to expedite development in aerodynamics and active controls
EXT	extended
F	point on maneuvering envelope corresponding to V_D at -1g load factor
F_{cc}	control column force
FAA	Federal Aviation Administration
FAR	Federal Aviation Regulation ("Part 25: Airworthiness Standards, Transport Category Airplanes" is mentioned in this report)
FCK	Fixed-camber Krueger flap leading edge device
G	vibratory acceleration normalized to gravity
GVT	ground vibration test
g	acceleration due to gravity
H	point on maneuvering envelope where the maximum negative lift coincides with -1g load factor
HS	high speed

Symbols for Report (Continued)

HS	horizontal stabilizer (to identify mode line)
INSTL	installed
i_H	horizontal incidence angle between the horizontal tail and the fuselage reference plane
KCAS	knots, calibrated air speed
KEAS	knots, equivalent air speed
LND	landing
L8	NASA Langley 8-foot wind tunnel
L/D	lift-to-drag ratio
LE	leading edge
LH	left hand
LMP	loads measurement program
LS	low speed
M, M_N, M_O	free-stream Mach number
M_D	dive Mach number
M_{MAX}	maximum Mach number
M_{MO}	maximum operating Mach number
M_{PEAK}	peak local Mach number
MAC	mean aerodynamic chord (also identified as c in the symbol $C \frac{c}{c}$)
MCAIR	McDonnell Aircraft Company low-speed wind tunnel
MTOGW	maximum takeoff gross weight
MZFW	maximum zero fuel weight
N_1	engine fan speed, expressed as percent of reference RPM
NST	Northrop subsonic wind tunnel
N_z	vertical load factor
OEW	operator empty weight
PDR	Preliminary Design Review
PSD	power spectral density
RET	retracted

Symbols for Report (Continued)

RF	range factor, defined as $\frac{V}{W_f} W$
RFD	refurbish for delivery
RH	right hand
RMS	root mean square
RSWL	reduced span winglet
S&C	stability and control
SAD	structural aerodynamic damping
SFC	engine specific fuel consumption
SYM	symbol
TEL	trailing edge left
TER	trailing edge right
TO	takeoff
TOFL	takeoff field length
V	aircraft velocity
V_A	design maneuvering speed
V_B	design speed for maximum gust intensity
V_C	cruise speed
V_D	dive speed
V_F	design flap speed
V_{REF}	reference speed corresponding to $M = 0.9$
V_S	stall speed
$V_{S_{1g}}$	stall speed at 1g
V_{MIN}	FAA-certified stall speed
V_{MO}	maximum operating speed
V_e	equivalent airspeed
V_2	takeoff safety speed
W, WT	aircraft gross weight
W_f	aircraft fuel flow

Symbols for Report (Continued)

W/δ	aircraft gross weight divided by ambient pressure ratio
W/L	winglet
W/O	without
WG	wing (to identify mode line)
WTT	wind tunnel test
X_{ORS}	wing station references measured along the wing rear spar
X_W	wing station references measured normal to the aircraft plane of symmetry
α	angle of attack
α_{V_2}	angle of attack at V_2
δ_F	wing flap setting angle, degrees
δ_r	rudder deflection angle, degrees
δ_s	slat deflection angle, degrees
δ_w	control wheel deflection, degrees
Δ	delta
η	span ratio, percent
B	sideslip angle, degrees

Symbols for Appendix A

A13 through 61	identification of test flights performed during winglet phases
ACCEL	accelerometer
AFCS	automatic flight control system, with specific units of interest identified as -1A channel, System 1, Roll Computer No. 1, Roll Computer No. 2
AIL	aileron
ALTDE	altitude
ARSPD	airspeed
AT/SC	autothrottle speed command
ATTIT	attitude
AUX	auxiliary
BOT	bottom

Symbols for Appendix A (Continued)

CT, CNT	count, a measurement unit
DEG	degree of angular measure, a measurement unit
DEG C, DEG F	degree Celsius, degree Fahrenheit, measurement units
DISCR	discrete
DPS	degrees per second, a measurement unit
EAFB	Edwards Air Force Base
ENGR	Engineering
FRNT	front
F/T	flight test
hp	pressure altitude
INBRD	inboard
INCOMP	incompressible flow
INHG	inches mercury, a measurement unit
INNER	inner
INS	inertial navigation system
JUNC	juncture, junction
KSI	one thousand pounds per square inch, a measurement unit
LHIB	left hand inboard
LHOB	left hand outboard
LOWR	lower
N_1	engine fan speed, expressed as a percent
N_2	engine core speed, expressed as a percent of reference RPM
OUTD, OUTBRD	outboard
PCT, PCNT	percent
POSIT, POSN	position
PPH	pounds per hour, a measurement unit
PRESS	pressure
PRI	primary
PROD	production

Symbols for Appendix A (Continued)

PSIA	pounds per square inch absolute, a measurement unit
PSID	pounds per square inch differential, a measurement unit
RHIB	right hand inboard
RHOB	right hand outboard
RSWLU	right side winglet left upper
SKN	skin
SP	space
STRES	stress
SUB	subcom, denoting a data system channel having a lower data rate than the primary channel
SURF	surface
T/C	trailing cone
TE	trailing edge
UPPR	upper
VFT	vertical fin tip
WING	wing
X/c	distance along local chord of wing or winglet, divided by chord length
XORS	wing station references measured along the wing rear spar

PROGRAM SUMMARY

The flight evaluation program was conducted using an aircraft supplied by Douglas. The aircraft (Ship 101) was leased from Continental Airlines and was returned to airline service upon program completion. Program activities consisted of detail design, winglet manufacture, aircraft preparation (including modification of the wing structure), installation of the winglets, ground and flight testing, and refurbishment for delivery (RFD) to airline service. The flight testing was structured so that key data comparisons of the baseline aircraft without winglets and the winglet-equipped aircraft would be made from back-to-back phases. Federal Aviation Administration (FAA) approvals were obtained at the appropriate stages of the program, particularly concerning the modifications made to and retained with the aircraft.

The flow of program tasks is illustrated in Figure 6. The program schedule is shown in Figure 7.

Specific portions of the detail design phases are discussed in the subsequent text. They include the loads and criteria analyses, structural design, stress analysis, and flutter analysis.

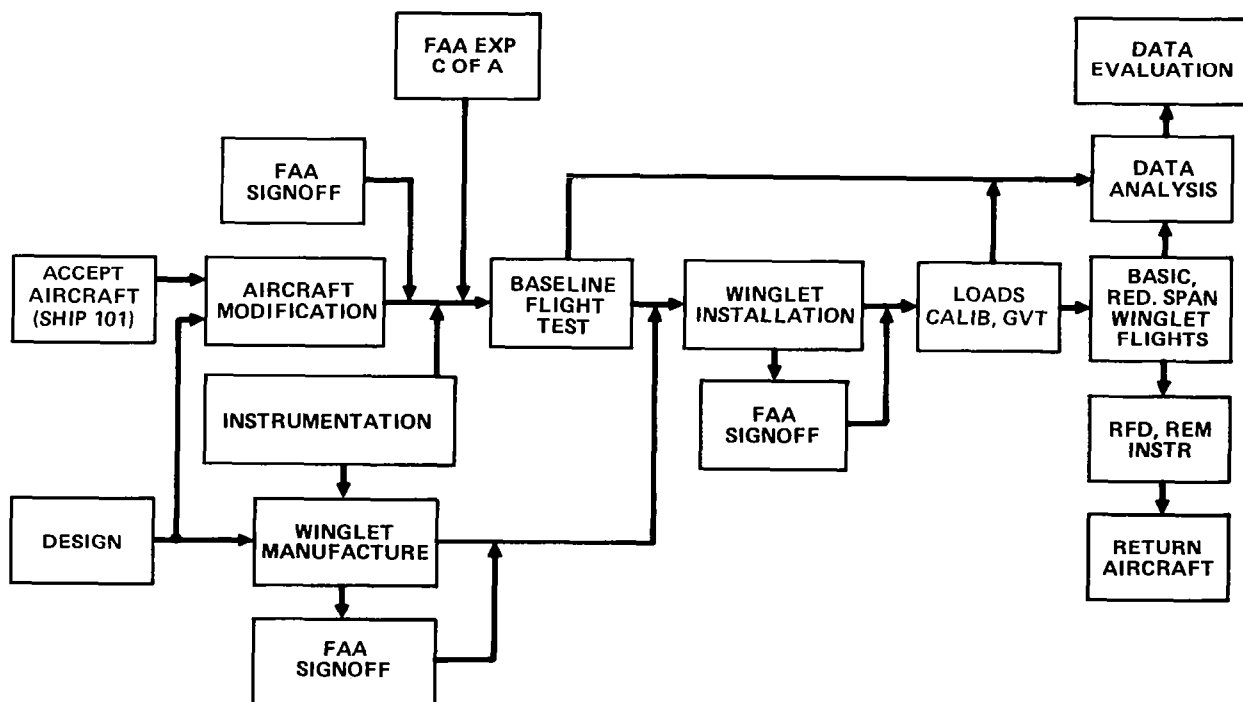


FIGURE 6. FLOW OF TASKS

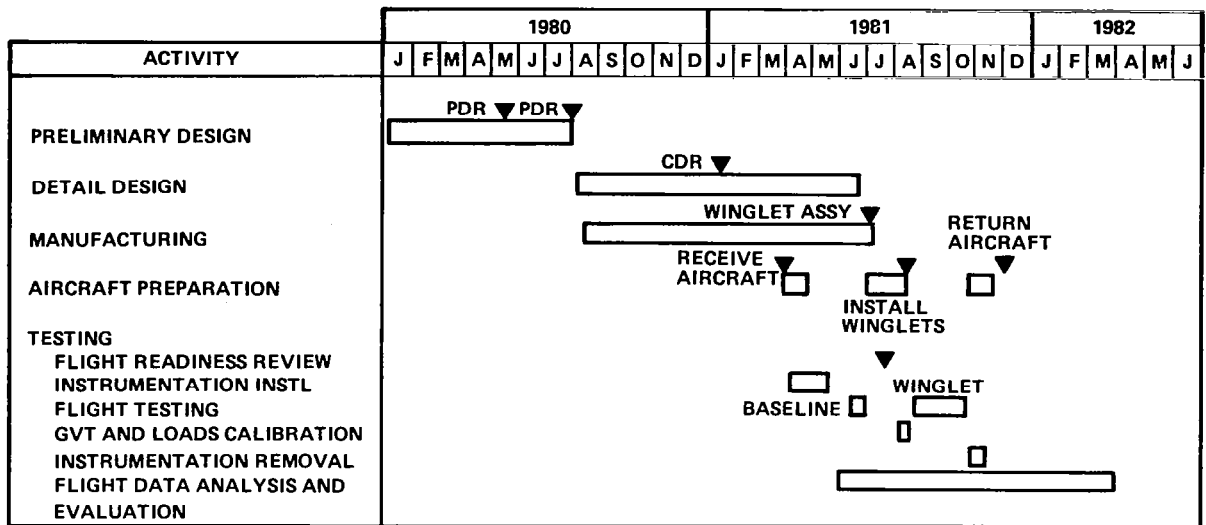


FIGURE 7. FLIGHT EVALUATION PROGRAM SCHEDULE

WINGLET INSTALLATION DESIGN AND ANALYSIS

Winglet Configuration

The winglet design used in the flight evaluation was a modified version of the design developed by Dr. R. T. Whitcomb of NASA Langley (Reference 1). The first modifications, consisting mainly of moving the lower winglet forward, were made during the high-speed tests (Reference 2) conducted in the Langley 8-foot wind tunnel on semispan models of the DC-10 Series 10 and 30 aircraft. Additional modifications were made prior to the wind tunnel tests run in the Ames 11-foot and 12-foot tunnels (Reference 3). These tests utilized full-span models of the DC-10 Series 30. Further modifications were made prior to flight evaluation. The differences between the DC-10 Series 10 flight configuration and the wind tunnel configuration evolved in the Reference 2 tests are shown in Figure 8. The figure shows the BWL having an upper true span of 3.23 m (10.6 ft). The changes comprised:

- A redefined leading edge fillet derived from the wind tunnel shape modifications. The redefinition was employed on the full-span models of Reference 4.
- The incorporation of the DC-10 Series 30 lower winglet as defined in Reference 3.
- The movement aft of the lower winglet so as to avoid occlusion of the existing production wing tip forward position light. With this position, the trailing edge location relative to the upper winglet leading edge was equivalent to the position which evolved in the DC-10 Series 10 semispan wind tunnel test.

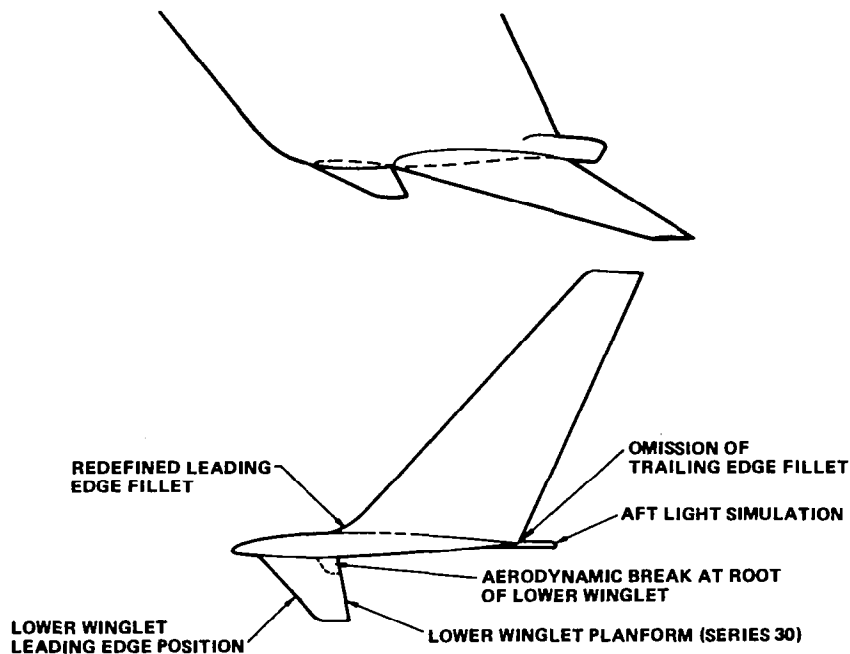


FIGURE 8. WINGLET GEOMETRY VARIATIONS FROM WIND TUNNEL MODEL

- A modification of the lower winglet trailing edge by a trailing edge break owing to juncture shape difficulties which became evident in full scale.
- The deletion of the outboard trailing edge fill near the upper winglet root. This fill was used in the semispan model of Reference 2, but the tests showed it offered no advantage over the true winglet surface alone.
- The addition of a fairing, simulating the aft position light installation, extended aft at the inboard juncture of the wing with the upper winglet. The plan view shape of this fairing was aligned with the outboard profile of the winglet near the trailing edge.

In addition to these detailed provisions, allowance was made in the winglet geometry for the aeroelastic twist differences between the 1g flight condition and the jig condition. The wind tunnel model was fabricated to reflect the 1g flight condition. In this way, the installed geometry was defined. An indication of the differences in the cruise and installed rigging is shown in Figure 9.

During the Douglas application studies, a trade study of the effect of winglet size was conducted. One conclusion was that a retrofit of winglets to the DC-10 Series 10 fleet would be feasible if a smaller winglet could be used. Thus the degree of strengthening required for the wing could be limited, primarily involving the upper panel stiffener reinforcing method devised for

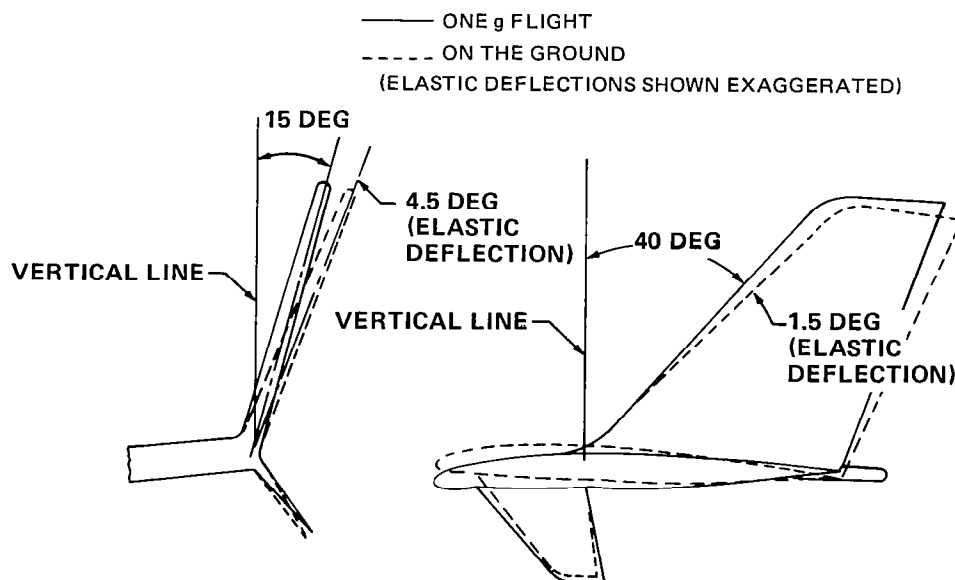


FIGURE 9. WINGLET RIGGING TO ACCOUNT FOR ELASTIC DEFLECTIONS

the flight evaluation aircraft. While the aerodynamic benefit was diminished compared with that of the larger basic winglet, the reduction in structural penalty made an attractive configuration. The reduced-span study configuration shape (dimensioned for full scale) is compared with the basic winglet in Figure 10.

Since the winglet span has a powerful effect on the amount of wing structure change required, it became important for the flight program to include evaluation of a reduced-span winglet. It was therefore decided to change the program plan to include a reduced-span winglet so that a back-to-back comparison could be made with the basic winglet. A practical method of obtaining a test configuration for the reduced-span concept was via a simple truncation of the basic winglet. The estimated performance difference between the study configuration of Figure 11 and the truncated winglet was very small (about 3 percent).

The geometry of the full-scale basic and reduced-span winglets is shown in Figure 11. The upper winglet was set at -2 degrees incidence relative to the fuselage centerline. The lower winglet was set at zero incidence. Neither surface was twisted.

Certain contingency provisions were included in the winglet design. These are illustrated in Figure 12, and consist of a bolt-on leading edge device for the upper winglet and a provision to move the lower winglet forward or remove it altogether.

The leading edge Krueger flap was manufactured as a result of data from the high lift wind tunnel tests of Reference 4. These data showed evidence of flow separation from the upper wing-

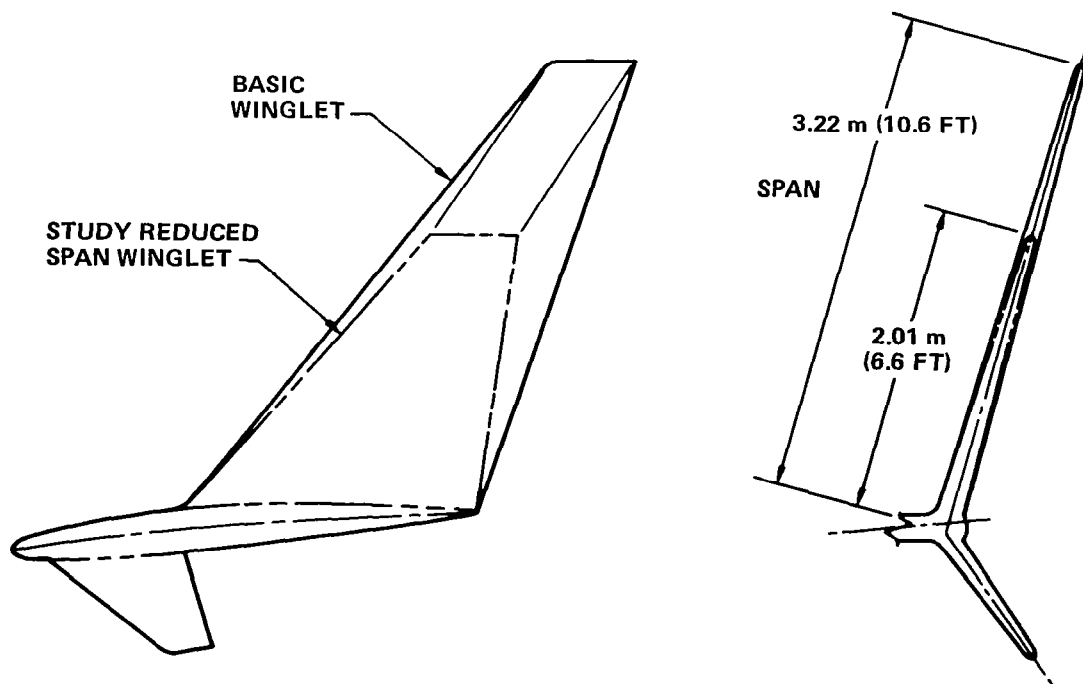


FIGURE 10. PRINCIPAL WINGLET CONFIGURATIONS FROM APPLICATION STUDIES

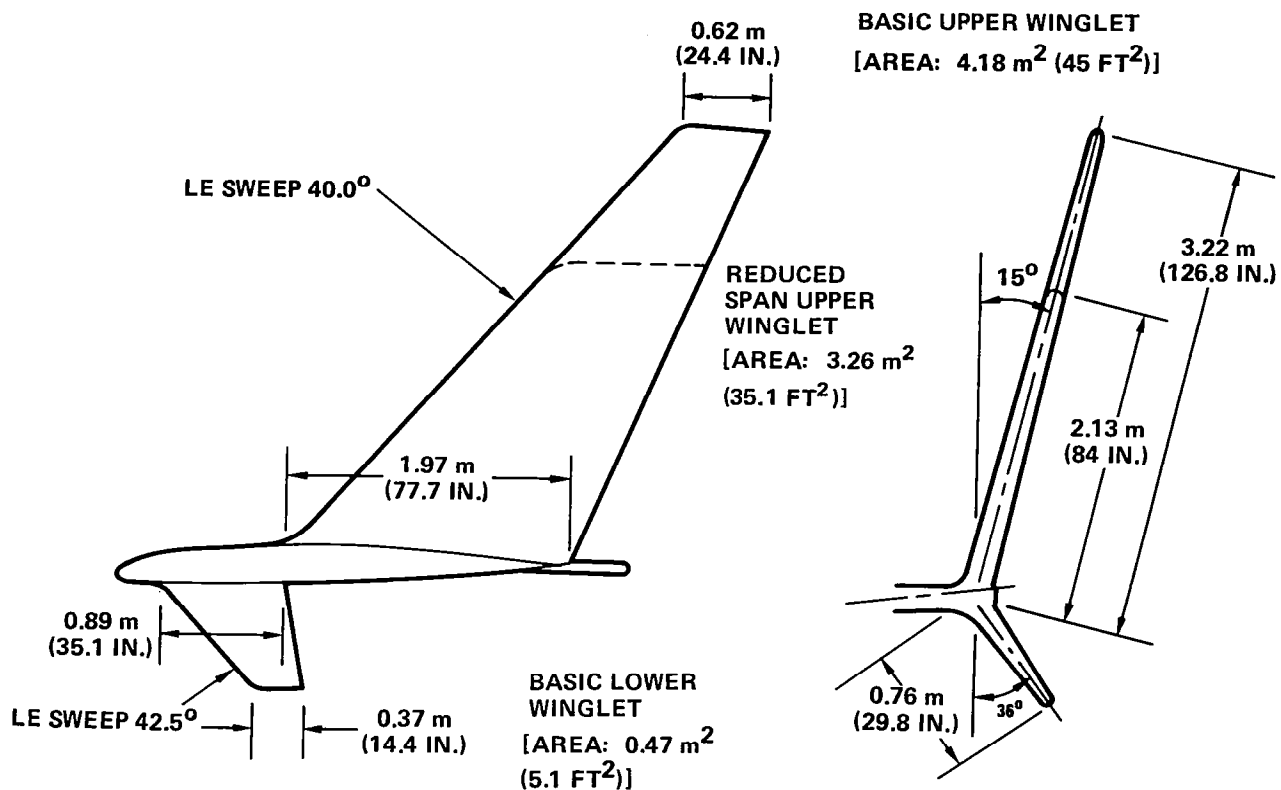


FIGURE 11. PLANNED WINGLET GEOMETRY

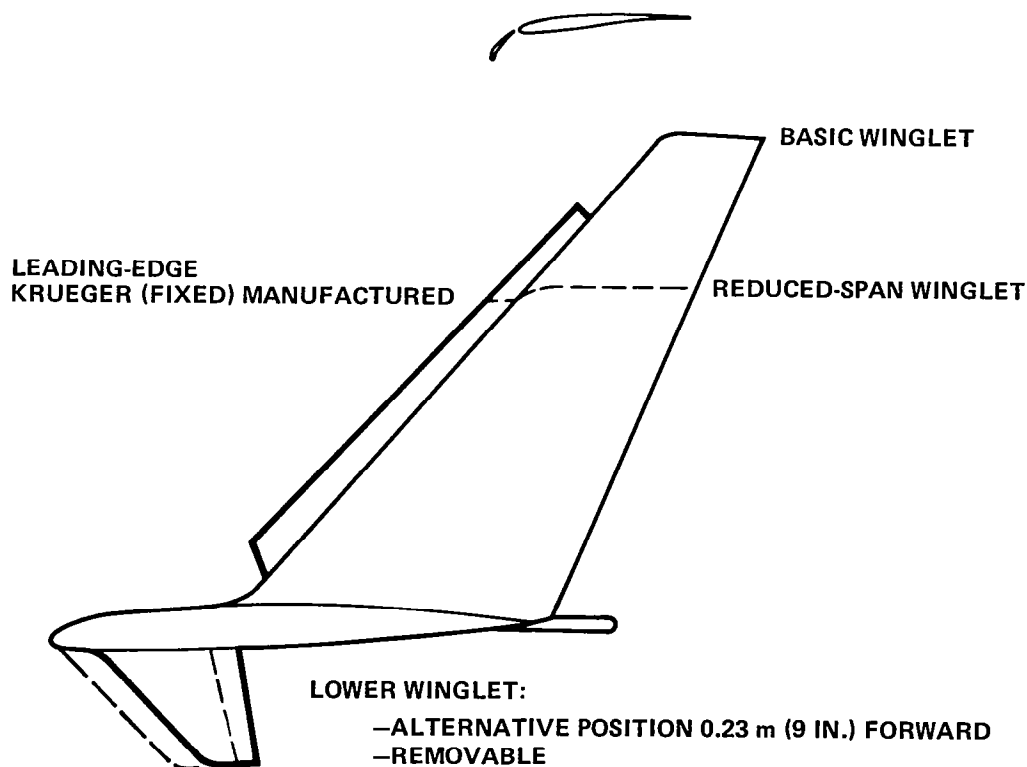


FIGURE 12. CONTINGENCY CONFIGURATIONS

let at high lift coefficient. Although the separation occurred at lift coefficients above those of normal operation, it was considered prudent to have a leading edge device available for installation on the winglet should the need arise. The leading edge device was a single-position (not deployable or retractable in flight) Krueger leading edge flap for the upper winglet. The geometry was determined by practical considerations which would permit extension from the lower surface of the upper winglet. The flap extended spanwise from 11 percent to 82 percent of the upper winglet span. This extension was chosen after consideration of articulation requirements. The Krueger chord was 16 percent of the local winglet chord and was deflected 50 degrees with a gap of 1.5-percent chord and -1.5-percent chord overhang. The Krueger was made adaptable to the reduced span winglet by trimming its length.

The additional contingency provision concerned the decision to locate the lower winglet farther aft to avoid occlusion of the forward position light. Should this position give rise to flow interference between upper and lower winglets, a potential problem area identified in earlier wind tunnel tests, a more forward position could be adopted or the lower winglet could be removed entirely, a condition that was investigated in the semispan wind tunnel test.

Structural Design Criteria

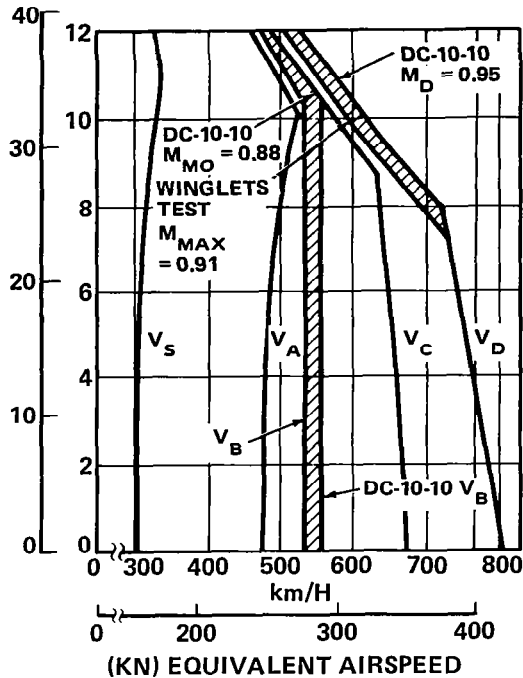
Owing to the need to minimize wing structure modifications which were to remain with the aircraft on return to airline service, it was determined that the aircraft should be flown at speeds, gross weights, cg limits, and load factors just sufficient to satisfy program objectives. Aircraft configuration requirements were derived from the test aircraft specification, and the data requirements defined later in this report. As a result of these considerations, the envelope limitations shown in Figure 13 and the maneuvering envelope of Figure 14 were applied.

FAR Part 25 static strength requirements (2.5g limit) governed the design of the winglet and its attachment to the wing. This design requirement provided substantial margins of safety in the new structure, hence no proof test for the winglet structure was needed. Design-level gust intensities for clear air turbulence were included in the design.

Specific criteria were applied to the design of the winglet so that aerodynamic data quality was preserved in the presence of flight deflections. No elastic buckling of the winglet skins was permitted up to the maximum 1g cruise condition.

Fatigue was not a consideration for the winglet flight test phase due to the limited flight test time; however, satisfactory fatigue life of the aircraft as refurbished for delivery was assured.

ALTITUDE
(1,000 FT) (1,000 m)



1,000 LB (1,000 kg)

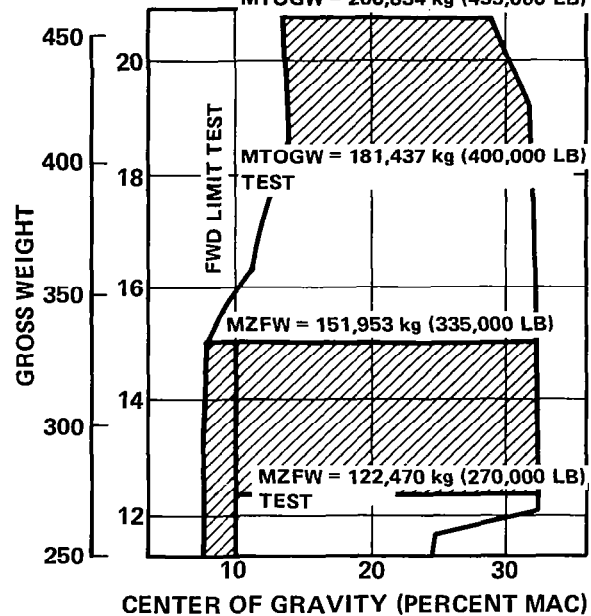


FIGURE 13. ENVELOPE LIMITATIONS

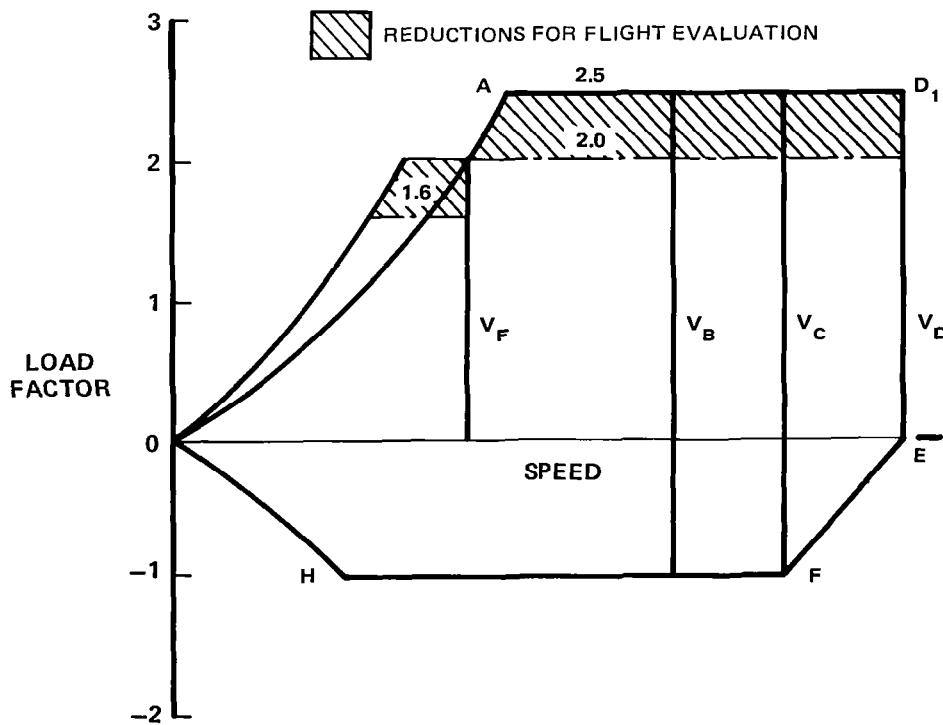


FIGURE 14. MANEUVERING ENVELOPE

Prediction of Flight Loads

Winglet loads were estimated using a combination of theoretical and wind tunnel test data. The resulting forces and moments were then applied to existing aeroelastic models of the wing structure to estimate the external loads. In addition, the influence of the winglet on the wing spanwise lift distribution was estimated.

In estimating the normal force (the main component of force on the winglet), several alternatives were considered, as shown in Figure 15. The normal force was first estimated using linear (vortex lattice) theory, but when the wind tunnel data of Reference 2 became available they showed these linear theory estimates to be too conservative. The Reference 2 data were obtained only at typical cruise lift coefficients — and, therefore, over only a limited angle-of-attack range — but they were extrapolated linearly to obtain the normal force coefficients at lower and higher angles of attack. These are shown as the “linear wind tunnel” data in Figure 15. Later, nonlinear data (the dashed curve in the figure), which showed the effects of load-shedding or “round-over” due to eventual flow-separation at the higher angles of attack, became available from the tests of Reference 3. These tests were made over a fairly extensive range of angles of attack and sideslip at Mach numbers up to 0.95. The nonlinear data were analytically corrected for Reynolds number effects, giving the dotted curve in Figure 15; however, the adjusted nonlinear coefficients were still lower than the linear wind tunnel coefficients at the higher angles of attack. Therefore, to provide a substantial degree of conservatism in the load estimates, the linear wind tunnel coefficients were used at the higher angles of attack. The

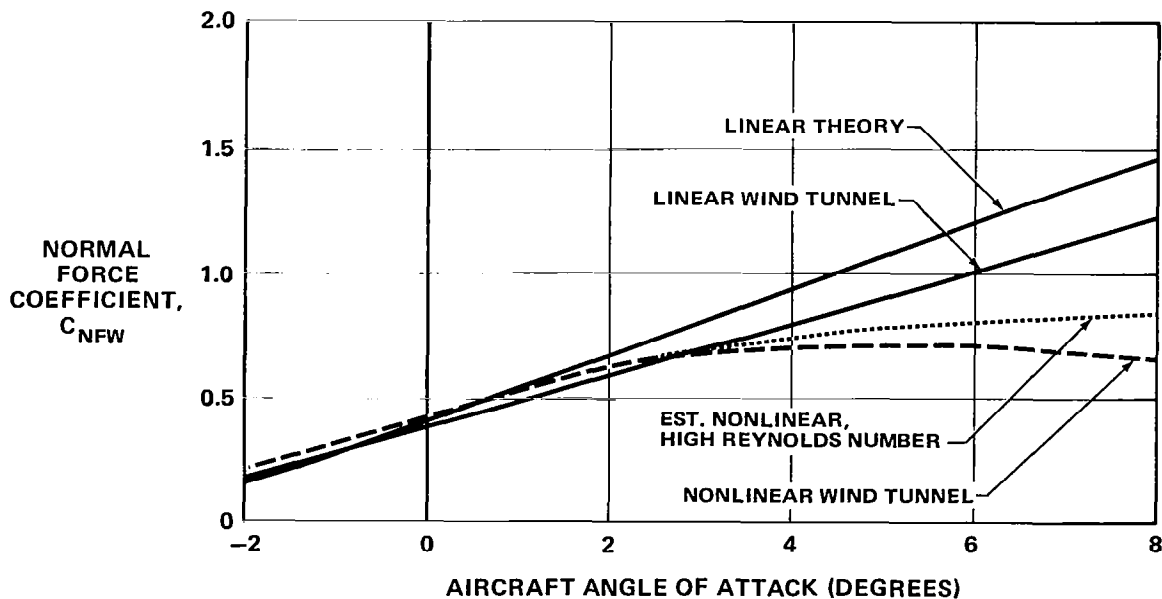


FIGURE 15. ALTERNATIVES FOR SELECTION OF WINGLET DESIGN LOADS

nonlinear data, on the other hand, gave the higher normal force coefficients in the lower angle-of-attack region, and so were used at these lower angles of attack.

Since the presence of the winglet modifies the wing spanwise lift distribution, the changes were estimated using nonplanar vortex lattice techniques. Baseline and additional lift distributions due to winglets were estimated and incorporated into the data base of the external wing loads program. One condition for estimated spanwise lift distribution with winglet compared to the baseline is shown in Figure 16. The data identify the discontinuities due to the detailed characteristics of the wing – for example, engine installations.

Structural Description

The structure which was designed for the tests consisted of an upper winglet, a lower winglet, and a wing box extension attached to the test aircraft wing box at the outer fuel closure bulkhead (Figure 17). In addition, the wing box upper skin panels were strengthened.

The winglet structure is shown in Figure 18. The upper winglet was designed with a primary structure of conventional metal construction having two spars with skins and ribs. The wing box extension spars were continuous with those of the upper winglet, with the rear spar spliced to the wing rear spar across the fuel bulkhead. Additional splicing was made to the skins, stringers, and fuel closure bulkhead through external splice plates and internal fittings. The new

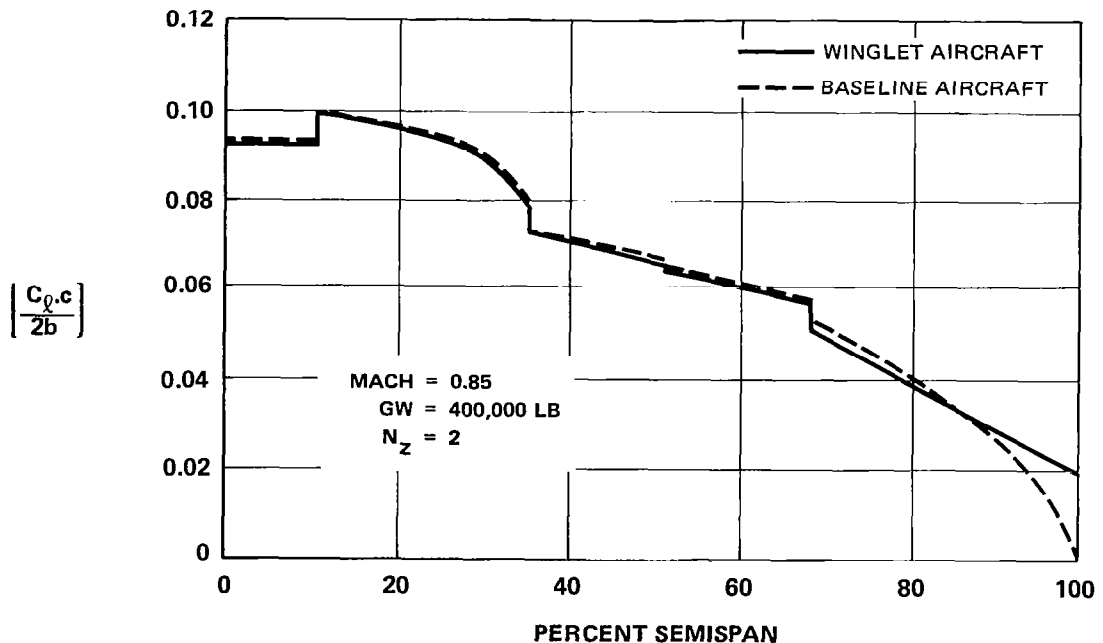


FIGURE 16. TYPICAL ESTIMATED SPANWISE WING LIFT DISTRIBUTION

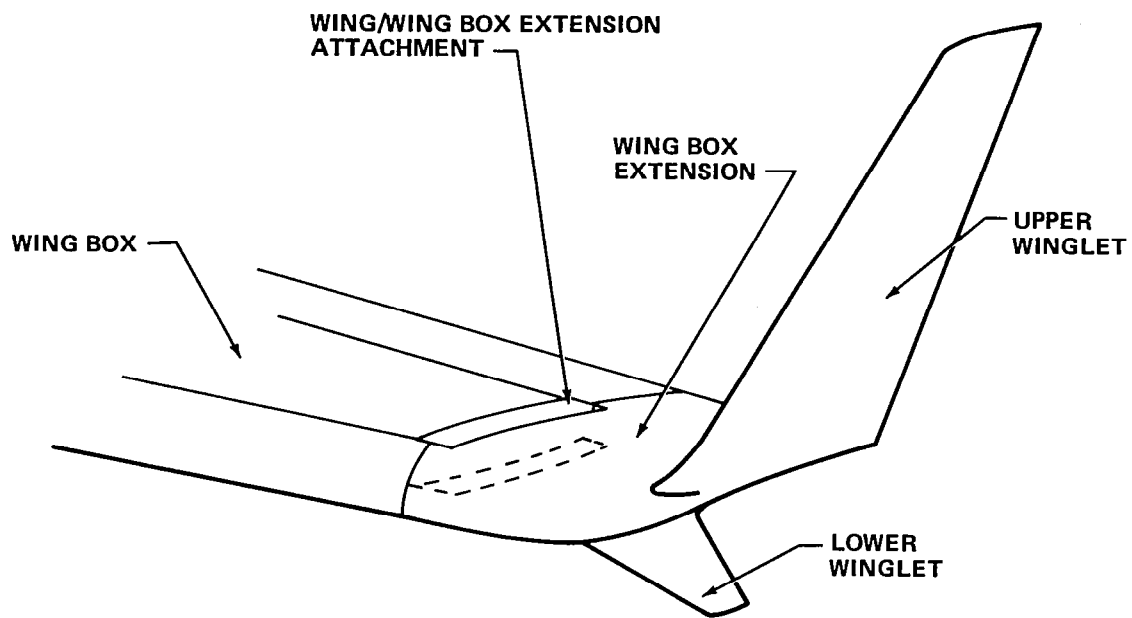


FIGURE 17. WINGLET INSTALLATION COMPONENTS

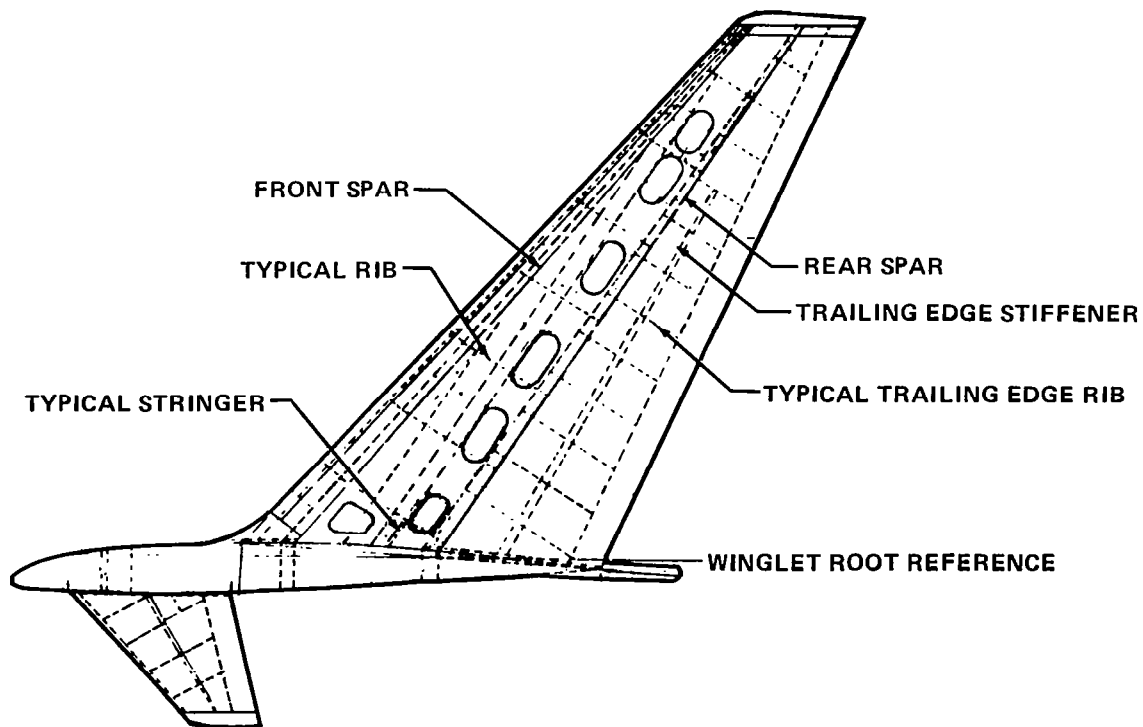


FIGURE 18. BASIC WINGLET STRUCTURAL CONFIGURATION

extension was constructed of conventional aluminum structure with skins and ribs. The leading and trailing edge assemblies of the wing box extension were modified production items. The fairing of the juncture between the upper winglet and the wing tip extension was merged at its aft end with a fairing representing the trailing edge position light installation. No operational light was installed at this position. An operational production wing tip light installation was included at each wing tip leading edge position.

Each lower winglet used a single aluminum spar with glass-fiber-epoxy laminate skins. This material was also used for the leading edge of the upper winglets, trailing edge and tip of the new wing box extensions, juncture fairing of the upper winglet leading edge, and the simulated wing tip aft light fairing. Mahogany was used for the tips of the BWL and RSWL upper winglets and the tips of the lower winglets. Conversion from BWL to RSWL was done in the field by cutting through the entire structure at the appropriate spanwise section and installing a new winglet tip.

The strengthening of the wing is shown in Figure 19. The upper panels were reinforced with angle members attached to the stringers (shown in the figure as S1 through S22) between the ribs (shown by their reference numbers, 737.6 through 1042.3). The reinforcing affected approximately 7.6 m (300 in.) inboard of the wing box extension attachment at reference station X_w 912.4. In general, the type of reinforcing was a simple angle. In the area of the extension attach-

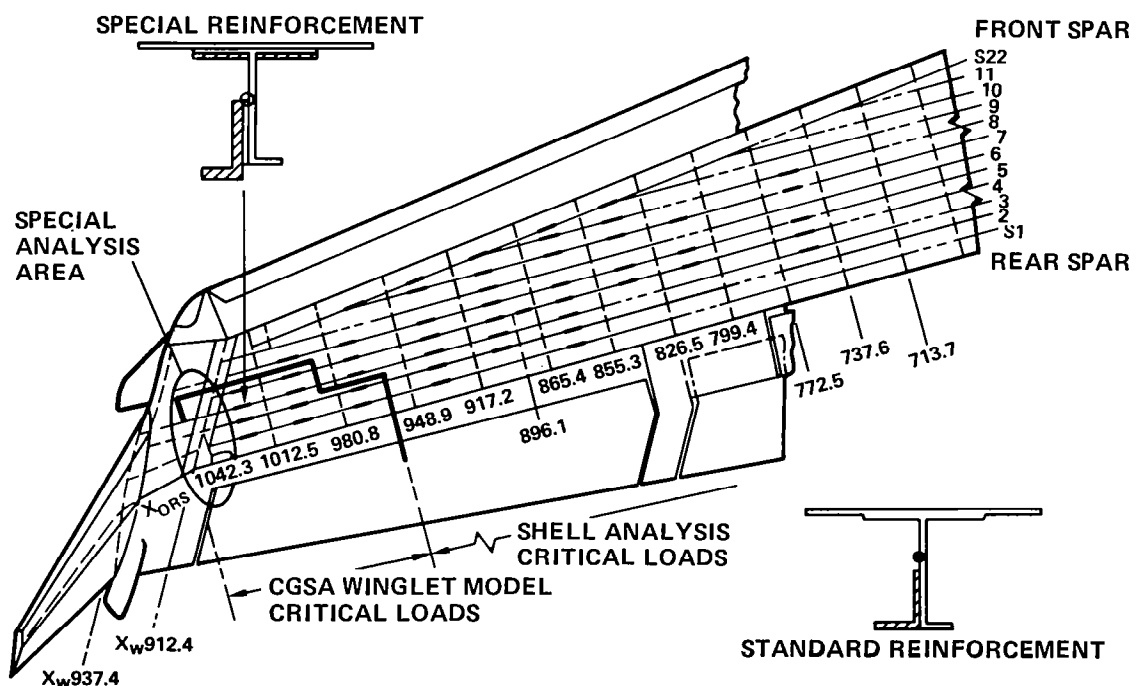


FIGURE 19. WING REINFORCEMENT - UPPER SURFACE

ment, one stringer was reinforced with a more substantial angle and doublers. The analysis methods used (see next section of this report) are also identified in Figure 19.

The spar cap and web splices were added to existing fastener locations in most cases. Some existing fasteners were replaced by larger ones, and new fasteners were added through skin doublers and plate splices between stringers. After removing the winglets and splice members during airplane reconfiguration, oversize fasteners were installed as necessary to restore integrity of the original box structure and fuel seal, and the remaining unused fastener holes were plugged. Wing-strengthening additions inboard of the splice remained with the aircraft after the test program.

The leading edge Krueger flap described earlier was designed and manufactured to bolt to the leading edge of the upper winglet. As fabricated for the BWL, the flap was 2.8 m (9.4 ft) long. The flap was constructed so that 0.8 m (2.5 ft) of the upper end could be trimmed in the field for the RSWL tests.

During the flight test phase, several aerodynamic configuration changes were made to the winglets, as described later in a discussion of test results. Appropriate structural alterations were made.

Stress Analysis

A finite element model was used to analyze the upper winglets, the wing box extension, and that portion of the existing wing approximately four wing tip chords inboard from the tip. The inboard end of this model was joined analytically to a shell analysis used for the inboard portion of the wing.

Flutter Analysis

The selection of the test configurations and flight conditions to be used in the flight flutter tests was based on flutter analysis results. This analysis predicted the important vibration modes, frequencies, and flutter-speed margins of the aircraft with winglets installed. The results of the analysis were verified later through a ground vibration test (GVT), conducted to measure the important mode shapes and frequencies.

The discrete mass representation of the aircraft with winglets consisted of concentrated masses on each of 55 bays, with each mass described by 6 degrees of freedom. The aircraft mass and stiffness properties were used to calculate unrestrained aircraft orthogonal modes. A set of orthogonal modes was computed for fuel loading conditions consisting of 0, 10.0, 12.5, 15.0, 17.5, 21.5, 40.0, 60.0, 80.0, and 100-percent fuel. Mass and stiffness symmetry about the aircraft centerline was assumed so only half the aircraft had to be analyzed.

The flutter analyses were performed using the standard "required damping versus velocity" methods. Symmetric and antisymmetric conditions were analyzed with unsteady aerodynamic influence coefficients (AIC) based on the Doublet Lattice Method. These coefficients were generated for $M = 0.9$, which is the flutter-critical Mach number for the DC-10. The unsteady aerodynamics included wing-winglet coupling effects.

The flutter analyses were performed for several altitudes with the resulting flutter speeds interpolated among altitudes to obtain a valid flutter speed at the correct 0.9 Mach number. Flutter speeds were normalized to a reference dive speed, V_{REF} , of 706 km/h (381 KEAS) which corresponds to $M = 0.9$ on the M_D/V_D boundary. Structural damping of $g = 0.02$ was assumed in all structural modes. Flutter was defined to occur when the value of damping reached zero. Various fuel loading conditions were analyzed to define the flutter speed as a function of fuel loading.

The critical flutter mode for the basic DC-10 Series 10 without winglets is a symmetric 3-Hz mode involving coupling between first wing bending and first wing torsion. The addition of the winglets reduced the flutter speed of the 3-Hz wing mode to $1.09 V_{REF}$ for fuel loading less than 12.5 percent. In addition, the winglets introduced a 4.5-Hz flutter mode involving second wing bending and second wing torsion. The minimum flutter speed of this 4.5-Hz flutter mode was $1.14 V_{REF}$. Because these adverse winglet effects were predicted, 226.80 kg (500 lb) of mass balance was installed in each wing tip to ensure adequate flutter margins for flight testing.

The flutter speeds for the 3-Hz (inner panel) and 4.5-Hz (outer panel) modes with the mass balance added are shown in Figure 20. The flutter speeds for the 4.5-Hz mode were higher than for the 3-Hz mode, and were above $1.2 V_{REF}$ at all fuel loadings. Flutter speeds for the 3-Hz mode on the other hand were above $1.2 V_{REF}$ only at fuel loadings above about 15 percent; below that they dropped to as low as $1.14 V_{REF}$. Because of this, the fuel loadings were kept above 24 percent (15,875.73 kg or 35,000 lb of fuel) for all tests except the flutter tests.

The flutter analysis for the conditions of Figure 20 showed that the subcritical damping was more than 2 percent at all speeds up to V_D , with no significant loss of damping as V_D was approached.

The results shown in Figure 20 were based upon theoretical analyses performed prior to the GVT. (The differences between GVT measured frequencies and theoretical frequencies are shown and discussed later in this report in the section titled Results and Discussion.) In order to assess the significance of these frequency differences, a flutter analysis was performed of the empty fuel configuration using the measured frequency data. The analysis using measured frequency data resulted in slightly higher flutter speeds for both the 3-Hz and 4.5-Hz flutter modes than did the corresponding flutter analysis using theoretical modal frequencies. Therefore, for conservatism, the theoretical modal frequencies were used for all flutter speed predictions.

FLUTTER SPEED

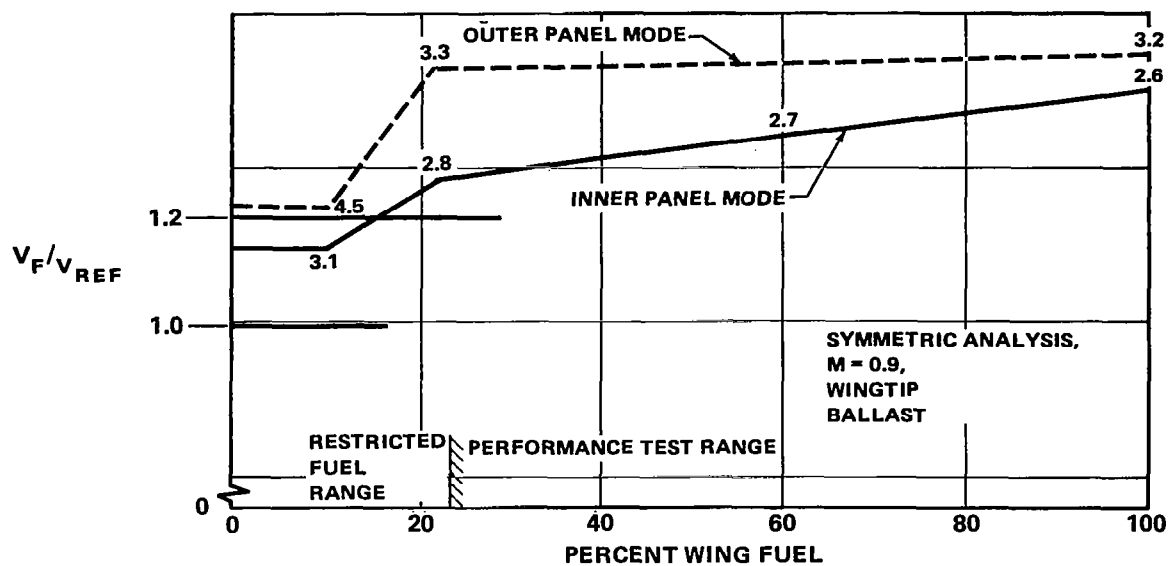


FIGURE 20. PREDICTED FLUTTER SPEED VERSUS WING FUEL – BASIC WINGLET

WINGLET MANUFACTURE

The main stages of winglet manufacture are illustrated in Figures 21 through 28. Figure 21 shows a stage in the profile machining of one of the upper winglet spars. This unit was machined from a hand forging using computer-aided manufacturing techniques. During machining and heat treatment, the spar was located by tabs along the length, these being removed in the final stages of fabrication. Figure 22 shows the winglet trailing edge assemblies being built on simple fixtures. The winglet spars were used essentially as location tooling during the winglet assembly.

Figure 23 shows spars in position, with a trailing edge assembly also in place. A more detailed view of the upper winglet structure, looking inboard, is shown in Figure 24. At this early stage, some instrumentation is already in place. The same assembly, looking outboard, is shown in Figure 25. The juncture of the upper winglet and wing box extension, at a later stage of the assembly when the extension skins were attached, is shown in Figure 26. Two stages of assembly of the lower winglets are shown in Figure 27, indicating the skin and rib assemblies forward and aft of the main spar. The completed assembly, without the lower winglet, is shown ready for installation in Figure 28.

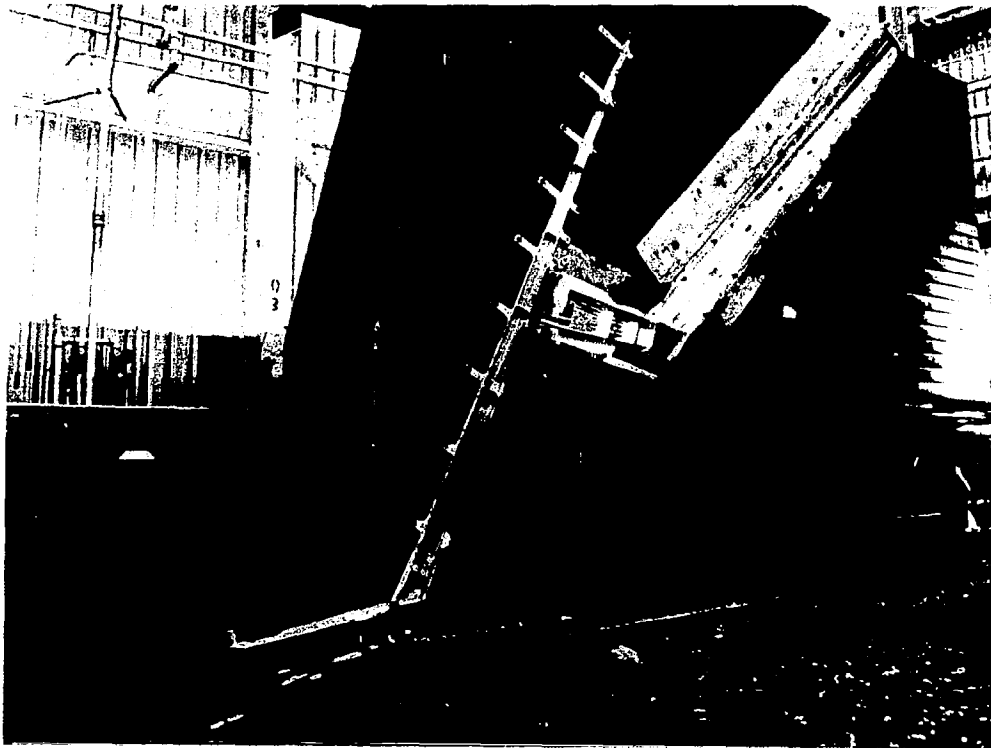


FIGURE 21. WINGLET SPAR MACHINING

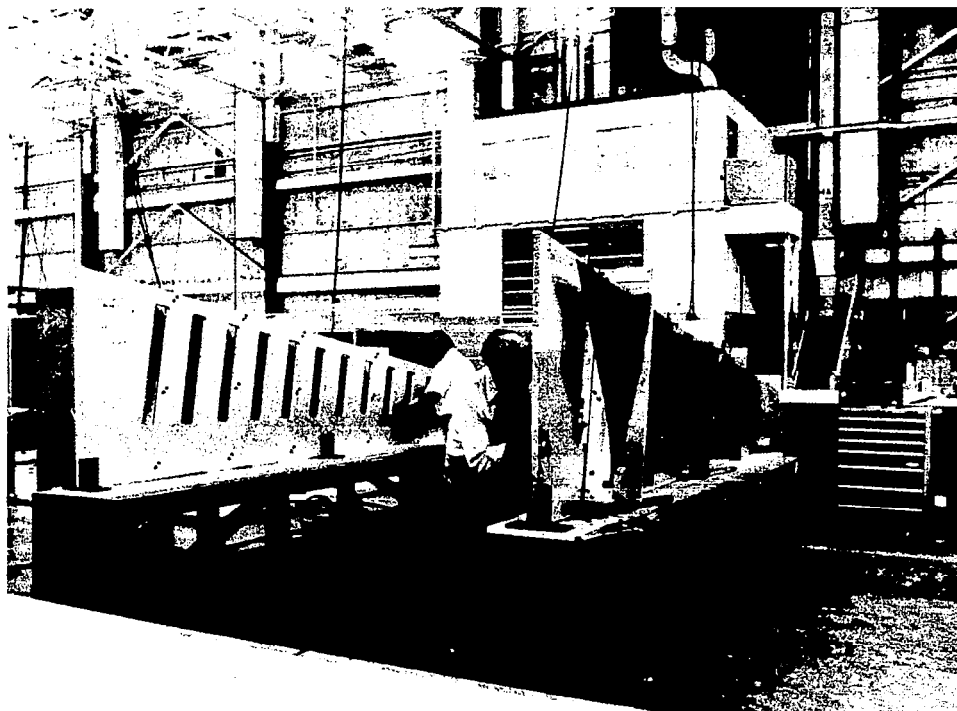


FIGURE 22. TRAILING EDGE ASSEMBLIES

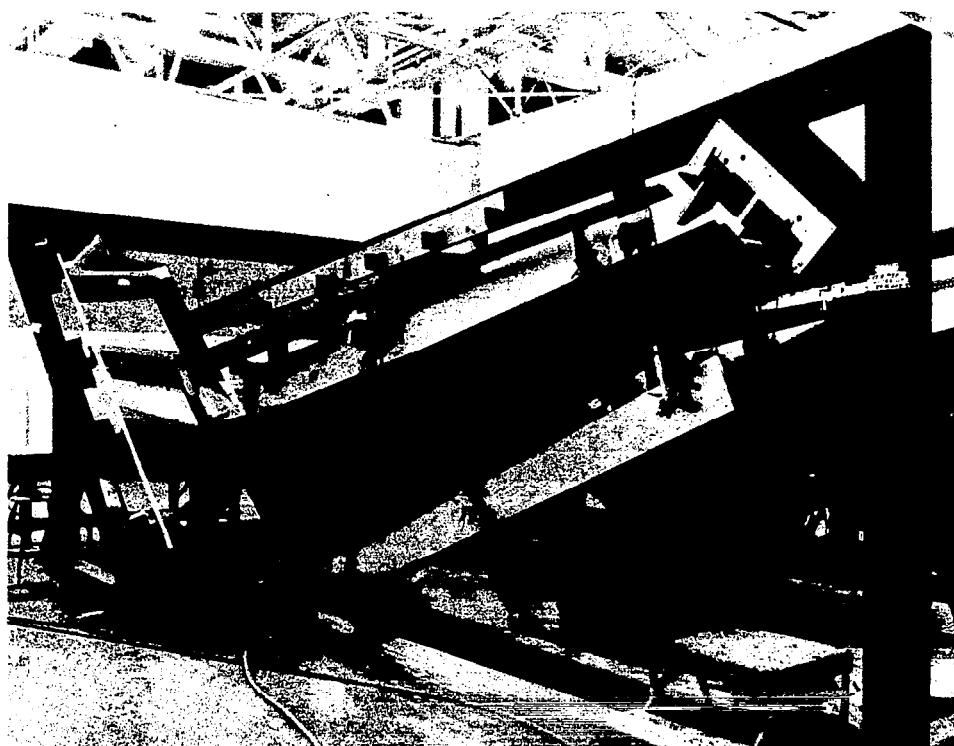


FIGURE 23. WINGLET – START OF ASSEMBLY

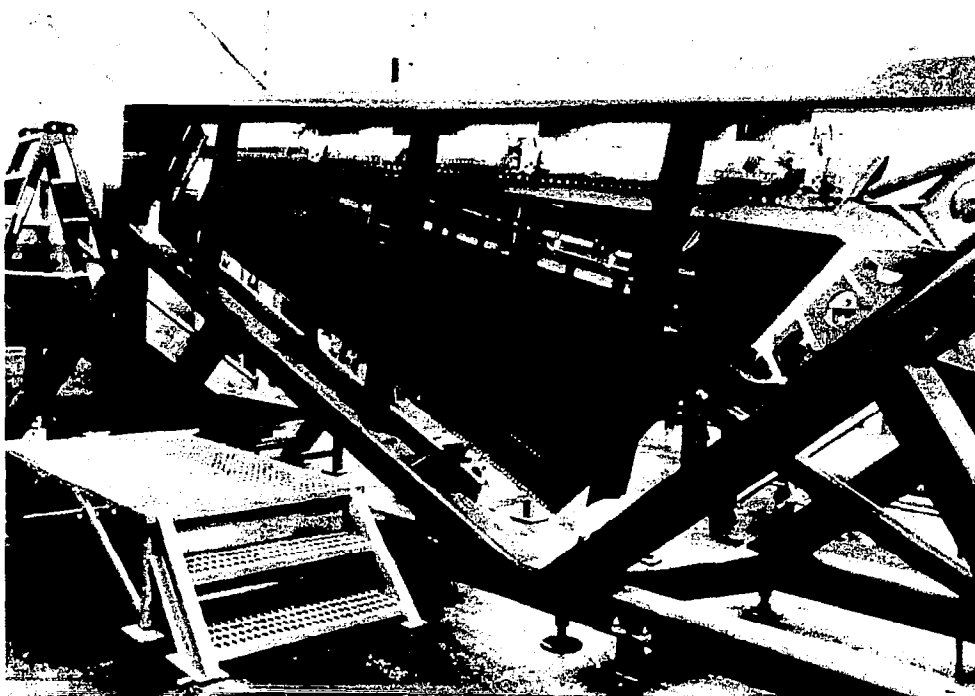


FIGURE 24. UPPER WINGLET SUBSTRUCTURE

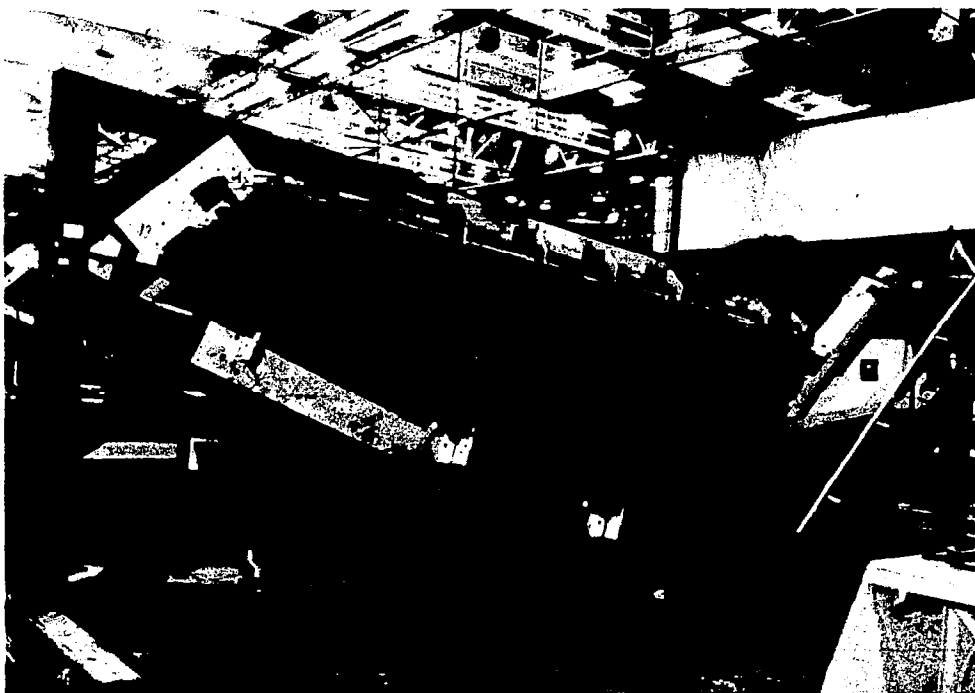


FIGURE 25. UPPER WINGLET ASSEMBLY

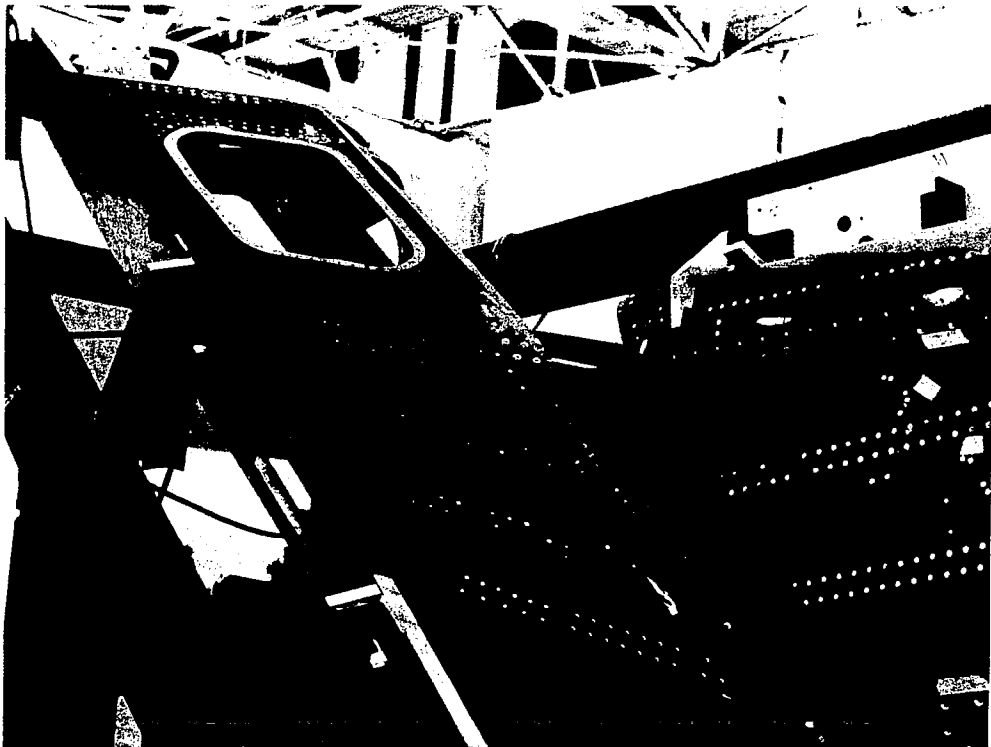


FIGURE 26. WINGLET AND WING BOX EXTENSION JUNCTURE

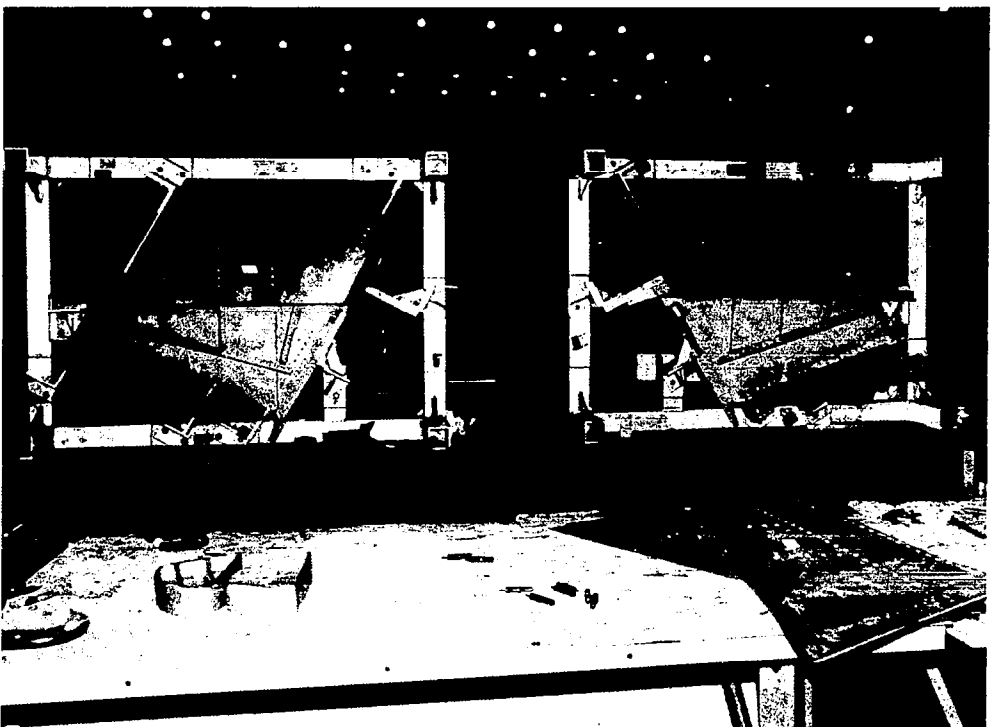


FIGURE 27. LOWER WINGLETS

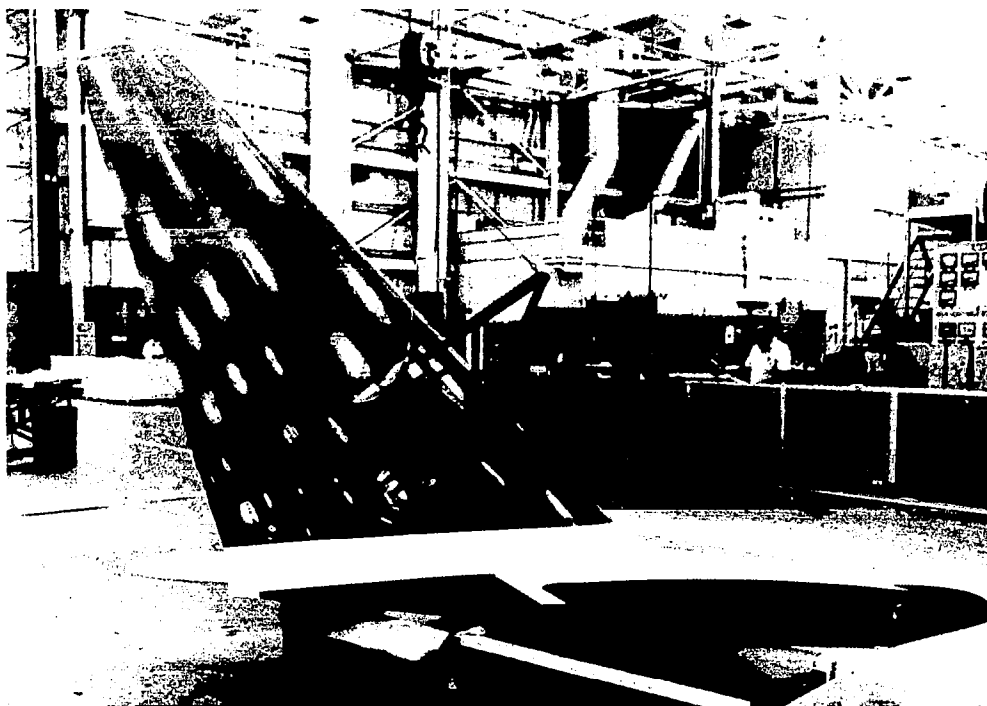


FIGURE 28. WINGLET AND WING BOX EXTENSION ASSEMBLY

AIRCRAFT PREPARATION AND WINGLET INSTALLATION

The aircraft preparation phase consisted of the baseline aircraft modification, the winglet installation, and the aircraft reconfiguration for airline service after the test. The three activities were conducted in the open using simple equipment.

The modification activity consisted primarily of strengthening the wing box. Upper skin stiffener reinforcements were inserted through the existing lower skin access panels and attached with the aid of simple location tools. During this work, instrumentation and test equipment were installed in the aircraft. Upon completion of this activity, the baseline flight test took place.

In the second stage, the winglet assemblies were installed. This installation required further structural work near the wing tip to make the connections. The winglet was installed using simple hoist equipment (Figure 29). The completed installation of the upper and lower winglet is shown in Figure 30. During the second stage, work to complete the instrumentation was undertaken.

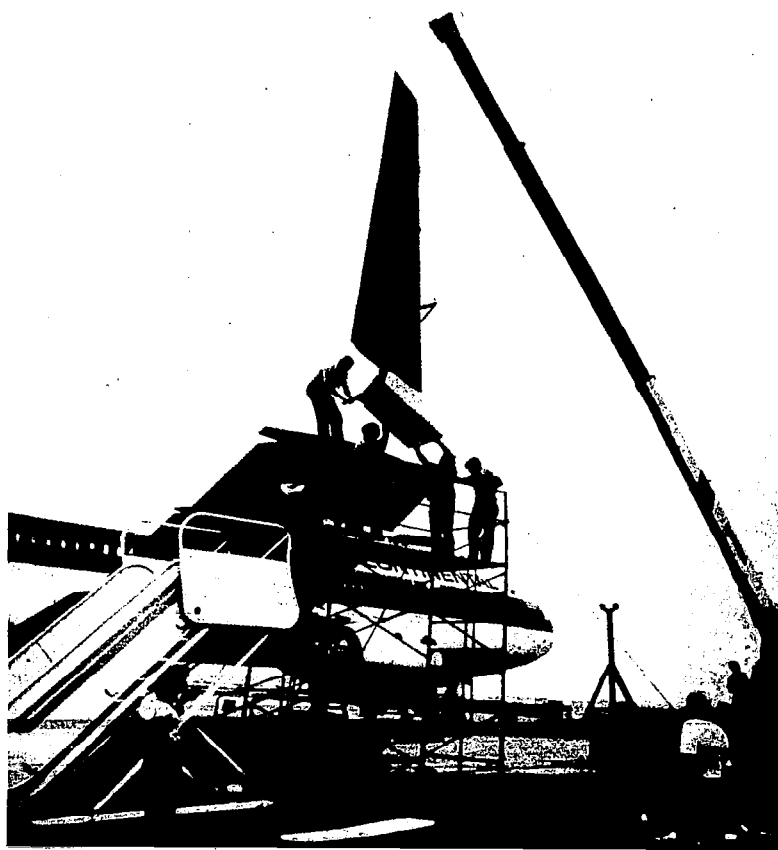


FIGURE 29. WINGLET INSTALLATION IN PROGRESS

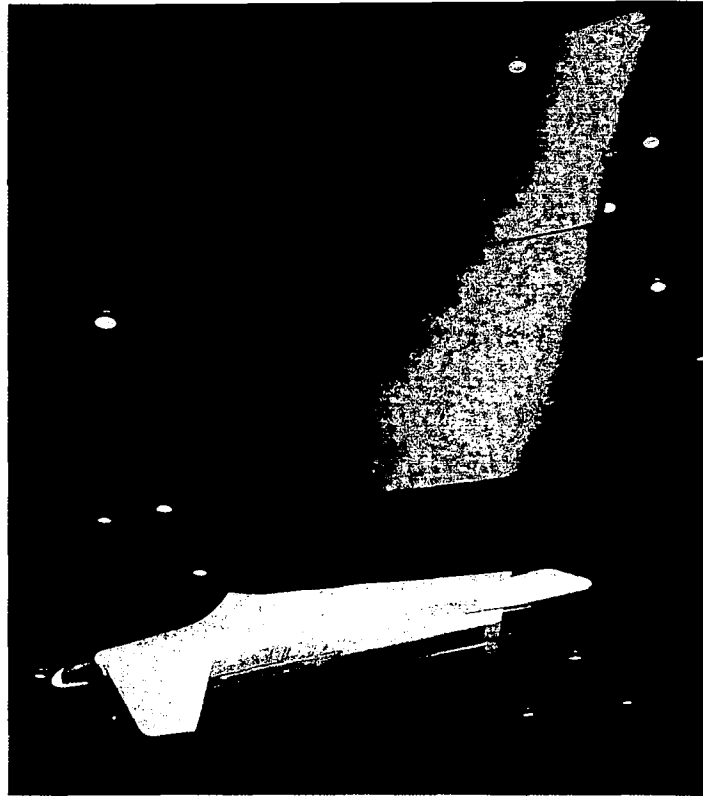


FIGURE 30. WINGLET INSTALLATION COMPLETE

After the winglet flight test, the aircraft was reconfigured to the baseline configuration with test equipment removed. New and splicing structures were removed. Items previously installed for wing box strengthening remained with the aircraft. The original wing tips were reinstalled and the aircraft refurbished prior to its return to airline service.

FLIGHT PROGRAM

Test Approach

In order to ensure accuracy in comparison and correlation, the flight test program was arranged to have back-to-back testing of the baseline and winglet aircraft in all key areas. The important areas for comparison were performance, stability and control, and loads. Structural and aerodynamic damping data were obtained from BWL testing only. The program was begun with tests of the baseline aircraft, continued with the BWL configuration, and completed with the RSWL. The flight test program is summarized in Figure 31. Test conditions, instrumentation, and tests performed are described further in subsequent parts of this section. A list of flight test measurements is presented in Appendix A.

Test Conditions

Aerodynamics — Evaluations were made in the following specific areas:

- Cruise drag improvement
- High-space buffet boundary
- Stall speeds and characteristics
- Low-speed drag improvement
- High- and low-speed stability and control (S&C) characteristics

	BASELINE	WINGLET	
		BWL	RSWL
PERFORMANCE CRUISE LOW SPEED	X X	X X	X X
STABILITY AND CONTROL	X STEADY SIDESLIP ONLY	X	X STEADY SIDESLIP ONLY
DIAGNOSTIC DATA FLOW VISUALIZATION (TUFTS) WING DEFLECTION MEASUREMENT (CAMERA) PRESSURE MEASUREMENTS (WING) PRESSURE MEASUREMENTS (UPPER WINGLET)	X X	X X X X	X X X X
STRUCTURAL AERODYNAMIC DAMPING		X	X ENVELOPE EXPANSION CHECK ONLY
LOADS MEASUREMENT (DOUGLAS) ADDITIONAL PRESSURE MEASUREMENT STRAIN GAUGES	X	X X	X X

FIGURE 31. FLIGHT TEST PROGRAM

The high-speed performance and buffet boundary test conditions are summarized in Figure 32. Performance evaluation data were obtained for typical cruise operating conditions. In addition, flights were made at lower Mach numbers to establish the incompressible drag. From these data, the aircraft drag coefficient was determined by obtaining the aircraft thrust required at the particular altitude and air speed. The range factor $[(V/W_p)W]$ was obtained from corresponding measurements of the air speed, fuel flow, and weight. Engine thrust was obtained by measurement of the engine fan speed, N_1 , and use of the engine performance computer decks.

Buffet onset data were determined by measuring normal acceleration during wind-up turns at high cruise Mach numbers. A buffet boundary investigation for the reduced-span winglet was classified as a contingency item for two reasons. First, on the basis of wind tunnel results, no change in the basic aircraft buffet characteristics was anticipated from the installation of winglets. Second, the RSWL would, because of its size, be expected to introduce a lesser effect on buffet C_L than the BWL, and consequently, if no change was observed for the larger winglet, it could confidently be assumed that no change would be present for the smaller. Consequently the RSWL was only to be evaluated for buffet characteristics if a significant impact was determined from the preceding BWL tests.

The low-speed performance test conditions are shown in Figure 33. Minimum stall speeds for both the baseline and BWL aircraft were evaluated at forward cg with the aircraft in the clean configuration and flap settings typical of takeoff and landing. During these tests, evidence of any buffet limitations was sought by use of accelerometer measurements in the cockpit cabin and on the winglet. It was intended that, should unacceptable buffet be encountered, a fixed leading edge device would be attached to the upper winglet leading edge and its effect measured.

Stall speeds were investigated for the baseline and BWL configurations. It was determined that stall characteristics were only required for the BWL. Low-speed stall characteristic tests for the RSWL were considered as a contingency only if the BWL tests showed a significant effect. Such a result was considered unlikely since wind tunnel tests for both the BWL and the RSWL did not indicate any significant change over the baseline aircraft, and since intuitively the RSWL should produce even less change. It was planned that, should there be a measured stall speed difference for the BWL, the RSWL would also be evaluated at the takeoff flap setting.

Low-speed drag polars were obtained for the baseline aircraft and for both winglet configurations by tests at the same flap settings, using engine N_1 as the measurement for the determination of thrust.

The stability and control test conditions are shown in Figure 34.

TEST CATEGORY	OBJECTIVES	BASELINE	WINGLET	TEST CONDITIONS			MEASUREMENTS
CRUISE CHARACTERISTICS	ESTABLISH BASELINE LEVEL	X		<u>MID/AFT CG (ALL TESTS)</u>			RANGE FACTOR, N_1
	EVALUATE BASIC UPPER AND LOWER WINGLETS		BWL	<u>W/δ</u>	<u>M</u>	<u>ALT</u>	
				1.4×10^6	0.82R, 0.83R	33,000	
				1.6×10^6	0.80, 0.81, 0.82R, 0.83R, 0.84	36,000	
				1.75×10^6	0.81, 0.82R, 0.83R	39,000	
	EVALUATE REDUCED-SPAN UPPER AND LOWER WINGLETS		RSWL				
INCOMPRESSIBLE DRAG	DETERMINE INCOMPRESSIBLE DRAG POLAR	X	BOTH	0.6×10^6	0.50, 0.55, 0.60, 0.65	17,000	
				0.8×10^6	0.55, 0.60, 0.65	23,000	
				1.0×10^6	0.60, 0.65	27,000	
BUFFET BOUNDARY	ESTABLISH BUFFET ONSET	X	BWL	1.6-g WIND-UP TURN M = 0.75, 0.80, 0.83 ALT = 36,000-38,000			NORMAL ACCELERATION
			RSWL	M = 0.83			ONLY IF CHANGE OBSERVED FOR BASIC WINGLET

R DENOTES REPEAT POINT

FIGURE 32. HIGH-SPEED PERFORMANCE TEST CONDITIONS

TEST CATEGORY	OBJECTIVE	BASELINE	WINGLET	TEST CONDITIONS	MEASUREMENTS
STALL CHARACTERISTICS	DETERMINE STALL CHARACTERISTICS		BWL	<u>FORWARD CG (ALL TESTS)</u> $\delta_F/\delta_S = 0/\text{RET}, 0/\text{T.O.}, 15/\text{T.O.}, 22/\text{T.O.}, 50/\text{LND}$ ALT = 10,000-15,000	STICK FORCES
			RSWL	$\delta_F/\delta_S = 15/\text{T.O.}, 50/\text{LND}$	STICK FORCES**
STALL SPEEDS	DETERMINE V_{MIN}	X	BWL	$\delta_F/\delta_S = 0/\text{RET}, 15/\text{T.O.}, 15/\text{LND}$ ALT = 10,000-15,000	$V_{S_{1g}}, V_{\text{MIN}}$ AT VARIED ENTRY RATES
			RSWL	$\delta_F/\delta_S = 15/\text{T.O.}$	ONLY IF CHANGE OBSERVED FOR BASIC WINGLET
LOW-SPEED DRAG	DETERMINE LOW-SPEED DRAG POLAR	X	BOTH*	SIX POINTS OVER RANGE OF 1.2 TO 1.5 V_{MIN} $\delta_F/\delta_S = 15/\text{T.O.}$ ALT = 10,000	N_1

R DENOTES REPEAT POINT

*EVALUATION OF WINGLET LEADING EDGE DEVICE, IF REQUIRED

**EVALUATED ONLY IF CHANGE OBSERVED FOR BASIC WINGLET

FIGURE 33. LOW-SPEED PERFORMANCE TEST CONDITIONS

TEST CATEGORY	OBJECTIVES	CONFIGURATION		TEST CONDITIONS	MEASUREMENTS
		BASELINE	WINGLET		
STATIC LONGITUDINAL STABILITY	VERIFY STABILITY AND CONTROL CHARACTERISTICS	X	BWL	HEAVY WT, AFT cg, HIGH ALT, $M_N = 0.85$	STANDARD STABILITY AND CONTROL PARAMETERS
LONGITUDINAL MANEUVERING STABILITY			BWL	MEDIUM WT, AFT cg, HIGH ALT, $M_N = 0.82$	
LONGITUDINAL TRIM			BWL	FOUR SPEEDS/CONFIG, CRUISE AND LANDING	
STEADY SIDESLIP			BWL, RSWL	CRUISE, TAKEOFF AND LANDING 2 SPEEDS/CONFIG, AFT cg	
DIHEDRAL STABILITY			BWL	HEAVY WT, MID AFT cg, $M_N = 0.88, 0.90$ HIGH ALT	
DUTCH ROLL CHARACTERISTIC			BWL	LIGHT CRUISE WT AND HEAVY LANDING WT CONFIG	
SPIRAL STABILITY			BWL	LIGHT WT, TAKEOFF AND LANDING CONFIG	
ROLL PERFORMANCE			BWL	MID cg, CRUISE AND LANDING CONFIG, 2 SPEEDS/CONFIG	

FIGURE 34. STABILITY AND CONTROL TEST CONDITIONS

The tests primarily concerned investigation of the DC-10 with the BWL. The choice of this configuration was based on wind tunnel results which indicated that the impact of winglets on stability and control characteristics should be small. Therefore, in order to ensure quantifiable results for winglet increments in S&C parameters, the larger winglet was employed. It was anticipated that if the BWL aircraft should be judged satisfactory from a handling-characteristics viewpoint the RSWL aircraft would also be satisfactory. The testing of static directional stability was required for the baseline and both winglet configurations in order to accurately distinguish any difference.

To evaluate winglet effects, flow visualization, measurements of pressures, and estimates of wing bending and twist deflection were obtained. The flow visualization was designed to identify the flow quality on the surfaces and at the juncture of winglet and wing at cruise and low speeds. Pressure measurements were taken on the upper winglet, outer wing, and aileron. Wing deflection data were used to calculate the impact of winglets on induced drag reduction.

Structural and Aerodynamic Damping (Flutter) — The test conditions were based on the results of the flutter analyses previously described, as verified by ground vibration testing, and are shown in Figure 35.

For the flight test with the BWL, two fuel configurations were defined. Clearance for the configuration representing the minimum amount of fuel to be used for subsequent performance

ACTIVITY	WINGLET CONFIGURATIONS	MEASUREMENTS
VIBRATION FLUTTER ANALYSIS	BWL, RSWL	FLUTTER SPEED MARGINS, MODES, FREQUENCIES
GROUND VIBRATION TEST	BWL	MODE SHAPES, FREQUENCIES
FLIGHT TEST	BWL <ul style="list-style-type: none"> ● 15,875.73 kg (35,000 LB) FUEL 7160 m (23,500 FT) TO 0.91 m (ENVELOPE CLEARANCE) ● 12.5 PERCENT FUEL 9,140 m (30,000 FT) ● 12.5 PERCENT FUEL FLUTTER CRITICAL CONDITION 7,160 m (23,500 FT) TO 0.91 m 	FREQUENCY, DAMPING VELOCITY CONDITIONS

FIGURE 35. FLUTTER TEST CONDITIONS

testing was made first. This fuel amount was 15 876 kg (35,000 lb). Subsequently, measurements at the 12.5-percent fuel flutter critical condition were obtained. The less critical performance fuel condition was tested at medium altitude to 0.91 Mach number. The flutter-critical condition required testing first at high altitude, then at medium altitude. Figure 36 shows the range of test speeds and altitudes superimposed on the DC-10 envelope.

It was originally intended that flutter testing with the RSWL would be limited to clearing the speed envelope with performance minimum fuel. As explained in the Results and Discussion section, this test was later considered unnecessary.

The flutter data were obtained from accelerometer information. Modal excitation was made by pilot-induced inputs in the flight controls. Damping values were obtained from the transient decay of the excited modes, as determined from time histories of symmetric and antisymmetric parameters. The symmetric excitation parameters were wing tip normal acceleration, winglet tip normal, winglet tip longitudinal, starboard engine normal, and cockpit normal. The antisymmetric excitation parameters were wing tip normal acceleration, winglet tip normal, and cockpit lateral.

Loads Measurement — The primary test objective was to determine the winglet impact on wing loads and the winglet load itself. In addition, the flight loads were monitored for potentially critical maneuvers. Additional data were required as a result of concern, arising from wind tun-

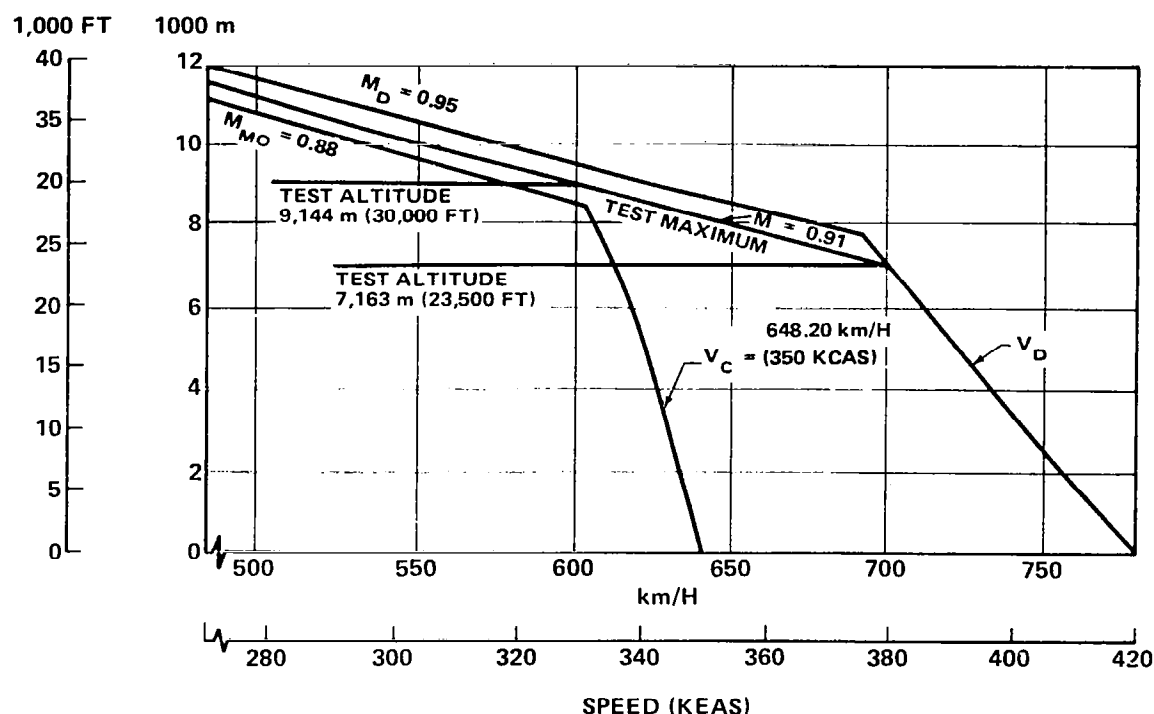


FIGURE 36. FLUTTER TEST SPEEDS AND ALTITUDES

nel data, that the outboard aileron could be subjected to a significant increase in load due to the winglet installation. Consequently, data requirements were set for the key items concerned, namely the outboard aileron, its actuating cylinder, and the most critical of the hinge brackets. The test parameters for the loads measurement program are shown in Figure 37.

The flight test measurements were made in a number of angle-of-attack surveys at a range of Mach numbers. The surveys were flown under 1g conditions and also during steady banked turns at 1.6g. Steady state yawing maneuvers were included at 1g for certain selected conditions so the effect of sideslip could be evaluated. High-lift data were included in the program.

ITEM	OBJECTIVES	BASLINE	WINGLET	MEASUREMENTS
UPPER WINGLET	ESTABLISH WINGLET ROOT LOADS; VERIFY WIND TUNNEL DATA	X	BWL, RSWL	STRAIN GAGES; PRESSURE SURVEY
WING, WING TIP	DETERMINE WINGLET IMPACT ON WING LOAD		BWL, RSWL	STRAIN GAGES; PRESSURE SURVEY
OUTBOARD AILERON	VERIFY WIND TUNNEL DATA		BWL, RSWL	PRESSURE SURVEY
AILERON ACTUATING CYLINDER	ESTABLISH AILERON HINGE MOMENTS		BWL, RSWL	STRAIN GAGES
AILERON HINGE BRACKET NO. 4	MAINTAIN ADEQUATE MARGINS OF SAFETY		BWL, RSWL	STRAIN GAGES

FIGURE 37. LOADS TEST PARAMETERS

Flight Instrumentation

The flight instrumentation consisted of the existing (or production) air data computer (ADC), an additional flight test ADC together with an inertial system, on-board monitoring equipment including a computer, pressure orifices and strain gauges, accelerometers, and visual aids.

Aerodynamics Data — Owing to the back-to-back nature of the performance tests, thrust-instrumented and calibrated engines were not required. However, air data and engine parameters were carefully measured.

The production ADC parameters measured were the captain's airspeed, altitude, pitot total pressure, static pressure, and total air temperature, and the first officer's airspeed, altitude, pitot total pressure, static pressure, and temperature.

For the flight test ADC, a trailing cone streamed from the vertical fin was provided to supply an error-free static pressure source. The test ADC parameters measured were:

- Keil pitot and auxiliary pitot compared with trailing cone static airspeed
- Total Keil pitot and auxiliary pitot pressure
- Trailing cone static pressure and altitude
- Inertial navigation system parameters
- Engine parameters: N_1 (fan speed), N_2 (core speed), exhaust gas temperature, and fuel flow using calibrated transmitters
- Other parameters, including angle of attack and of sideslip; pitch, roll, and yaw rates; surface and system positions, and cabin pressure. Surface instrumentation consisted of the pilot-operated flight control positions, flight control forces, and control surface positions. Buffet onset characteristics were obtained from cockpit, cabin, and wing accelerometers. In order to measure the buffet response in the stall tests, accelerometers were installed on the horizontal stabilizer front spar, the outboard elevator balance weights, and the vertical stabilizer tip.

Flow visualization was obtained on the left winglets and the winglet by means of tufts. The tufts were viewed from both the DC-10 cabin and a chase aircraft.

Pressure distribution measurements were obtained on the right outer wing and upper winglets to determine span loads on the wing and upper winglets. A single row of orifices near the wing tip was considered sufficient to determine the additional wing span loading due to the winglet, since this is the only area where the wing load distribution is significantly affected.

Over the remainder of the wing, complete span load distribution data had been established from previous DC-10 test programs. In addition to the wing pressure orifice row, pressure measurements were obtained on the right outboard aileron. The locations of the pressure orifices, and the camera targets used for photographic measurements of wing deflection, are shown in Figure 38.

Flutter — The flutter instrumentation consisted of accelerometers located in the winglets, wing tips, starboard wing engine, horizontal and vertical stabilizers, and captain's seat (Figure 39). All accelerometers except those mounted on the starboard wing and engine were also used for buffet measurements. Figure 39 also shows accelerometers, which were used solely for buffet data, at the tail engine, elevator tip, and aircraft center of gravity.

In addition to the accelerometers, aileron, elevator, and rudder surface position instrumentation was used. Data from the structural aerodynamic damping (SAD) tests, as well as from the stall tests previously mentioned, were telemetered to the Douglas Flight Control and Data Center to allow real time monitoring. These data were also recorded on the onboard data system tape recorder. The SAD tests were observed from a chase airplane supplied by NASA Dryden.

Loads — The load instrumentation consisted of strain gauges and pressure orifices on the wing and upper winglet. Pressure instrumentation locations are shown in Figure 38. Calibrated strain gauges were installed in the winglet near its root. The wing was instrumented with un-

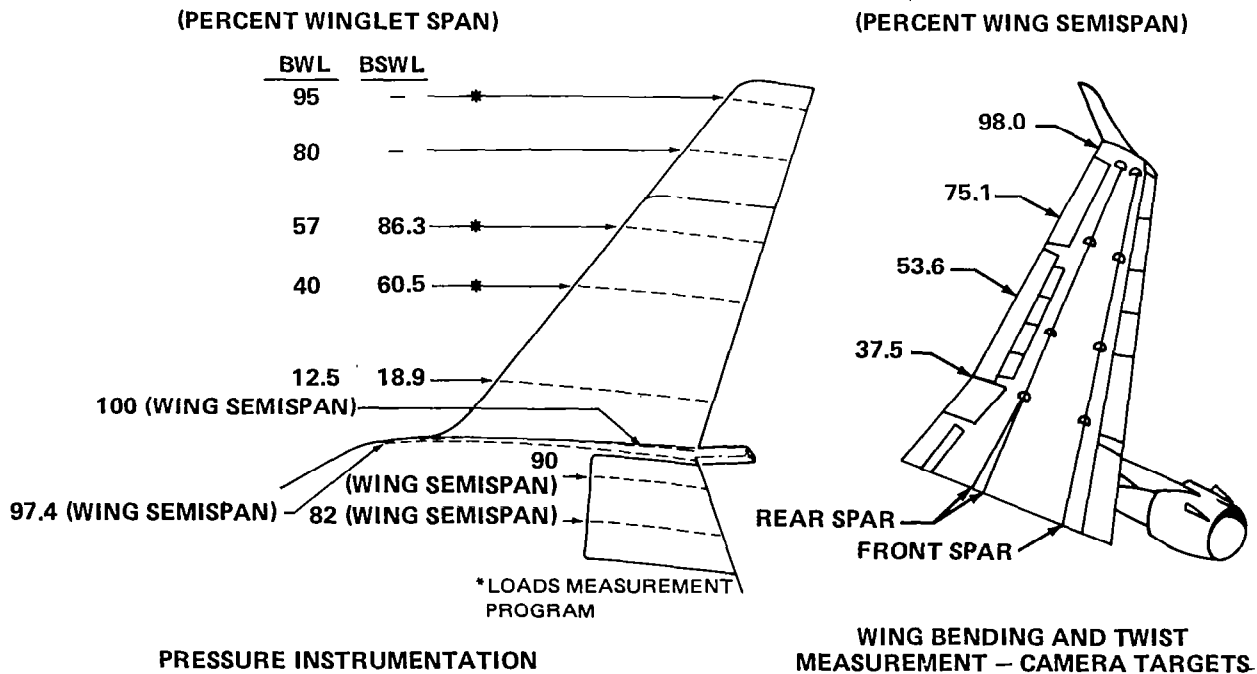


FIGURE 38. WING AND WINGLET PRESSURE AND DEFLECTION INSTRUMENTATION

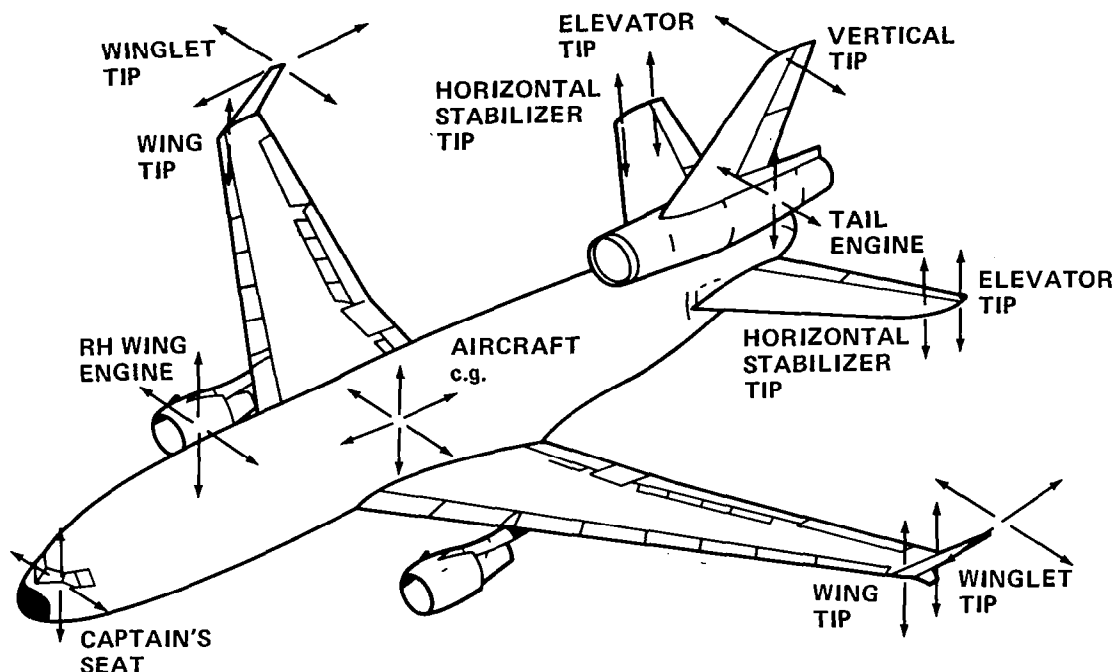


FIGURE 39. ACCELEROMETER LOCATIONS

calibrated strain gauges at three spanwise positions. The readings on these gauges were used in back-to-back comparisons with winglet on and winglet off. The winglet off condition was related to previously available data. The winglet strain gauges were calibrated by the point load method described in Reference 4. This method required the application of point loads to a number of locations on the front and rear winglet spars.

Flight Data System

The flight data system, using the Douglas facilities, enabled the test aircraft to link up with the operating base at Yuma and the flight test center at Long Beach. The system provides direct output of data in engineering units, and real time data presentations.

Through telemetry and microwave transmission, real time data could be transmitted to the test facilities. In addition to data transfer by normal communications, airborne recorded tape data could be dumped from Yuma to Long Beach.

Preflight Ground Tests

Ground Vibration Test (GVT) — Prior to the BWL flight tests, a GVT was conducted to measure the important mode shapes and frequencies of the test aircraft with the BWL installed. Due to extensive DC-10 GVT experience and data, a complete vibration modal survey was not

justified. Because the winglet installation primarily affected the wing modes, the GVT focused on the important modes for the wing, engine, and winglet. In addition, the amplitude and phases of the aircraft extremities (vertical and horizontal stabilizer, tips, engine nacelles, wing tips, and upper winglet tips) were measured.

Symmetric and antisymmetric frequency sweeps were made over a range of 1 to 20 Hz. The sine-dwell method was used to measure the modes, and decay records were employed to calculate the modal damping. Normalized modal deflection and mode lines were then calculated.

Strain Gauge Calibration Tests — Calibration tests were conducted for the gauges at the aileron actuator, hinge bracket, and winglet root. Conventional techniques were used for the aileron components, with excellent correlation. The winglet strain gauges were calibrated using the point method previously described. Point loads were applied from an adjacent rig to eight different positions on the winglet, and influence coefficients were derived for the gauges. Correlation with prediction was excellent.

Flight Test Program

The baseline flight test program was conducted from Long Beach and consisted of 11 flights designated A2 through A12. (Flight A1 was the delivery flight from Continental Airlines.) These flights were primarily devoted to cruise and low-speed performance.

The BWL test phase began with a general handling and envelope expansion flight from Long Beach to Edwards Air Force Base. From Edwards, a series of flights completed the envelope expansion and the structural and aerodynamic damping program. Satisfactory data were obtained. Chase plane support was provided by the NASA Dryden Flight Research Center. The BWL performance testing began with transfer of the test aircraft to the Douglas facility at Yuma, Arizona. During this flight, evidence of low-speed buffet was observed. As a result, development activity was introduced into the program aimed at identifying and resolving the problem. This addition required changes to the originally planned program. However, the BWL phase was accomplished in all essentials. The details of the development activity are described in the Results and Discussion section. The results of flight tests performed during the BWL phase are shown in Figure 40.

Upon completion of the BWL phase of the test program, the upper winglet span was reduced for the RSWL phase. Owing to the results and quantity of data obtained in the BWL phase, the previously planned envelope expansion test was eliminated. For the same reason, changes to the other parts of the originally planned program were made. Some development tasks were also conducted. In addition, a test was added to measure the effect of drooping the outboard ailerons. RSWL phase objectives were accomplished in all essentials, and the aircraft was returned to Long Beach for the refurbishment program. The results of flight tests performed during the RSWL phase are shown in Figure 41.

FLIGHT NO.	CONFIGURATION					TESTS PERFORMED									COMMENTS
	CONFIG	LOWER WL	FCK	VORT (1 OR 2)	MODE	SAD	HS BUFFET	CRUISE PERF		LS DRAG	LS BUFFET	STALLS	S AND C	LMP	
A-13	1	X				X						STICK SHAKER		X	FIRST FLIGHT WITH WINGLETS, CHASE, LIMITED FLOW VISUALIZATION FLUTTER: M = 0.70, 0.75, 0.80, 0.84, 0.86, 0.87; 24% FUEL; h _p = 7163 m (23,500 FT)
A-14	1	X				X									M = 0.87, 0.88, 0.89, 0.90, 0.91; 24% FUEL; h _p = 7163 m (23,500 FT)
A-15	1	X				X									M = 0.75, 0.80, 0.84, 0.86, 0.88, 0.89; 12.5% FUEL; h _p = 9144 m (30,000 FT)
															M = 0.70, 0.75, 0.80, 0.84, 0.86, 0.88, 0.89; 12.5% FUEL; h _p = 7163 m (23,500 FT)
A-16	1	X				X									M = 0.89, 0.90, 0.91; 12.5% FUEL; h _p = 7163 m (23,500 FT)
A-17	1	X											X	X	TUFT FLOW VISUALIZATION, CHASE, STATIC DIRECTIONAL
A-18	1	X									X		X		TUFTS AND TARGETS REMOVED, STATIC DIRECTIONAL
A-19	1	X							X		X				TARGETS REINSTALLED
A-20	1	X						X	X		X				
A-21	1	X					X	X			X				
A-22 & A-23	1	X													NO DATA, FERRY TO EAFB AND RETURN (STATIC DISPLAY)
A-24	1	X												X	LOST TRAILING CONE, PROGRAM NOT COMPLETED
A-25	1	X												X	TAKEOFF AND LANDING LOADS
A-26	1	X												X	LOADS PROGRAM COMPLETED
A-27	2	X	BASIC								X				TUFT FLOW VISUALIZATION
A-28	3		BASIC								X				LOWER WINGLET REMOVED, TUFT FLOW VISUALIZATION
A-29	4		BASIC	1							X				VORTILET 1 INSTALLED, TUFT FLOW VISUALIZATION
A-30	5		BASIC								X				LEFT KRUEGER FLAP DEFLECTION ADJUSTED TO 48 DEGREES; RIGHT KRUEGER FLAP DEFLECTION ADJUSTED TO 40 DEGREES
A-31	6		EXTENDED								X				KRUEGER EXTENDED TO WINGLET ROOT, DEFLECTIONS SAME AS A-30

FIGURE 40. FLIGHT TESTS PERFORMED DURING EVALUATION OF BASIC WINGLET (PAGE 1 OF 2)

FLIGHT NO.	CONFIGURATION			TESTS PERFORMED											COMMENTS
	CONFIG	LOWER WL	FCK	VORT (1 OR 2)	MODE	SAD	HS BUFFET	CRUISE PERF		LS DRAG	LS BUFFET	STALLS	S AND C	LMP	
A-32	7	X	EXTENDED								X				LOWER WINGLET REINSTALLED, BOTH KRUEGER FLAP DEFLECTION ADJUSTED TO 40 DEGREES
A-33	8		EXTENDED							X					BOTH KRUEGER FLAP DEFLECTIONS ADJUSTED TO 40 DEGREES; POLARS INCOMPLETE
A-34	8		EXTENDED							X					DRAG POLARS INCOMPLETE ON ACCOUNT OF UNSTABLE ATMOSPHERE
A-35	8		EXTENDED									X			STALL SPEED TEST INCOMPLETE ON ACCOUNT OF LOSS OF TRAILING CONE, TARGETS REMOVED
A-36	8		EXTENDED									X			INSTRUMENTATION ABORT
A-37	8		EXTENDED							X	X				
A-38	8		EXTENDED									X			
A-39	8		EXTENDED							X		X			STALL SPEEDS AND DRAG POLARS COMPLETED
A-40	8		EXTENDED									X	X		STALL CHARACTERISTICS, LOW-SPEED STABILITY AND CONTROL, WEATHER ABORT
A-41	8		EXTENDED									X	X		STALL CHARACTERISTICS AND LOW-SPEED STABILITY/ CONTROL COMPLETED
A-42	9												X		HIGH-SPEED STABILITY/ CONTROL PARTIALLY COMPLETED
A-43	9												X		HIGH-SPEED STABILITY/ CONTROL COMPLETED
A-44	9							X	X						TARGETS INSTALLED, CRUISE PERFORMANCE NOT COMPLETED
A-45	9										X				TUFT FLOW VISUALIZATION, NO CHASE
A-46	9							X	X						CRUISE PERFORMANCE COMPLETED
A-47	10	X		2	X					X	X				TUFT FLOW VISUALIZATION
A-48	11			2	X						X				TUFT FLOW VISUALIZATION
A-49	12	X	SHORTENED	2							X				MOD6 REMOVED, LAST BASIC WINGLET FLIGHT

FIGURE 40. FLIGHT TESTS PERFORMED DURING EVALUATION OF BASIC WINGLET (PAGE 2 OF 2)

FLIGHT NO.	CONFIGURATION					TEST PERFORMED								COMMENTS
	CONFIG	LOWER WL		FCK		AIL DROOP	HS BUFFET	CRUISE PERF		LS DRAG	LS BUFFET	S AND C	LMP	
		BASIC	EXT CHORD	UPPER WL	LOWER WL			INCOMP	HS					
A-50	13			X						X	X			TUFT FLOW VISUALIZATION
A-51	14							X	X		X			
A-52	14									X	X			TUFT FLOW VISUALIZATION
A-53	14							X	X			X		CRUISE PERFORMANCE (LOWER WINGLET OFF) COMPLETED, STATIC DIRECTIONAL STABILITY
A-54	15	X							X		X			
A-55	15	X						X	X					COMPLETED CRUISE PERFORMANCE (LOWER WINGLET ON)
A-56	15	X											X	LOADS PROGRAM COMPLETED
A-57	16	X		X							X			TUFT FLOW VISUALIZATION
A-58	17		X	X	X					X	X			TUFT FLOW VISUALIZATION
A-59	18		X											HIGH-SPEED FLOW VISUALIZATION
A-60	18		X					X	X		X			WING BENDING AND TWIST MEASUREMENT
A-61	18		X			X		X	X		X			WING BENDING AND TWIST MEASUREMENT, 3-DEGREE DROOPED AILERONS

FIGURE 41. FLIGHT TESTS PERFORMED DURING EVALUATION OF REDUCED-SPAN WINGLET

RESULTS AND DISCUSSION

Baseline Phase

Flight Test Program — The planned objectives for this phase were achieved. Some deviations from the original test plan were required, but sufficient data were obtained to adequately establish a basis with which to compare the results of the winglet phases of the program.

Aerodynamics — The results showed that the test aircraft performance was representative of that of the DC-10 in-service fleet. Also, engine performance levels were found to be typical of those of fleet airplanes with similar service time.

Loads Measurement — Some data points originally planned for strain gauge measurement were not obtained during baseline phase. However many of these data were obtainable from similar points obtained during the aerodynamics testing. Sufficient data were obtained to establish a sound basis for testing in the subsequent phases of the program.

Basic Winglet Phase

Ground Vibration Test — The GVT results are summarized in Figure 42 which lists frequencies of the important symmetric and antisymmetric modes. Theoretical modal frequencies are

EMPTY FUEL
BASIC WINGLET
AIRCRAFT ON SUPPORT SYSTEM

	MODE DESCRIPTION	FREQUENCY, Hz		PERCENT DIFFERENCE
		THEORY	MEASURED	
SYMMETRIC MODES	FIRST WING BENDING	1.73	1.61	7.4
	WING ENGINE YAW	1.98	1.95	1.5
	WING ENGINE PITCH WITH WINGLET IN PHASE	3.40	3.23	5.3
	WING ENGINE PITCH WITH WINGLET OUT-OF-PHASE	3.83	3.82	0.3
	HORIZONTAL STABILIZER BENDING	4.21	4.10	2.7
	WING FORE AND AFT BENDING WITH WINGLET IN PHASE	5.05	4.64	8.8
	WING FORE AND AFT BENDING WITH WINGLET OUT-OF-PHASE	5.30	5.46	-2.9
ANTISYMMETRIC MODES	WING ENGINE YAW	2.05	1.96	4.6
	FIRST WING BENDING	2.48	2.21	12.2
	VERTICAL STABILIZER BENDING			
	HORIZONTAL STABILIZER OUT-OF-PHASE	3.56	3.27	8.8
	SECOND WING BENDING WITH ENGINE PITCH	3.84	3.79	1.3
	WING FORE AND AFT BENDING WITH WINGLET IN PHASE	5.24	5.05	3.7
	SECOND WING BENDING	6.59	6.37	3.4
	WINGLET BENDING WITH WING FORE AND AFT IN PHASE	7.31	8.20	-12.0

FIGURE 42. GROUND VIBRATION TEST RESULTS

also presented for comparison. In general, good agreement exists between theoretical and measured frequencies except for the symmetric and antisymmetric first wing bending modes and the higher-frequency modes involving winglet flexibility. Experience has shown that the first wing bending modal frequencies can be affected significantly by the support system stiffness. Only theoretical estimates of the support system stiffness and winglet stiffness were used for the text program. The effect of these frequency differences on the aircraft flutter characteristics were discussed in the Flutter Analysis section presented earlier.

Figures 43 through 45 offer comparisons of mode shapes and node lines for the important modes which couple to produce the critical 3-Hz symmetric wing flutter mode. Good agreement is shown for both mode shapes and node lines for the wing, winglet, and engine. The scale of the mode shape lines is greatly exaggerated for purposes of clarity.

Flight Test Program — The planned objectives for this phase were achieved. In addition, development activity, primarily the result of the low-speed buffet investigation, was inserted into the program.

Two of the three contingency configurations (see Figure 12) were employed. As a result of the encounter with unacceptable low-speed buffet on the initial BWL performance evaluation flight, the contingency leading edge Krueger flap was extensively exercised during low-speed testing. In addition, the effect of removing the lower winglet was investigated in low-speed and high-speed conditions.

The development activity gave rise to a number of configurations beyond the BWL and its contingency modifications. All the configurations tested in the BWL phase are described in Figure 46. The rationale for those configurations — other than the baseline — is explained in subsequent sections. In Figure 46, Configuration 1 is the original BWL, Configuration 2 is Configuration 1 with the Krueger flap fitted to it, and Configuration 3 is Configuration 2 with the lower winglet removed. More extensive modifications were then made, the chief features of which are illustrated in Figures 47 and 48. A description of the specific configurations, consistent with that in Figure 46, follows:

- Configurations 4 and 5: Configuration 3 with Vortilet Number 1, Krueger flap angle adjustments being applied in the latter case. This vortilet is defined as an upper winglet leading edge dorsal fin which originated at the aft edge of the wing tip forward light lens and extended to the upper winglet leading edge just below the lower end of the Krueger flap (8 percent of the winglet span). It was fabricated from plate material with an aerodynamically sharp leading edge and negligible thickness.
- Configurations 6 and 8: Configuration 3 with an extended Krueger flap. The flap modification (Figure 49) consisted of a 0.61-m (24-in.) addition to the upper winglet Krueger flap which began on the flap's lower edge and extended to the winglet root. The extension was of similar section to that previously fabricated.

FREQUENCY: 1.610 Hz
SYMMETRY: SYMMETRIC

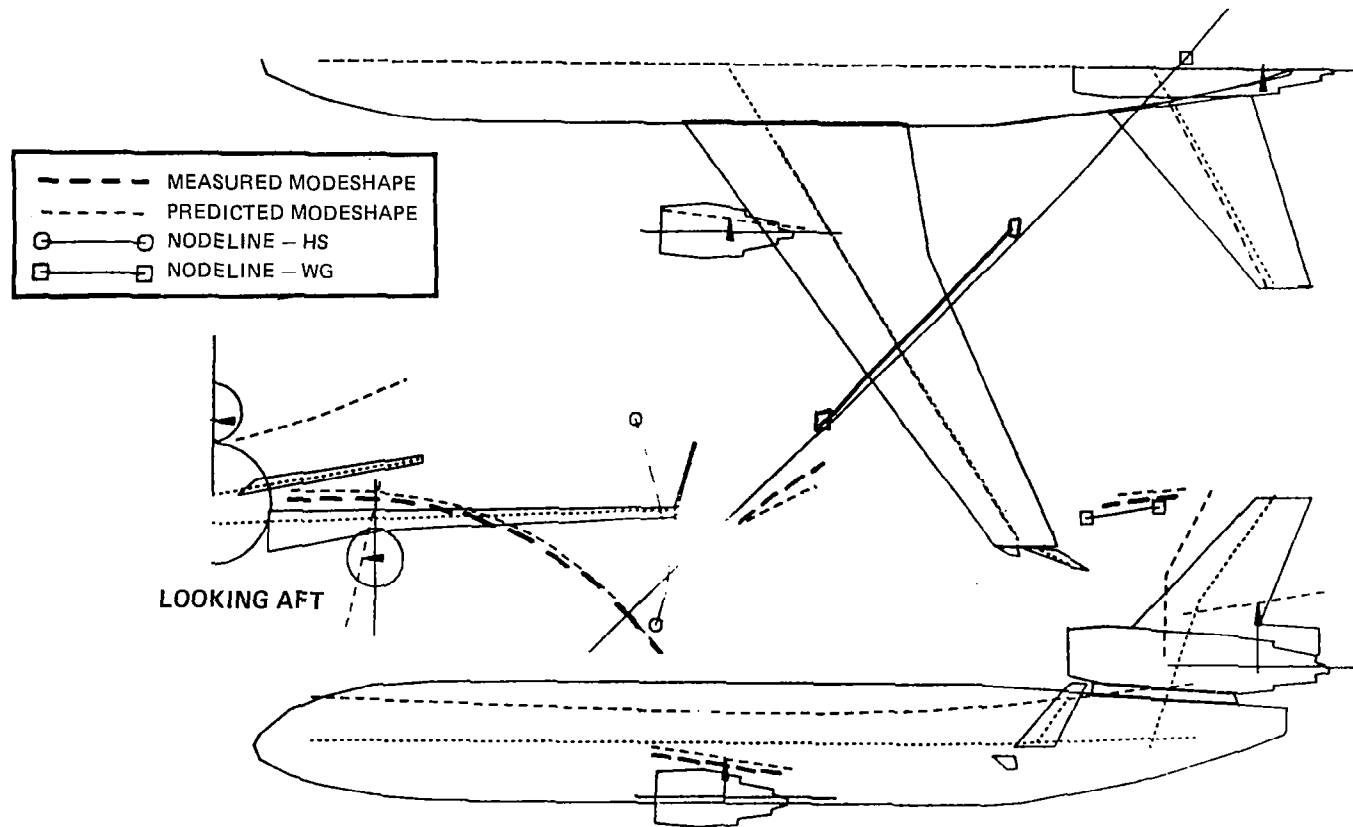


FIGURE 43. GVT FIRST WING BENDING MODES

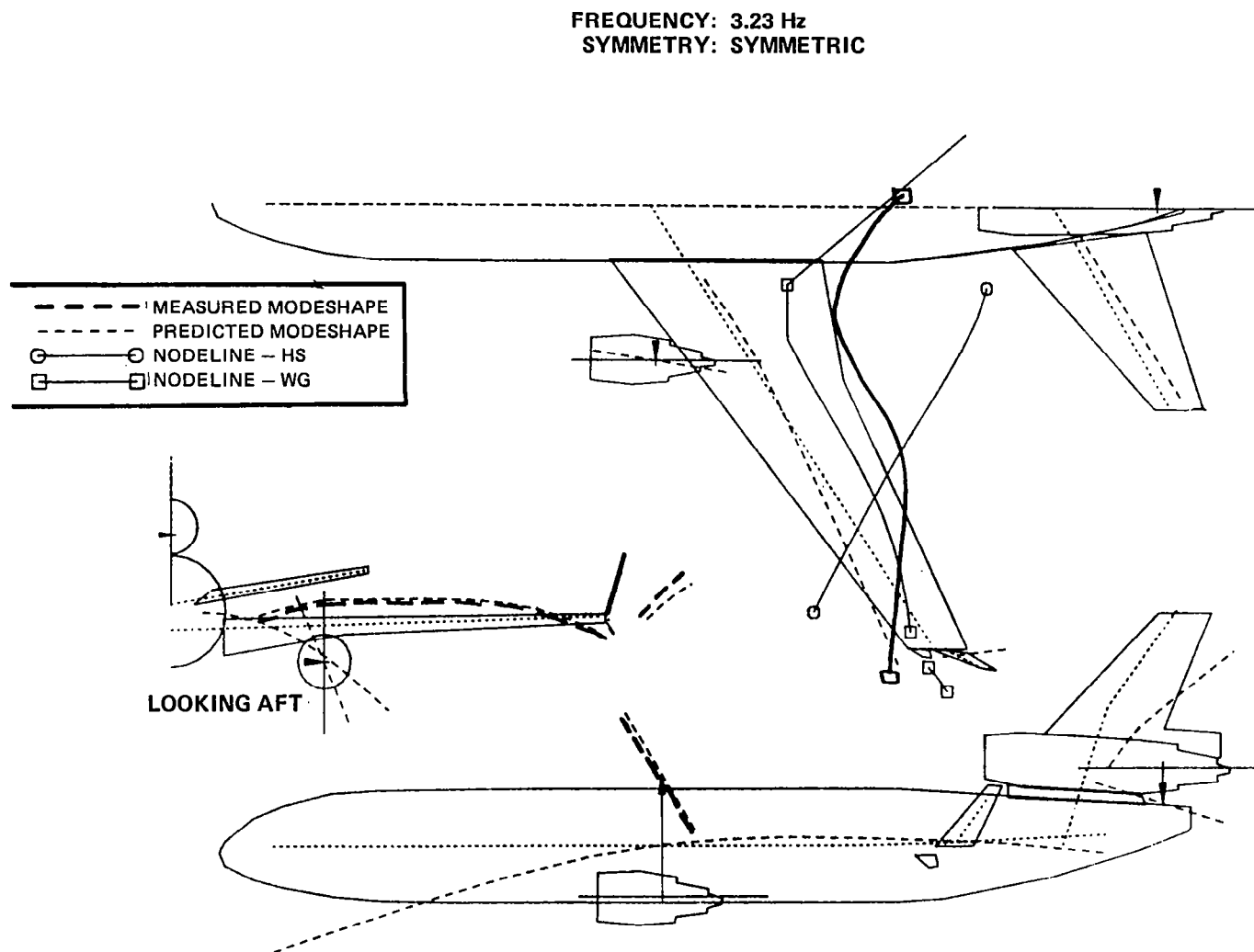


FIGURE 44. GVT WING ENGINE PITCH MODE WITH WINGLET IN PHASE

FREQUENCY: 3.82 Hz
SYMMETRY: SYMMETRIC

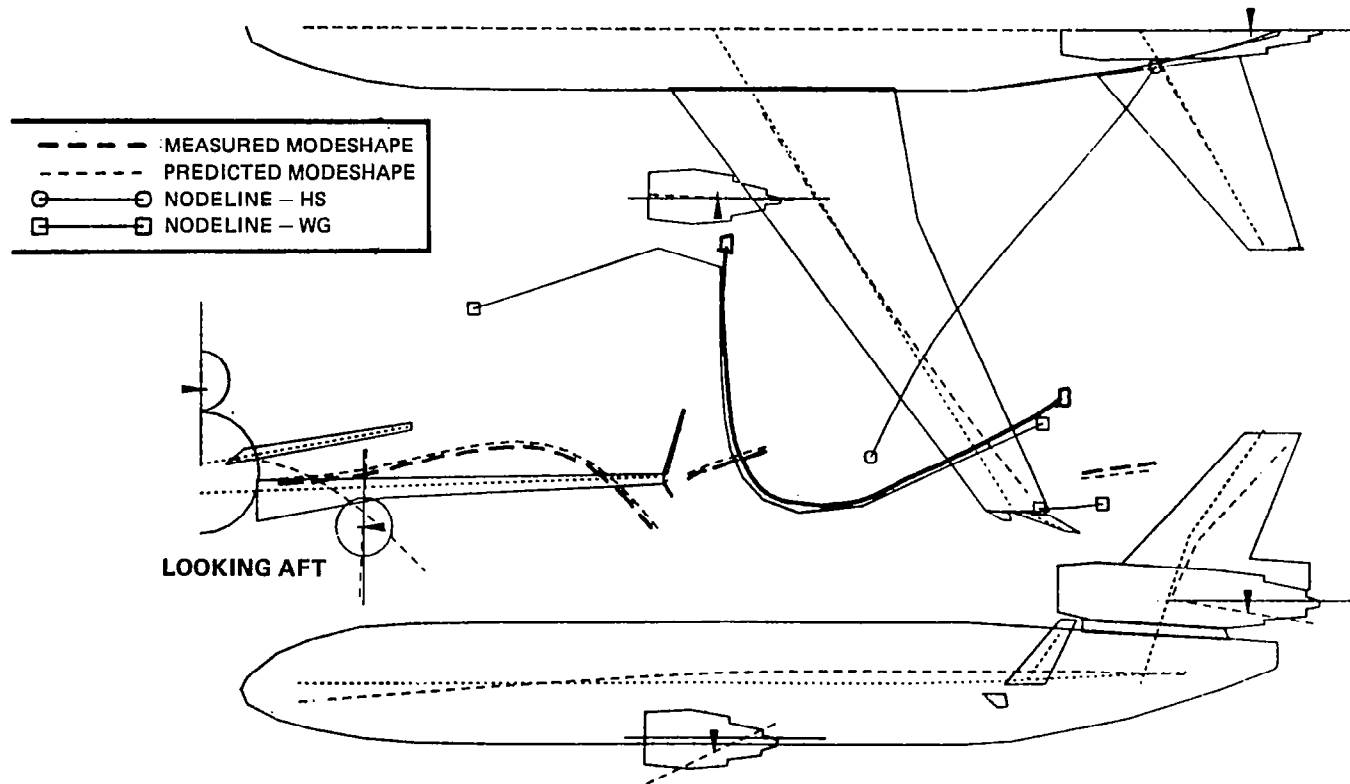


FIGURE 45. GVT WING ENGINE PITCH MODE WITH WINGLET OUT OF PHASE




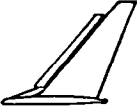

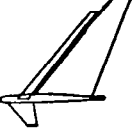




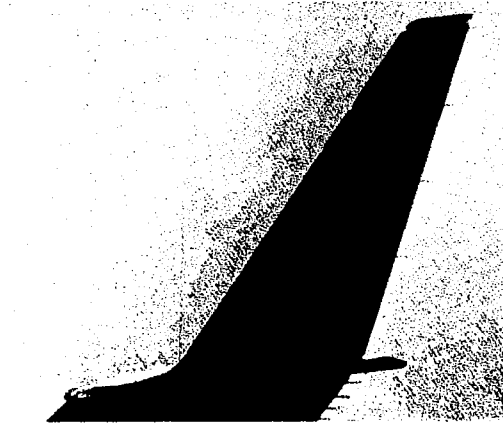
CONFIG NO.	1	2	3	4, 5	6, 8	7	9	10	11	12
PHYSICAL APPEARANCE										
DESCRIPTION	BASIC UPPER AND LOWER WINGLET AS ORIGINALLY DESIGNED	CONFIGURATION NUMBER 1 WITH KRUEGER FLAP ATTACHED TO UPPER WINGLET WITH 50-DEGREE DEFLECTION	CONFIGURATION NUMBER 2 WITH LOWER WINGLET REMOVED	CONFIGURATION NUMBER 3 WITH VORTILET 1 INSTALLED. VORTILET STARTED AT AFT END OF WING TIP LIGHT AND ENDED AT LOWER END OF KRUEGER FLAP KRUEGER FLAP DEFLECTION CONFIG NO. LH RH 6 45 40 8 40 40 NO. LH RH 4 50 50 5 45 40	BASIC UPPER WINGLET WITH KRUEGER FLAP EXTENDED TO WING TIP KRUEGER FLAP DEFLECTION CONFIG NO. LH RH 6 45 40 8 40 40	BASIC UPPER WINGLET WITH KRUEGER FLAP EXTENDED TO WING TIP AND DEFLECTED 40 DEGREES BASIC LOWER WINGLET INSTALLED	BASIC UPPER WINGLET WITHOUT LOWER WINGLET OR LEADING EDGE DEVICE	LARGE VORTILET 2 INSTALLED WHICH EXTENDED FROM AFT EDGE OF WING TIP LIGHT TO UPPER WINGLET LEADING EDGE AT ABOUT 37 PERCENT SPAN. MODIFIED (DROOPED LEADING EDGE) AIRFOIL ABOVE VORTILET 2. BASIC LOWER WINGLET INSTALLED	CONFIGURATION NUMBER 10 WITHOUT LOWER WINGLET	CONFIGURATION NUMBER 10 WITH MODIFIED AIRFOIL REMOVED AND KRUEGER FLAP INSTALLED ABOVE VORTILET 2
FLIGHT NO.	A13-A26	A27	A28	4: A29 5: A30	6: A31 8: A33-A41	A32	A42-A46	A47	A48	A49

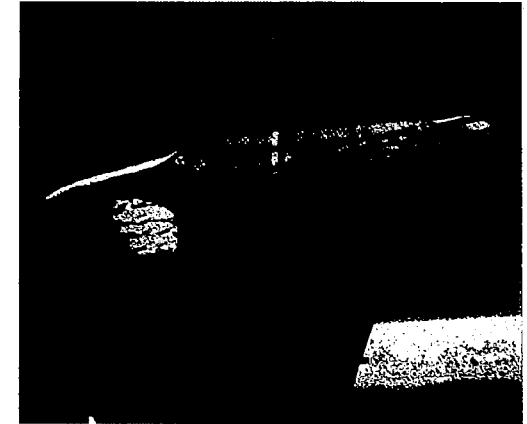
FIGURE 46. CONFIGURATION IDENTIFICATION
FOR BASIC WINGLET FLIGHT PROGRAM



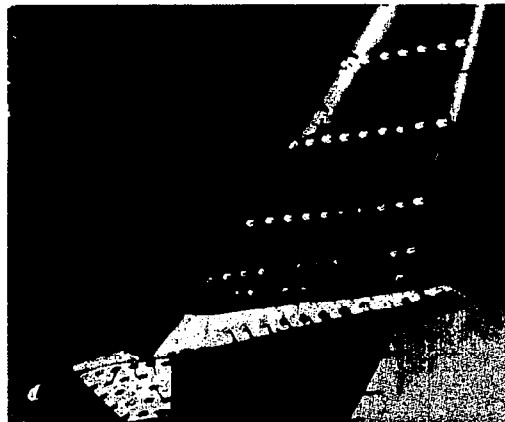
**BASIC UPPER WINGLET
AND LOWER WINGLET**



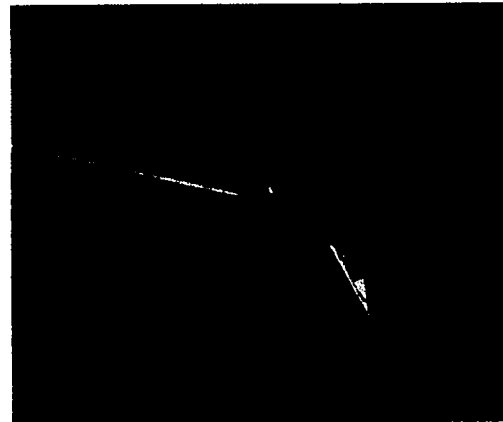
**BASIC UPPER WINGLET
WITHOUT LOWER WINGLET**



WING TIP LIGHT FAIRINGS



UPPER WINGLET KRUEGER FLAP

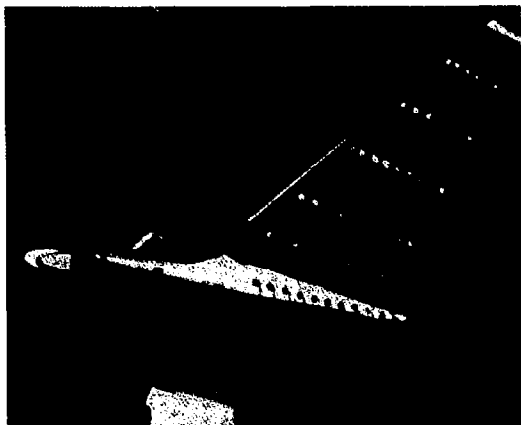


UPPER WINGLET KRUEGER FLAP



**KRUEGER FLAP EXTENSION
TO WINGTIP**

FIGURE 47. BASIC WINGLET CONFIGURATION FEATURES



OUTBOARD VIEW OF
VORTILET NO. 1



VORTILET NO. 2 WITH MOD 6



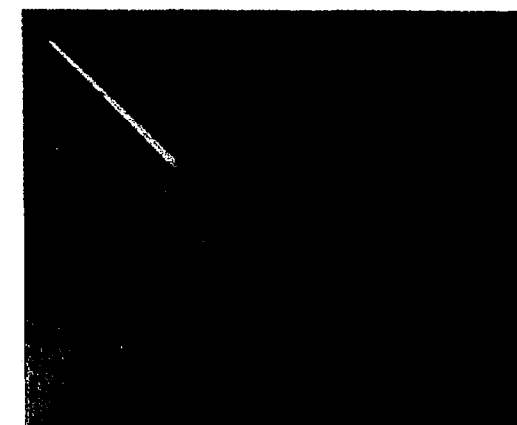
VORTILET NO. 2 WITH
SHORTENED KRUEGER FLAP



INBOARD VIEW OF
VORTILET NO. 1



VORTILET NO. 2 WITH MOD 6



VORTILET NO. 2 WITH
SHORTENED KRUEGER FLAP

FIGURE 48. BASIC WINGLET CONFIGURATIONS WITH VORTILETS

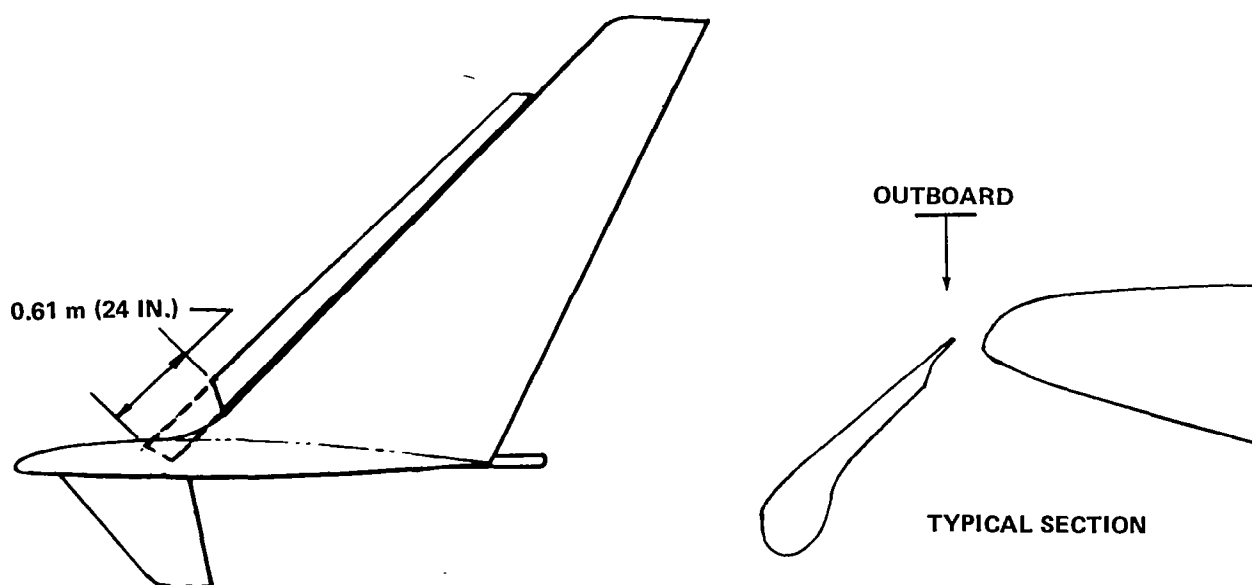


FIGURE 49. LEADING EDGE KRUEGER FLAP GEOMETRY FOR BASIC UPPER WINGLET

- Configuration 7: Configuration 8 with the lower winglet installed.
- Configuration 9: Configuration 1 without the lower winglet.
- Configuration 10: Configuration 1 but with the addition of Vortilet Number 2 and Winglet Airfoil Modification Number 6 (MOD 6). Vortilet Number 2 was an upper winglet leading edge dorsal fin which originated at the aft edge of the wing tip forward light lens and extended to a point on the upper winglet leading edge which was 38 percent of the winglet span above the winglet root. It was fabricated of fiberglass and foam over a metal plate "backbone." The leading edge radius was approximately 1.4 cm (0.75 in.) and the sides were contoured to blend smoothly at its junction with the winglet. MOD 6, which was selected from a number of alternatives, was a modification to the leading edge region of the basic winglet airfoil. The leading edge radius was increased from 0.5 to 1.5 percent chord. The modification was achieved by fitting a foam and fiberglass glove to the existing winglet. The glove extended from the most upward edge of Vortilet Number 2 to the winglet tip. The glove extended from the leading edge aft to 0.4-percent chord on the upper surface and to 31.6-percent chord on the lower surface.
- Configuration 11: Configuration 10 without the lower winglet.
- Configuration 12: Configuration 10 with MOD 6 removed and the Krueger flap installed above the vortilet.

As the program progressed, it became clear that the eventual configuration should attempt to balance or resolve two characteristics of the original BWL which were in apparent conflict —

first, that the lower winglet was beneficial in improving cruise performance; second, that the lower winglet adversely contributed to the low-speed buffet. This investigation was continued into the RSWL phase.

Flutter — Frequency and damping data from the flutter tests of Configuration 1 are shown in Figures 50 and 51 for the 3-Hz and 4.5-Hz modes respectively. The figures also include the analytical predictions and are for the flutter-critical condition (see Figure 20) of 12.5-percent fuel at 7 163 km (23,500 ft) with symmetric excitation.

The test results show the frequency and damping of both modes to be relatively constant over the test speed range from 0.70 to 0.91 Mach number. There is no loss of damping as 0.91 Mach number is approached. The test conditions of 12.5-percent fuel at 9 144 km (30,000 ft) and 15 876-kg (35,000-lb) fuel at 7 163 km (23,500 ft) showed similar trends and damping levels for symmetric excitation. The antisymmetric excitation conditions were more highly damped than the symmetric conditions by 1.5 to 2 percent C/C_c for these test configurations.

The predicted subcritical flight frequencies closely match the measured frequencies for both the 3-Hz and 4.5-Hz modes. For the 3-Hz mode, the predicted damping, although generally in good agreement with that measured, was slightly lower than the measured damping at the

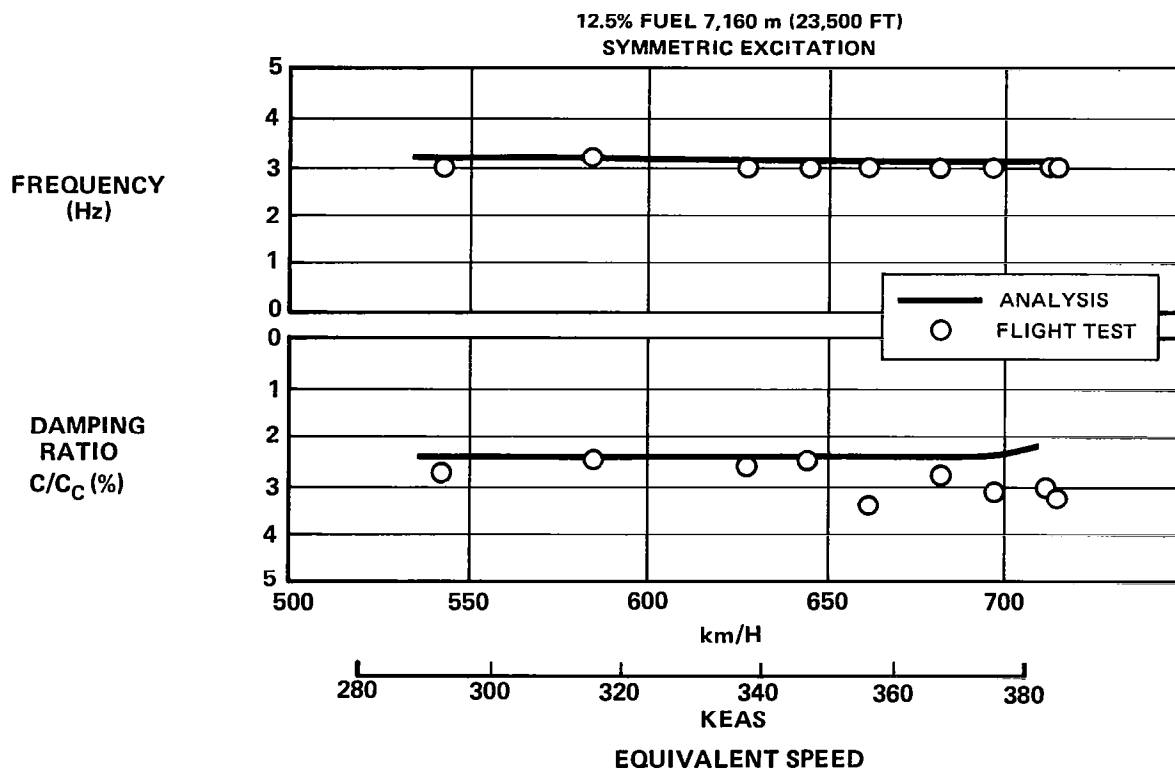


FIGURE 50. FREQUENCY AND DAMPING CHARACTERISTICS – 3Hz MODE
(DETERMINED FROM WING TIP NORMAL ACCELERATION)

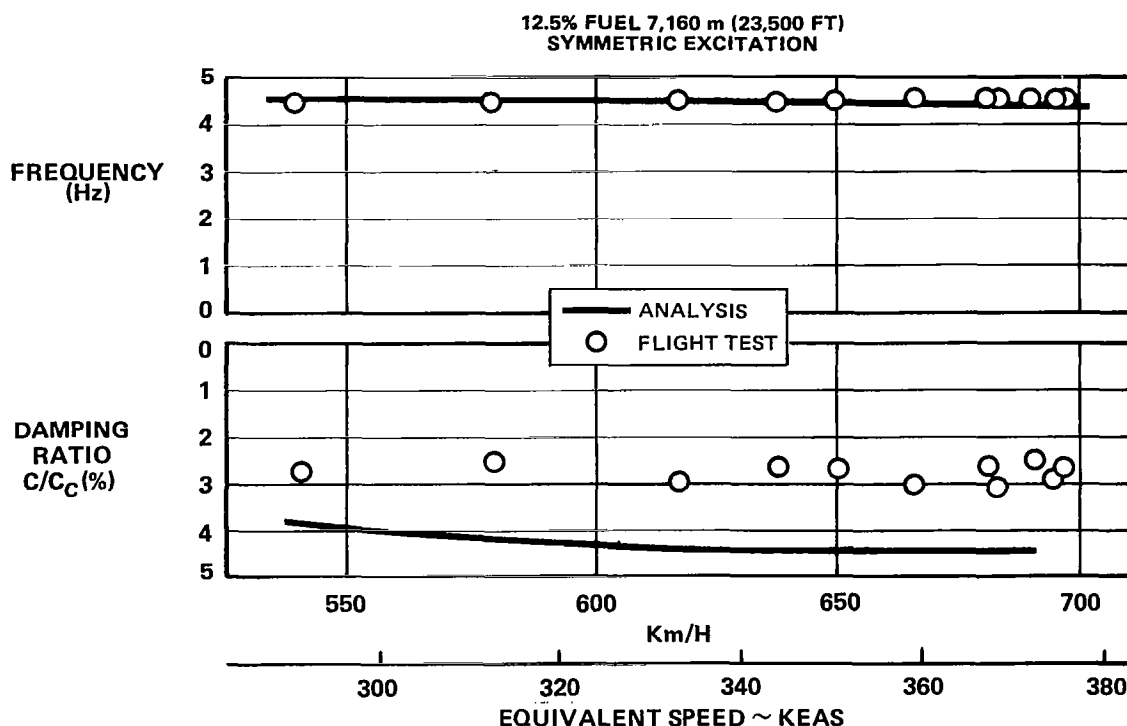


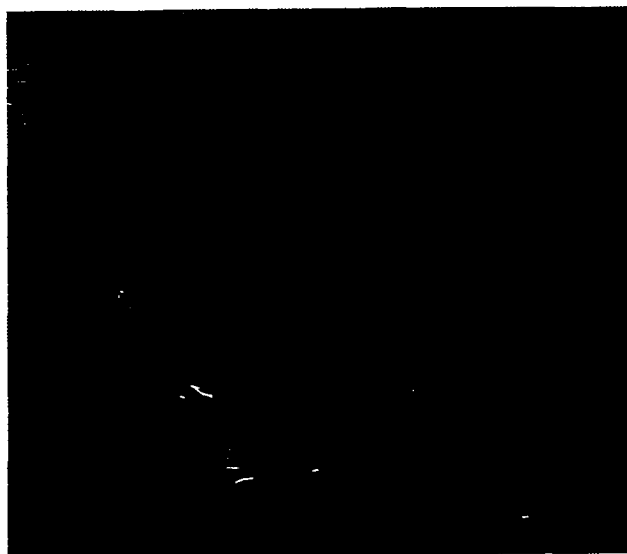
FIGURE 51. FREQUENCY AND DAMPING CHARACTERISTICS – 4.5 Hz MODE
(DETERMINED FROM WINGLET LONGITUDINAL ACCELERATION)

higher Mach numbers, and was therefore conservative. For the 4.5-Hz mode, the predicted damping was higher than that measured by approximately 1.5 percent C/C_c , and was therefore unconservative.

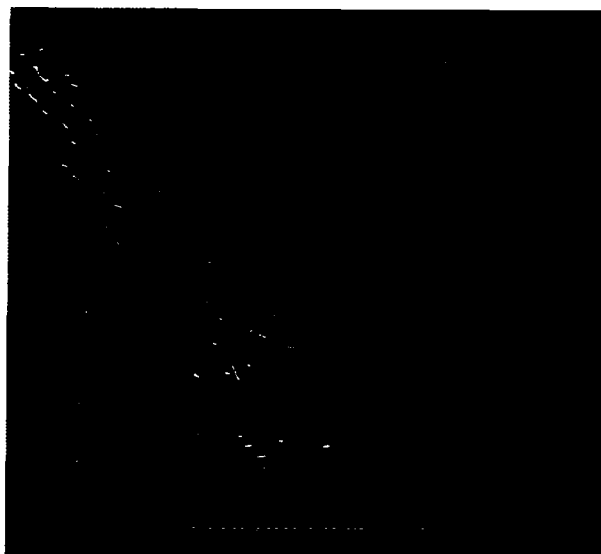
The effect on the flutter speed of the 4.5-Hz mode due to the 1.5-percent C/C_c difference between predicted and measured damping was estimated by reducing the predicted damping of the 4.5-Hz mode by 1.5-percent C/C_c over the entire speed range and calculating the new flutter speed. This resulted in a 1.5-percent reduction in flutter speed. However, the reduced flutter speed was still above $1.2 V_D$.

These data show good correlation with the predicted results discussed previously in relation to Figure 20. The prediction method is considered verified by the data for design purposes, particularly since the methodology, applied to the critical mode, is slightly conservative.

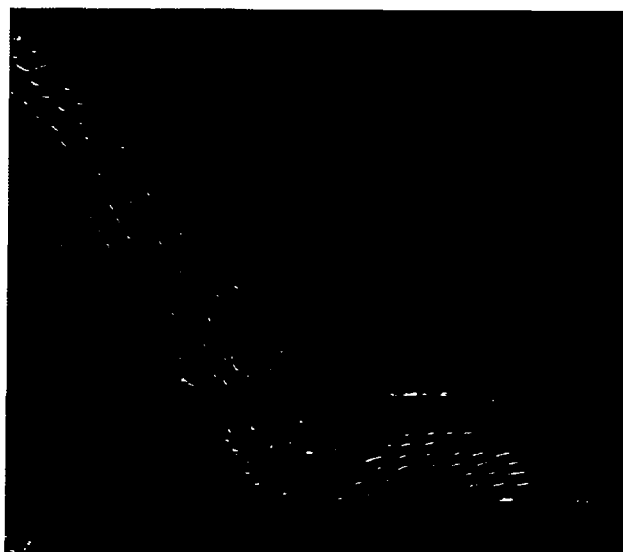
Low-Speed Buffet — The first flight (A-17) after the flutter program was dedicated to flow visualization and buffet evaluation of the BWL, Configuration No. 1. An early assessment of any potential low-speed problem was desired, particularly since the wind tunnel investigations (Reference 4) had indicated the possibility of flow separation prior to wing stall. Figure 52 illustrates the flow separation experienced in the wind tunnel. For angles of attack below the



$\alpha = 9 \text{ DEGREES } (< \alpha_{V_2})$



$\alpha = 13 \text{ DEGREES } (\cong \alpha_{V_2})$



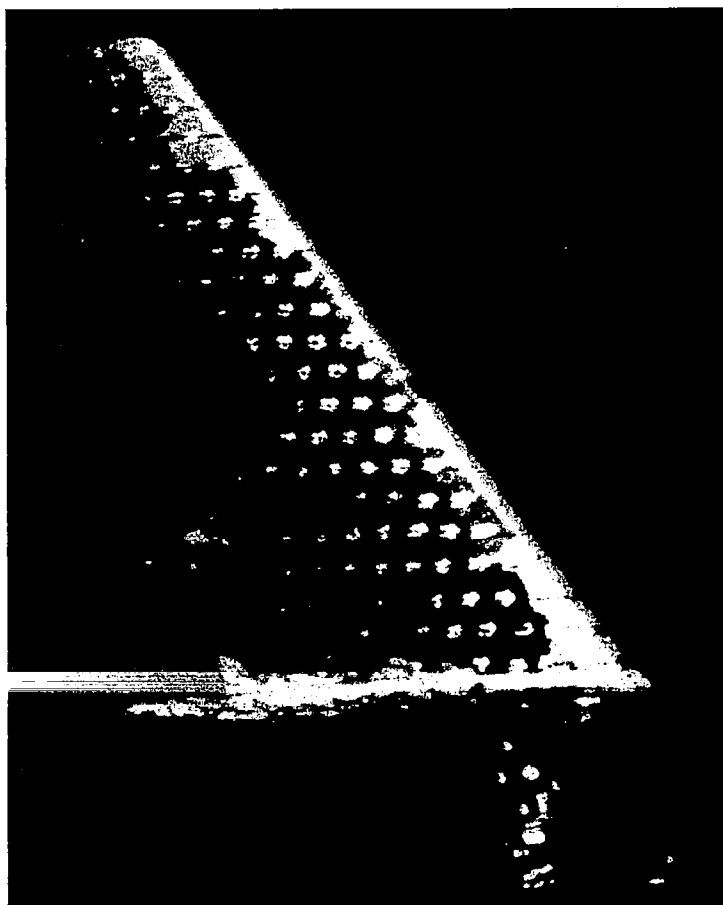
$\alpha = 15 \text{ DEGREES } (> \alpha_{V_2})$

FIGURE 52. WINGLET FLOW AT LOW SPEED IN THE AMES 12-FOOT WIND TUNNEL

critical takeoff condition, $1.2 V_{\text{MIN}}$, the flow is streamwise on both the wing and winglet except for local spanwise flow at the winglet trailing edge. At the $1.2 V_{\text{MIN}}$ condition, significant spanwise flow has developed. Beyond the V_2 condition but prior to stall, the flow on the winglet and locally on the wing has separated.

During the flight tests, buffet occurred at the critical takeoff and landing conditions of $1.2 V_{\text{MIN}}$ and $1.3 V_{\text{MIN}}$, respectively. Flow visualization observations made from the DC-10 cabin and

a chase aircraft indicated that the buffet corresponded to a completely separated flow on the suction side of both the upper and lower winglets. The flow separation developed gradually. At lifting conditions corresponding to $1.5 V_{MIN}$ where there was no buffet, the upper winglet had no separated flow (see Figure 53) although the flow on the lower winglet was about 70-percent separated. As the flight speed was reduced, flow separation migrated from the lower winglet into the root region of the upper winglet; the flow separation on the upper winglet got progressively worse until at $1.2 V_{MIN}$ an unacceptable buffet was felt in the cockpit. The buffet was characterized by a strong vertical bounce component which, according to the pilot, would make the airplane uncertifiable. The extent of the flow separation at $1.2 V_{MIN}$ is shown in the photographs of Figures 54 and 55. The flow patterns shown are similar to those obtained in the wind tunnel tests, except that the separation occurred in the wind tunnel at higher lift coefficients.

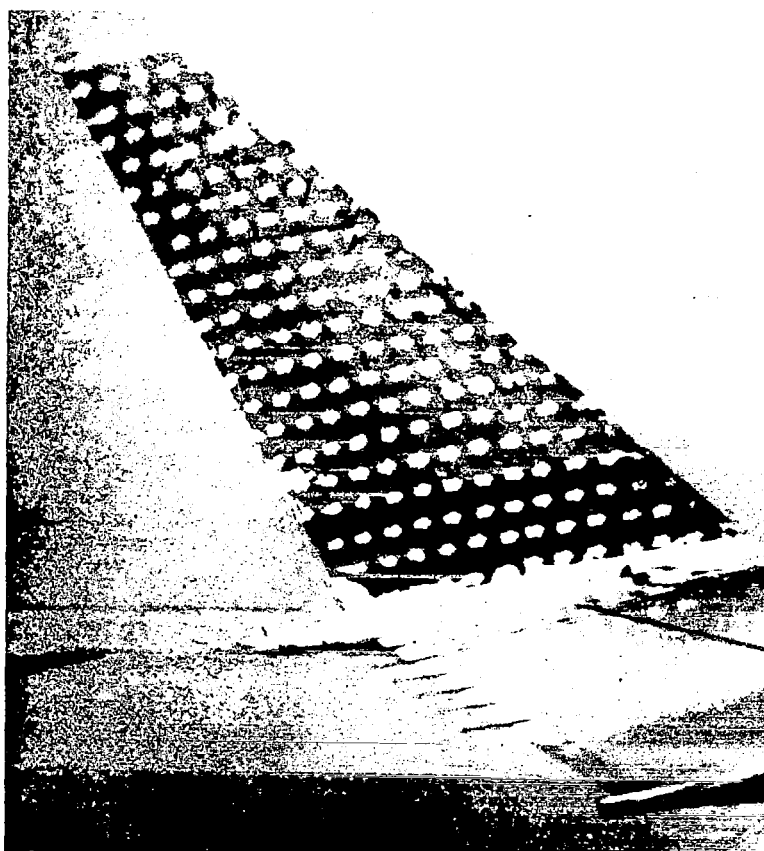


CONFIGURATION

- BASIC UPPER WINGLET WITH LOWER WINGLET
- NO LEADING-EDGE DEVICE
- $\delta_F = 15 \text{ DEG}$
- $\delta_F = \text{TAKEOFF}$

WINGLET FLOW ATTACHED
NO BUFFET

FIGURE 53. WINGLET FLOW IN LOW-SPEED FLIGHT — INBOARD (SUCTION) SIDE,
 $C_L = 0.96, V/V_{S_{MIN}} = 1.5$



CONFIGURATION

- BASIC UPPER WINGLET WITH LOWER WINGLET
- NO LEADING-EDGE DEVICE
- $\delta_F = 15 \text{ DEG}$
- $\delta_S = \text{TAKEOFF}$

WINGLET FLOW SEPARATED.
SEPARATION CARRIES OVER TO
WING TIP – MODERATE BUFFET

FIGURE 54. WINGLET FLOW IN LOW SPEED FLIGHT – INBOARD (SUCTION) SIDE,
 $C_L = 1.5$, $V/V_{S_{MIN}} = 1.2$

As a result of the findings from this flight, an extensive effort was undertaken to find a configuration with acceptable buffet characteristics. Since characteristics of buffet and flow separation did not appear to depend on the configuration of flaps and slats, the investigation was restricted mainly to the configuration having 15-degree flaps and slats extended in the takeoff position.

Figure 56 provides a summary of the configurations for which buffet and flow separation were observed. The first two rows on the chart provide pilot's comments on the buffet levels for the speed conditions corresponding to an all-engine takeoff ($1.35 V_{MIN}$) and an engine-out takeoff ($1.2 V_{MIN}$). The third row provides the pilot's comments regarding the presence of the objectionable vertical bounce component in the buffet. The fourth row presents sketches of the flow visualization observed on the suction side of the upper and lower winglets at the $1.2 V_{MIN}$ condition. The last row of the chart presents the peak-to-peak acceleration measured at the pilot's seat for each of the configurations. The consensus on the meaning of these measurements and their correlation with the flight experience was used to develop criteria for acceptability which is summarized in Figure 57. The instrumentation system has an approximate 0.03g peak-to-peak

CONFIGURATION

- BASIC UPPER WINGLET WITH LOWER WINGLET
- NO LEADING EDGE DEVICE
- $\delta_F = 15 \text{ DEG}$
- $\delta_S = \text{TAKEOFF DEVICE}$

UPPER WINGLET ATTACHED,
LOWER WINGLET SEPARATED –
MODERATE BUFFET

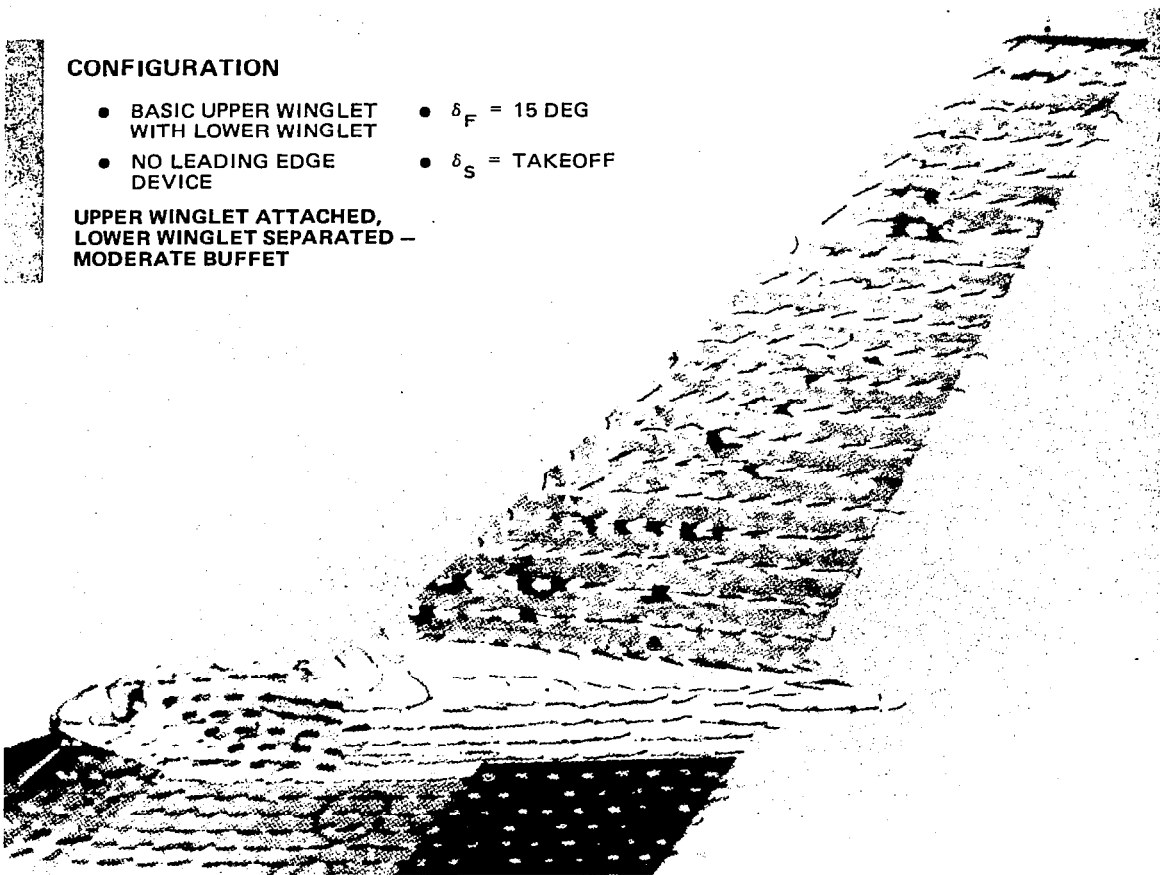
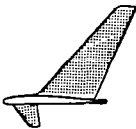

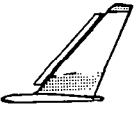

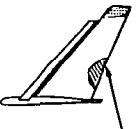

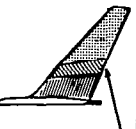
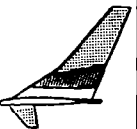
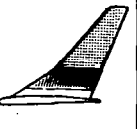



FIGURE 55. WINGLET FLOW IN LOW SPEED FLIGHT – OUTBOARD (PRESSURE) SIDE,
 $C_L = 1.5, V/V_{S_{MIN}} = 1.2$

noise level. Evaluation of the aircraft buffet characteristics without winglets indicated that they were in the normal range. The range of potentially acceptable configurations is from 0.03 to 0.06g depending on buffet intensity changes caused by small angle-of-attack changes and on changes with normal maneuvering. The closer to 0.03, the higher the confidence level of acceptability. The presence of a pronounced vertical bounce component was deemed unacceptable.

The first attempt to eliminate the buffet problem was to install the Krueger flap that had been fabricated as a result of the wind tunnel findings. As can be seen from Figure 56 for Configuration 2, the character of the flow was significantly different, but the buffet character remained unchanged. Next, the lower winglet was removed because it was clear from the flow visualization that the separated flow wake from the lower winglet was migrating into the root section of the upper winglet. With this configuration (Number 3), the buffet onset was delayed to a higher lift coefficient, but the level of buffet at $1.2 V_{MIN}$ was basically unchanged.

$\delta_F = 15 \text{ DEGREES}$ $\delta_S = \text{TAKEOFF}$

CONFIGURATION NUMBER	1	2	3	4	6	7	9	10	11	12
CONFIGURATION DESCRIPTION	BASIC UPPER AND LOWER WL	UPPER AND LOWER WL WITH FCK	UPPER WL WITH FCK	UPPER WL AND FCK AND VORTI	UPPER WL AND FCK EXT	UPPER AND LOWER WL AND FCK EXT	UPPER WL ONLY	VORT 2 WITH MOD 6 AND LOWER WL	VORT 2 WITH MOD 6 W/O LOWER WL	VORT 2 WITH FCK AND LOWER WL
FLIGHT	A-17	A-27	A-28	A-29	A-31	A-32	A-44/A-45	A-47	A-48	A-49
BUFFET AT 1.35 V _{MIN}	LIGHT	LIGHT	VERY LIGHT	VERY LIGHT	NONE	PERCEPTIBLE	PERCEPTIBLE	LIGHT	LIGHT	LIGHT
BUFFET AT 1.20 V _{MIN}	MODERATE	MODERATE	MODERATE	MODERATE	LIGHT	MODERATE	LIGHT	MODERATE	MODERATE	MODERATE
VERTICAL BOUNCE AT 1.20 V _{MIN}	YES	YES	YES	YES	BARELY	YES	JUST BARELY	BARELY	BARELY	NO (LATERAL COMPONENT)
WING FLOW VISUALIZATION	SEPARATED	SEPARATED	SEPARATED	ATTACHED	ATTACHED	SEPARATED	ATTACHED	ATTACHED	ATTACHED	ATTACHED
WINGLET FLOW VISUALIZATION AT 1.20 V _{MIN}										
					INTERMITTENT SEPARATION	NO CHASE	INTERMITTENT SEPARATION			NO CHASE
PILOT SEAT ACCELERATION AT V = 1.20 V _{MIN} (PEAK TO PEAK)	0.080	0.200	0.175	0.170	0.045	0.150	0.060	INSTRUMENTATION INOPERATIVE	INSTRUMENTATION INOPERATIVE	0.125

ATTACHED
STREAMWISE
FLOWSEPARATED
FLOWSPANWISE
FLOWINTERMITTENT
SEPARATIONFLOW VISUALIZATION SHOWN ON THE INBOARD SURFACE OF UPPER WINGLET AND
OUTBOARD SURFACE OF LOWER WINGLETFIGURE 56. SUMMARY OF LOW-SPEED BUFFET
CHARACTERISTICS - BASIC WINGLET

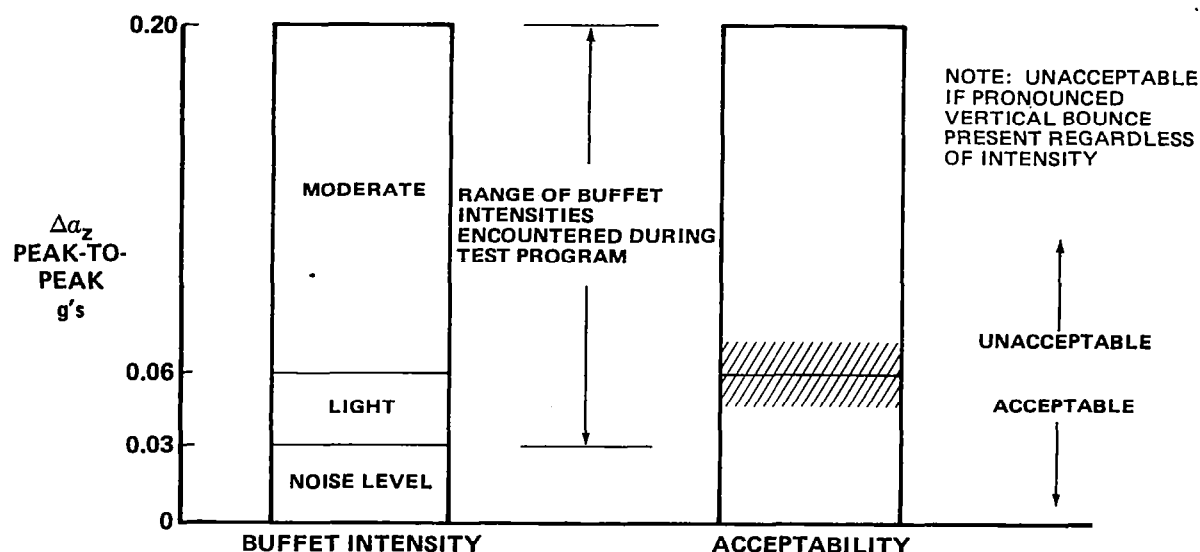


FIGURE 57. WINGLET LOW-SPEED BUFFET - ACCEPTABILITY CRITERIA

At this point it appeared that the problem was being controlled by the root and that the separated flow was washing out onto the wing thus contributing to the vertical bounce component. In order to relieve the root loading and to generate some vortex flow to help clean up the separation, a highly swept dorsal (denoted as Vortilet 1) was added to the unprotected root region (Configuration 4). The buffet levels, as well as the amount of separated flow, were reduced but the configuration was still unacceptable.

Recognizing the importance of the root region, it was decided to remove the vortilet and extend the leading edge device down to the wing. This resulted in an acceptable configuration (Number 6). The flow was basically attached except for the small region at the tip which was not protected since the Krueger was not full span. The buffet intensity was significantly reduced, with the vertical bounce component barely perceptible. Figure 58 presents the effect of the Krueger flap on the section loading at 57 percent of the winglet span. It shows that without the Krueger there was separated flow over most of the chord, but with the Krueger there was essentially no separation. From the winglet section lift it is clear that the Krueger flap allows the winglet to continue to load up as the airplane lift increases to the V_2 condition. Analysis of the other section data yields similar results.

Because the presence of the lower winglet is important from cruise performance considerations, it was reinstalled and the resulting configuration (Number 7) tested. The problem of the migration of the separated flow on the lower winglet into the upper winglet root region apparently reoccurred because this configuration proved unacceptable.

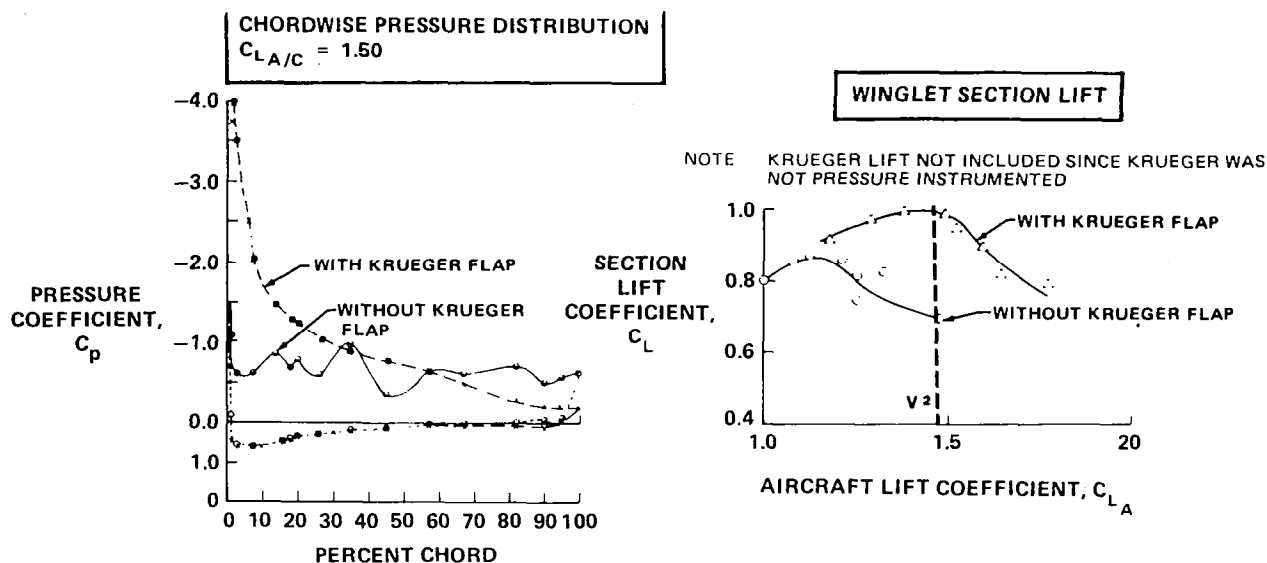


FIGURE 58. EFFECT OF WINGLET KRUEGER FLAP ON WINGLET SECTION LOADING ($\eta = 57\%$)

Both the Krueger flap and lower winglet were removed for a cruise flight and the buffet characteristics evaluated. The final analysis of the buffet for this configuration (Number 9) showed it to be acceptable, but the flow on the winglet was still separated over 75 percent of the span. This separation was shown to result in a significant reduction in the drag improvement due to the winglet.

In order to evaluate further the potential for an acceptable configuration without a leading edge device, an alternate planform with modified airfoil leading edges was evaluated. The airfoil modification was developed analytically and the airfoil/planform change was evaluated in a concurrent Douglas low Reynolds number wind tunnel test on another transport configuration. The results indicated that the winglet remained separation-free down to the wing stall and thus was a good candidate for flight evaluation. As shown earlier in Figure 56, three variations of this configuration were evaluated. The highly swept dorsal effected an attached flow area inboard with significant spanwise flow but the flow on the outboard panel remained separated. Installing the leading edge device on the outboard panel with the original airfoil shape prevented the flow from separating outboard but resulted in a very complicated three-dimensional flow pattern inboard with significant areas of local flow separation. With the gradients relieved in one area degraded flow resulted in another area. None of the three configuration variations evaluated produced an acceptable configuration.

In summary, of all the basic winglet configurations evaluated for low-speed buffet characteristics, two (Numbers 6 and 9) were considered to be acceptable. Both had the lower winglet removed and one had a Krueger leading edge device extended to the winglet root on the

upper winglet. The implications of the lower winglet removal on high- and low-speed performance benefits for winglets will be discussed in subsequent sections.

Low-Speed Drag — Although the primary emphasis for the application of winglets has been the reduction of cruise drag, a substantial drag reduction in takeoff and approach has also been found through analytical estimates and wind tunnel investigations (Reference 3). Figure 59 shows the low-speed drag improvement of the flight-tested BWL having an extended Krueger leading edge flap and no lower winglet (Configuration 6). The figure includes the drag reduction for the winglet aircraft relative to the baseline for two representative takeoff flap settings compared with values obtained from wind tunnel investigations (Reference 4). It should be noted that while the flight-tested drag increment for the 15-degrees flap deflection was obtained by direct comparison with the baseline aircraft, no baseline data were collected for a similar comparison at the zero-degree flap setting. Therefore, a baseline zero-degree-flap drag level was developed by adjusting the existing DC-10 performance manual drag polar by the variation between the manual level and measured drag values obtained during the baseline test phase for the 15-degrees flap setting.

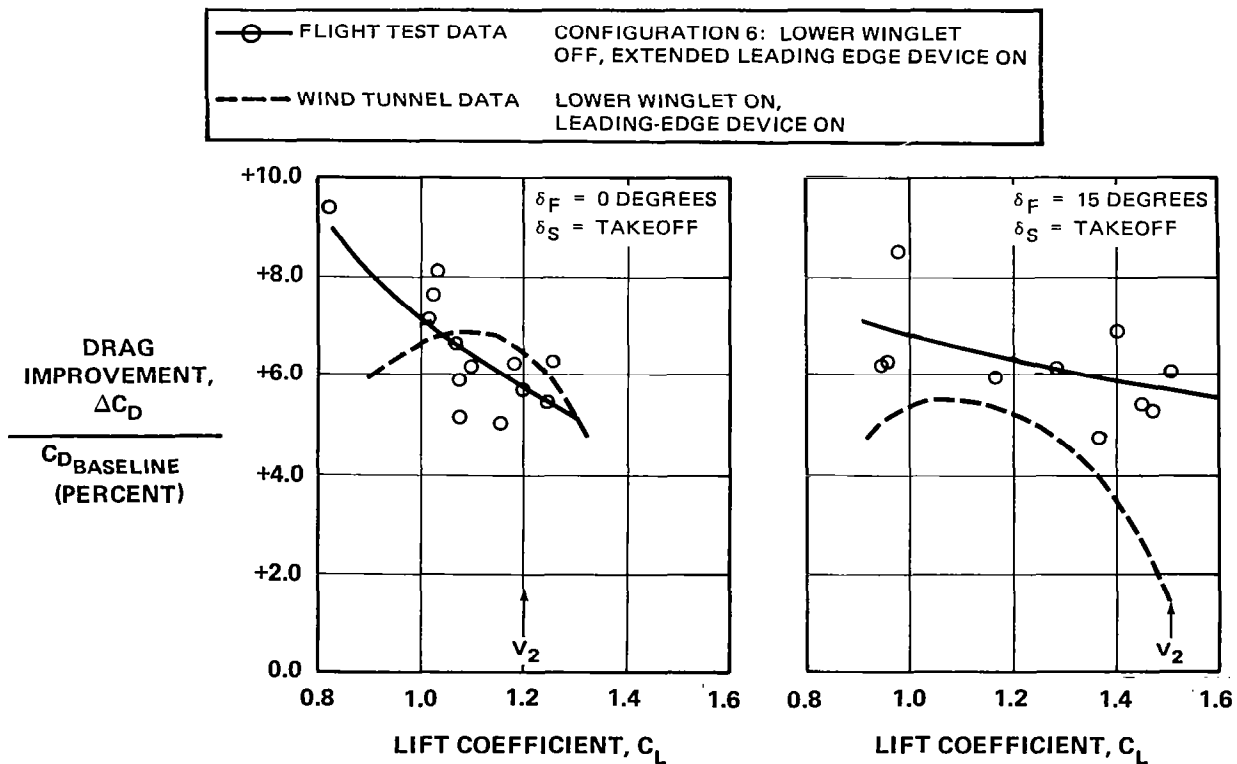


FIGURE 59. LOW SPEED DRAG IMPROVEMENT – BASIC WINGLET

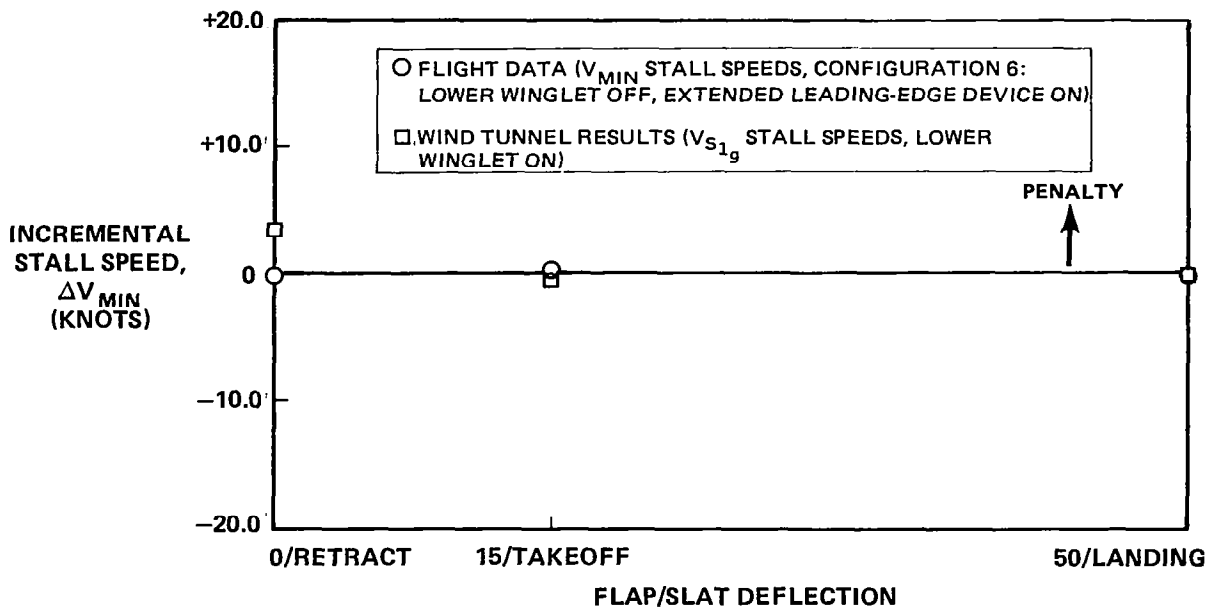


FIGURE 60. EFFECT OF WINGLET ON MINIMUM STALL SPEED

The fairing through the flight test data points represents the difference between fairings of the winglet and baseline drag polars. At the lift coefficient representative of engine-out climb speed (V_2), the winglet drag improvement is 5.7 percent at both zero- and 15-degrees flap deflection. These values equal or exceed pretest estimates based on wind tunnel data. It should be noted that the wind tunnel data given include the effect of the lower winglet. However, the wind tunnel investigation indicated a drag penalty for the leading edge device whereas in flight the leading edge device effected a marked improvement in the flow separation characteristics of the upper winglet.

Stall Speeds and Characteristics — Stall speeds were determined for three flap settings during both the baseline and winglet test program phases. The minimum stall speeds were determined by performing a series of stalls at different deceleration rates and interpolating to determine the minimum speed with a 0.51 m/s^2 (1.0 kt/sec) deceleration (FAA requirement). A comparison of the incremental V_{MIN} stall speeds between the BWL-equipped and baseline aircraft is presented in Figure 60. Also shown are speed increments based on maximum lift coefficients obtained during wind tunnel studies (Reference 4). The wind tunnel increments correspond to $1g$ stall speeds since deceleration cannot be simulated in the wind tunnel. It is evident from the figure data that the aircraft stall speeds are essentially unaffected by the presence of winglets, and that these results are in excellent agreement with the wind tunnel results. It is concluded — on the basis of this correlation for the basic winglet and on wind tunnel results for the reduced-span winglet — that the reduced-span configuration similarly would not affect stall speeds.

Stall characteristic tests were conducted on the aircraft with the basic winglets installed. Stall characteristics were examined at an aft cg in the following flap/slat configurations: 0/Retract, 0/Takeoff, 15/Takeoff, 22/Takeoff, and 50/Landing with the landing gear extended. All stalls were accomplished in straight flight with symmetric idle power. The entry rates during these tests varied between 0.26 m/s^2 (0.5 kt/sec) and 1.0 m/s^2 (2.0 kt/sec).

Positive and adequate control about all axes was maintained up to the stall and through the recovery from the stall. No unsatisfactory characteristics were recorded or reported by the flight crew.

Cruise Performance — The cruise performance improvement was determined from both the measured drag coefficient as determined from engine fan speed (N_1) and from range factor as determined from aircraft weight, speed, and measured fuel flow. In order to evaluate the range factor, an engine fuel flow analysis was required to determine if any engine deterioration occurred during the test program of nearly 200 flight hours. Only small adjustments were found to be necessary.

Figure 61 shows the correlation of the cruise performance benefit as measured by drag coefficient (determined from N_1) and by range factor with the BWL and RSWL. These data are for a Mach number range from 0.8 to 0.85. Excellent correlation is seen. For this report, the cruise performance benefit for winglets is presented as incremental drag coefficient relative to the baseline aircraft without winglets. However, it can be concluded that these benefits are synonymous with either a drag or range factor measurement.

All commercial transports step-climb by cruising at constant altitudes and then stepping to higher altitudes as fuel is burned off in order to operate near the maximum lift-to-drag ratio. As such, they have to operate over a range of lift coefficients. For the Series 10 intermediate range version of the DC-10, typical cruise lift coefficients vary from about 0.42 to 0.5 with 0.47 being a representative average. Normal cruise Mach number is from 0.82 to 0.83. The test aircraft was flown over a W/δ and Mach number range in order to adequately define its characteristics over this envelope. In addition, since the winglet is a device to improve the induced drag, an incompressible drag polar was also flown ($0.5 < M < 0.65$) for the baseline and each winglet configuration that was tested for cruise performance. This was done in order to determine whether the winglet would exhibit any compressibility effects.

Figure 62 summarizes the cruise drag improvement for the basic winglet, giving the percent drag improvement relative to the baseline airplane without winglets. Since the lower winglet was shown to be a major contributor to the low-speed buffet in the takeoff configuration, and was found in wind tunnel tests to reduce cruise drag 0.5 percent, it was removed to evaluate its effect on the cruise performance. The figure shows the measured drag improvement with and

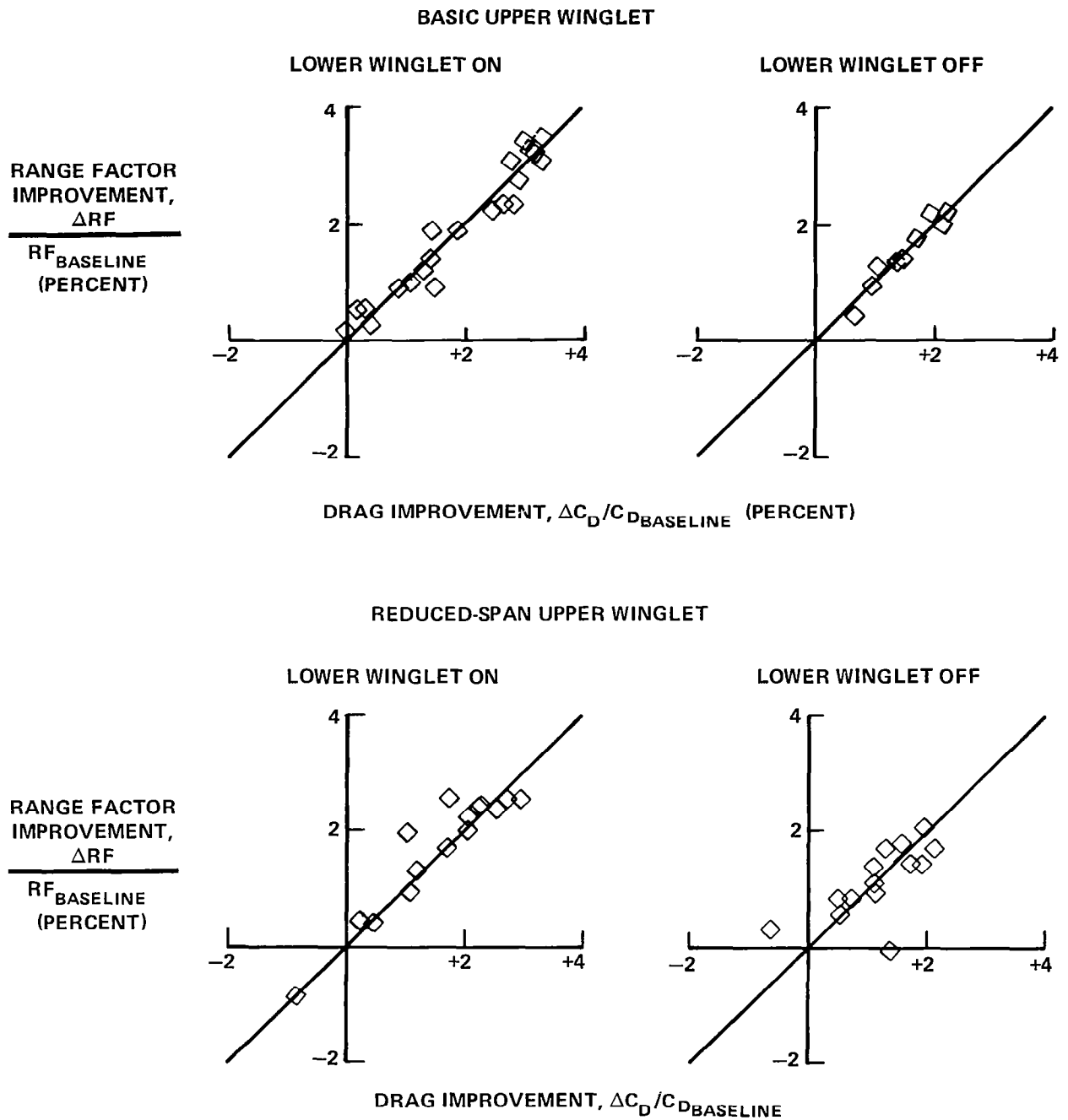


FIGURE 61. CORRELATION OF MEASURED RANGE FACTOR AND DRAG IMPROVEMENTS FOR THE BWL AND RSWL ($0.80 \leq M \leq 0.85$)

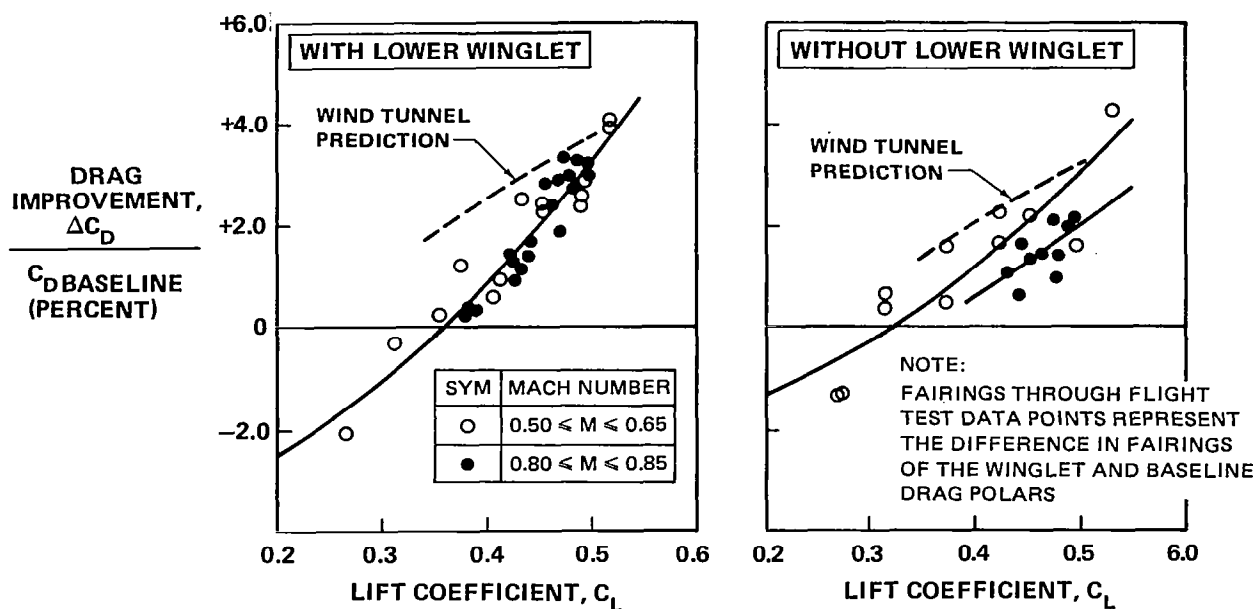


FIGURE 62. CRUISE DRAG IMPROVEMENT – BASIC WINGLET

without the lower winglet installed. Also shown is the wind tunnel prediction based on Reference 2 but adjusted for wing aeroelastic effects. It should also be noted that the analytical prediction using a nonplanar vortex lattice method is also in good agreement with the wind tunnel prediction.

With the lower winglet installed (left side of Figure 62), the flight-measured level was about 0.4 percent less than the prediction at the highest lift coefficient of DC-10 Series 10 operation ($C_L = 0.5$). At lower lift coefficients the discrepancy was greater suggesting a significant parasite drag penalty at zero lift. At $C_L = 0.47$, which is an average cruise condition for the DC-10 Series 10, the measured improvement was 2.5 percent compared to a predicted 3.4 percent (75 percent of prediction). The data for the lower winglet installed would also suggest that whatever is causing the shortfall is probably not related to compressibility effects because the compressible and incompressible data are in good agreement. Results with the lower winglet removed, however, suggest that this conclusion may be fortuitous.

The effect of removing the lower winglet is illustrated on the right side of Figure 62. At incompressible Mach numbers, the improvement is about the same as with the lower winglet installed, but at cruise Mach numbers there appears to be a significant compressibility penalty and at $C_L = 0.47$ the improvement is reduced to 1.5 percent. The benefit of the lower winglet measured in the wind tunnel was about 0.5 percent (also in agreement with vortex lattice calculations). The flight data suggest that this benefit is considerably larger (1 percent at $C_L = 0.47$, $M = 0.82$) and is related to compressibility effects.

Figures 63 through 65 present tuft photographs at cruise conditions ($M = 0.82$) for the suction surface (inboard) and pressure surface (outboard) of the upper winglet and the suction surface (outboard) of the lower winglet. The flow quality was excellent with no indications of large spanwise flow areas or areas of flow separation.

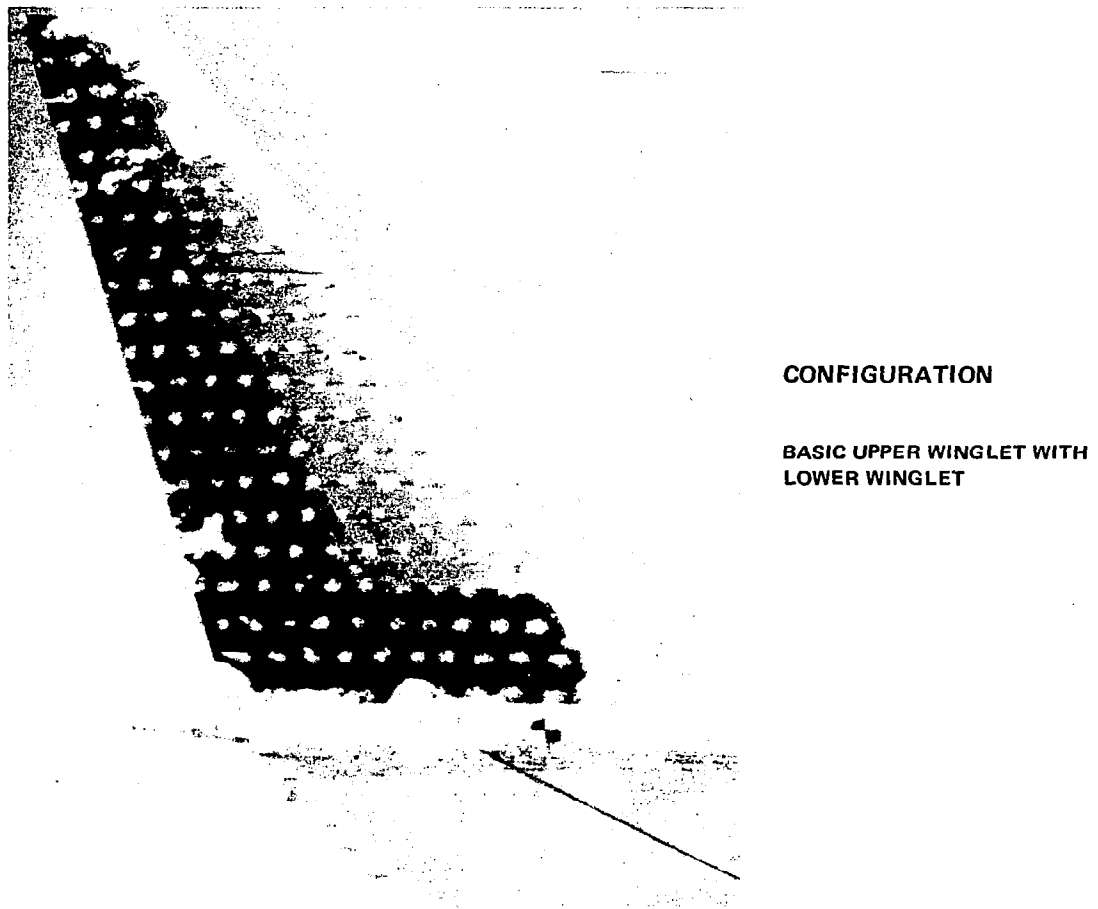
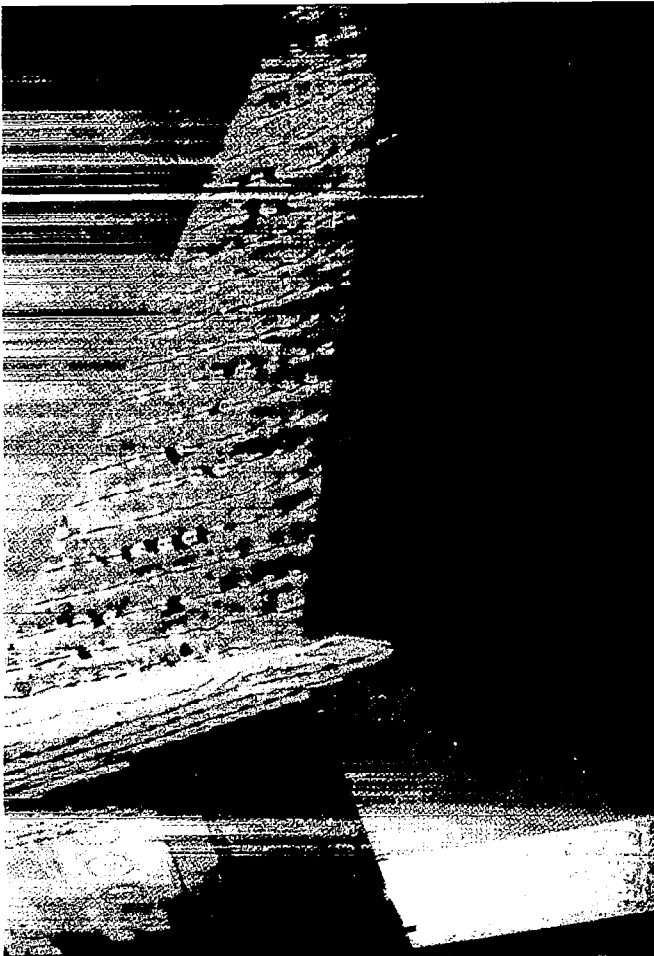


FIGURE 63. UPPER WINGLET FLOW IN CRUISE FLIGHT – INBOARD (SUCTION) SIDE

To try to explain the apparent performance shortfall at the lower lift coefficients, the effects of the winglets on wing deflection and twist were examined. Before the flight tests, the wing twist was estimated for $M = 0.82$ and $C_L = 0.45$. The calculations showed the twist increased from zero degrees at about the wing Yehudi break to about 0.35 degree at the wingtip. Vortex lattice calculations showed this amount of twist would increase the induced drag of the airplane by about 0.4 percent. The dashed line of Figure 62, labeled wind tunnel prediction, incorporates



CONFIGURATION

BASIC UPPER WINGLET WITH
LOWER WINGLET

FIGURE 64. UPPER WINGLET FLOW IN CRUISE FLIGHT – OUTBOARD (PRESSURE) SIDE,
 $M = 0.82$

this adjustment, i.e., the rigid-wing wind tunnel improvement was reduced by 0.4 percent at all lift coefficients. For the evaluation aircraft, wing bending and twist deflection were estimated* in order to determine the incremental wing twist resulting from the winglets. It was concluded that the derived wing deflections were in reasonable agreement with the preflight estimate. Further, these data were evaluated over a lift coefficient range from 0.3 to 0.5 at incompressible Mach numbers and C_L from 0.4 to 0.5 at compressible Mach numbers. The winglets were found to have essentially the same incremental twist independent of lift coefficient or Mach number. This would seem to rule out aeroelastic effects as a contributor to the shortfall or trend with lift coefficient.

*Although instrumentation had been provided for the photographic recording of wing deflections, the flight-measured data contained anomalies. The estimations referred to were therefore made using other data from the flight program, namely information from the performance flights and loads programs. After the flight program was completed, a test of the camera and wing target system was conducted on a DC-10 on the ground. The test was run because it had been suggested that fuselage pressurization could have caused the cabin window used for camera observation to act as a distorting lens. The results of the test confirmed the suggestion, and it is therefore concluded that the flight camera records are unusable.

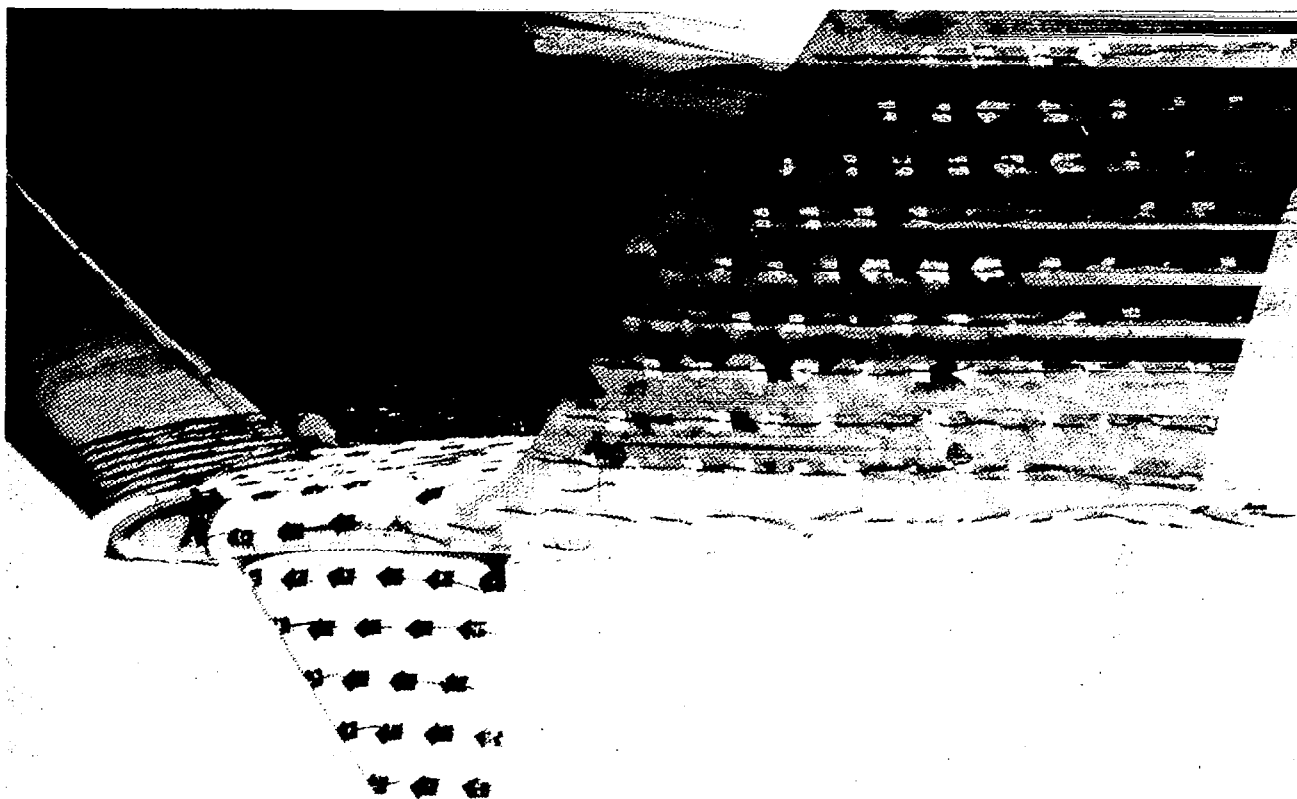


FIGURE 65. LOWER WINGLET FLOW IN CRUISE FLIGHT – OUTBOARD (SUCTION) SIDE

Figure 66 shows the measured pressure distribution at three winglet stations for 0.82 Mach number and 0.5 lift coefficient with the lower winglet on. It can be seen that a significant leading edge suction peak is present resulting in a fairly strong shock wave, particularly on the winglet outer span. While the pressure distribution at the 12.5-percent station is in reasonably good agreement with the wind tunnel measurements, at the 80-percent station the shock appears to be significantly stronger, both in peak Mach number and in the magnitude of the compression. These stronger shocks may be adversely affecting cruise performance of the winglet. However, referring to Figure 62, this is the very condition where the measured benefit is closest to the prediction. Clearly, there may be compensating effects in the nature of the improvement characteristics, e.g., shock losses being offset by the induced drag improvement due to the higher winglet loading.

The trailing edge recompressions do not indicate a flow separation except possibly at the 95-percent span station where the trailing edge does not recompress as well as at the other stations. There was no evidence of flow separation from the in-flight cruise tuft surveys.

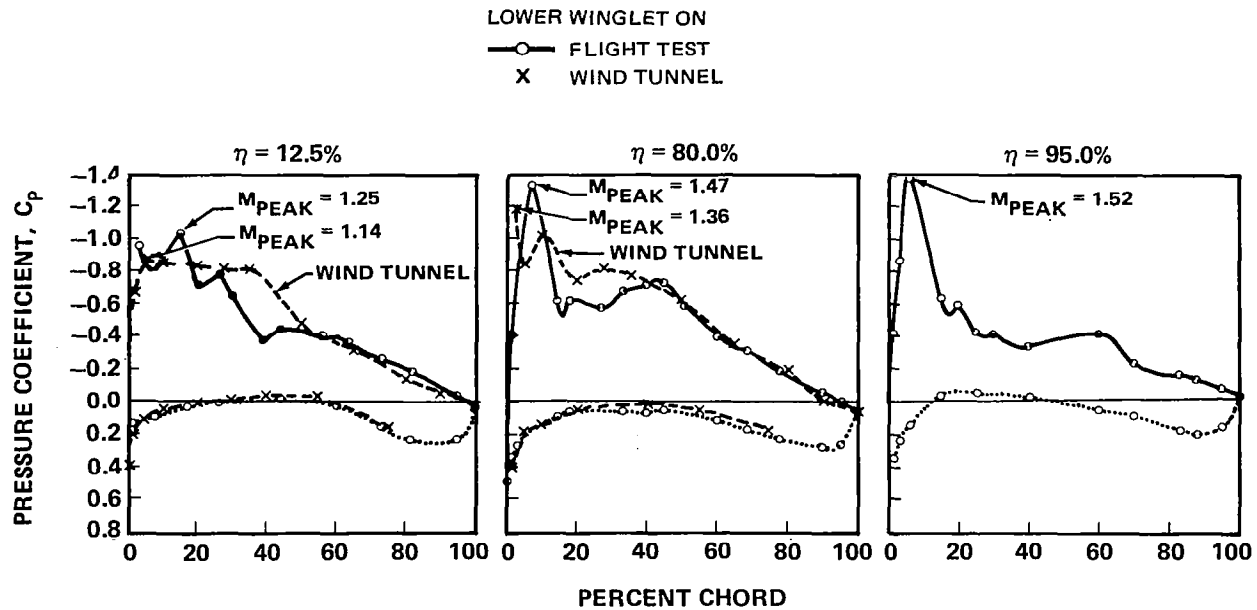


FIGURE 66. BASIC WINGLET PRESSURE DISTRIBUTION AT CRUISE

Figures 67 through 69 show the variations of winglet pressure distributions with lift coefficient for winglet spanwise stations of 12.5, 80.0, and 95.0 percent. The stronger shock wave on the outer panel is also evident at the lower lift coefficients; however, it does not appear to be any stronger relative to the wind tunnel value than was measured at higher lift coefficients. These results suggest that at least part of the performance shortfall may be related to compressibility effects but that the trend with lift coefficient is not.

The upper winglet pressure distributions with the lower winglet off are compared in Figure 70 to those with the lower winglet on. These pressures suggest that the additional penalty due to the removal of the lower winglet relative to the estimate may be caused by shock losses on the inboard upper surface of the upper winglet. The pressures are only slightly affected outboard but the suction peaks are increased and the shock strengths increase accordingly inboard. Figure 70 shows that the effect is nearly all related to the upper winglet loading as the pressure distribution on the wing tip seems minimally affected by the absence of the lower winglet.

The winglet span loads and normal force coefficients are shown in Figures 71 and 72, respectively. While there may be differences in the peak suction pressures from wind tunnel to flight, the span loads and normal force coefficients show excellent agreement with the wind tunnel-measured values, both in the level and the variation with airplane lift coefficient. In other words, the winglet was loading in flight the way the wind tunnel results had predicted it would.

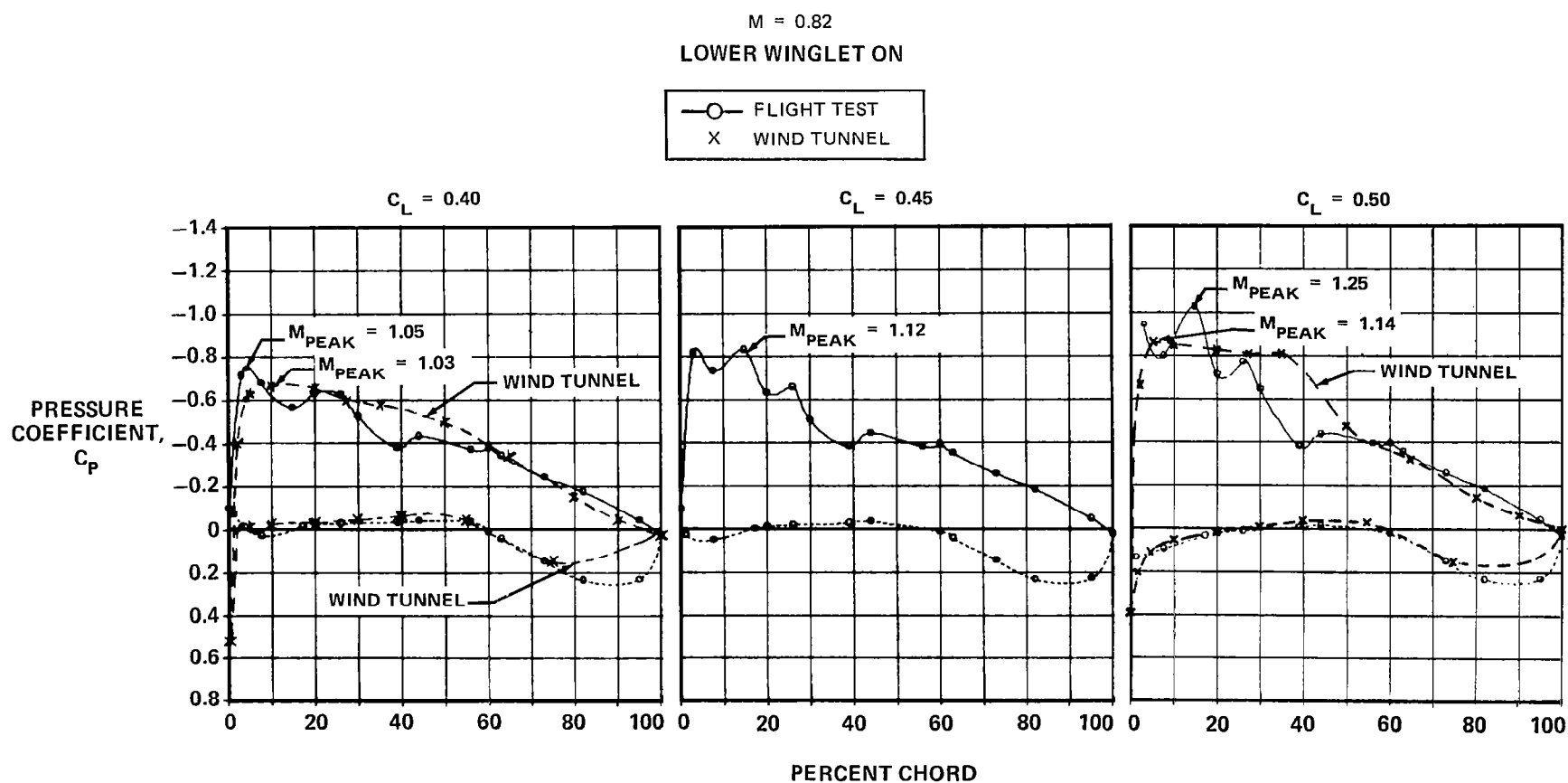


FIGURE 67. EFFECT OF LIFT COEFFICIENT ON BASIC WINGLET PRESSURE DISTRIBUTION AT CRUISE – 12.5-PERCENT SPAN

M = 0.82
LOWER WINGLET ON

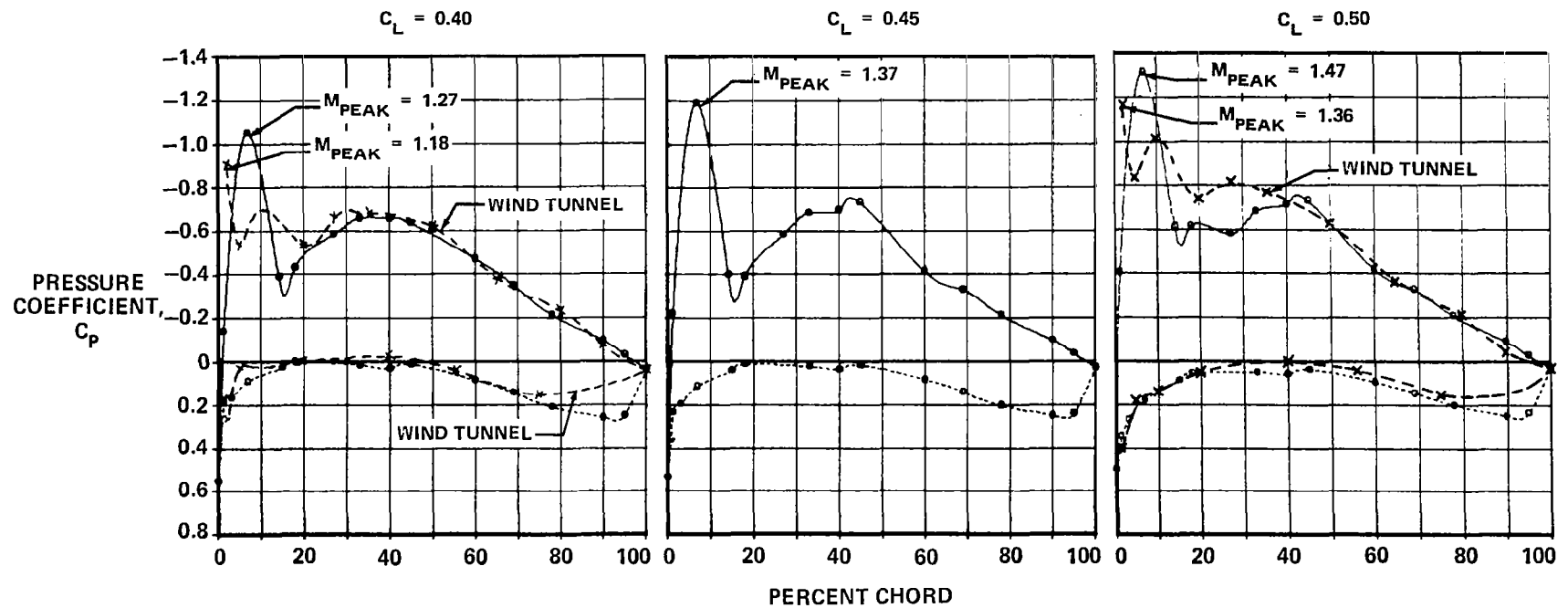
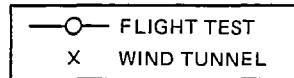


FIGURE 68. EFFECT OF LIFT COEFFICIENT ON BASIC WINGLET PRESSURE DISTRIBUTION AT CRUISE - 80-PERCENT SPAN

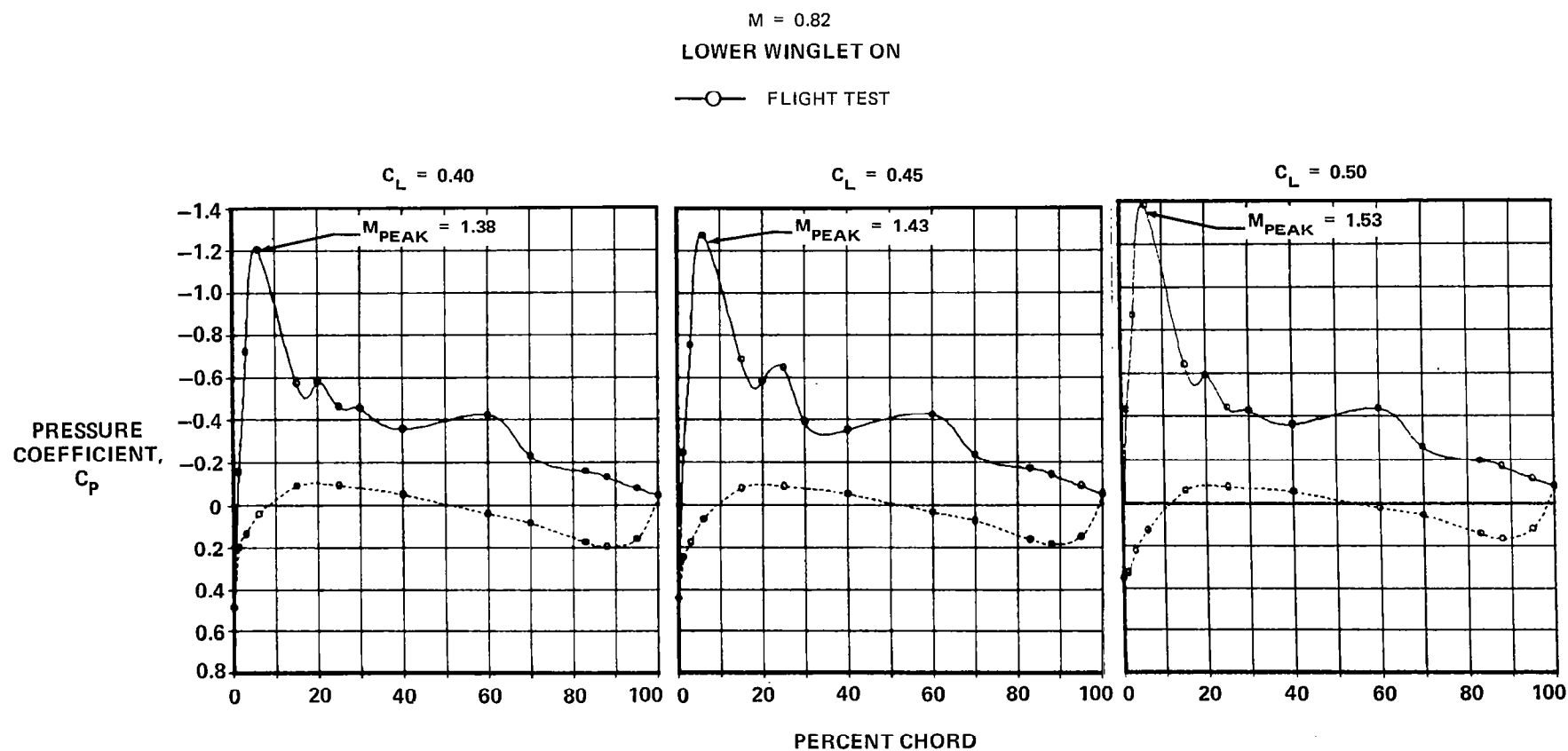


FIGURE 69. EFFECT OF LIFT COEFFICIENT ON BASIC WINGLET PRESSURE DISTRIBUTION AT CRUISE – 95-PERCENT SPAN

$$M = 0.82, C_L = 0.5$$

○ LOWER WINGLET ON
△ LOWER WINGLET OFF

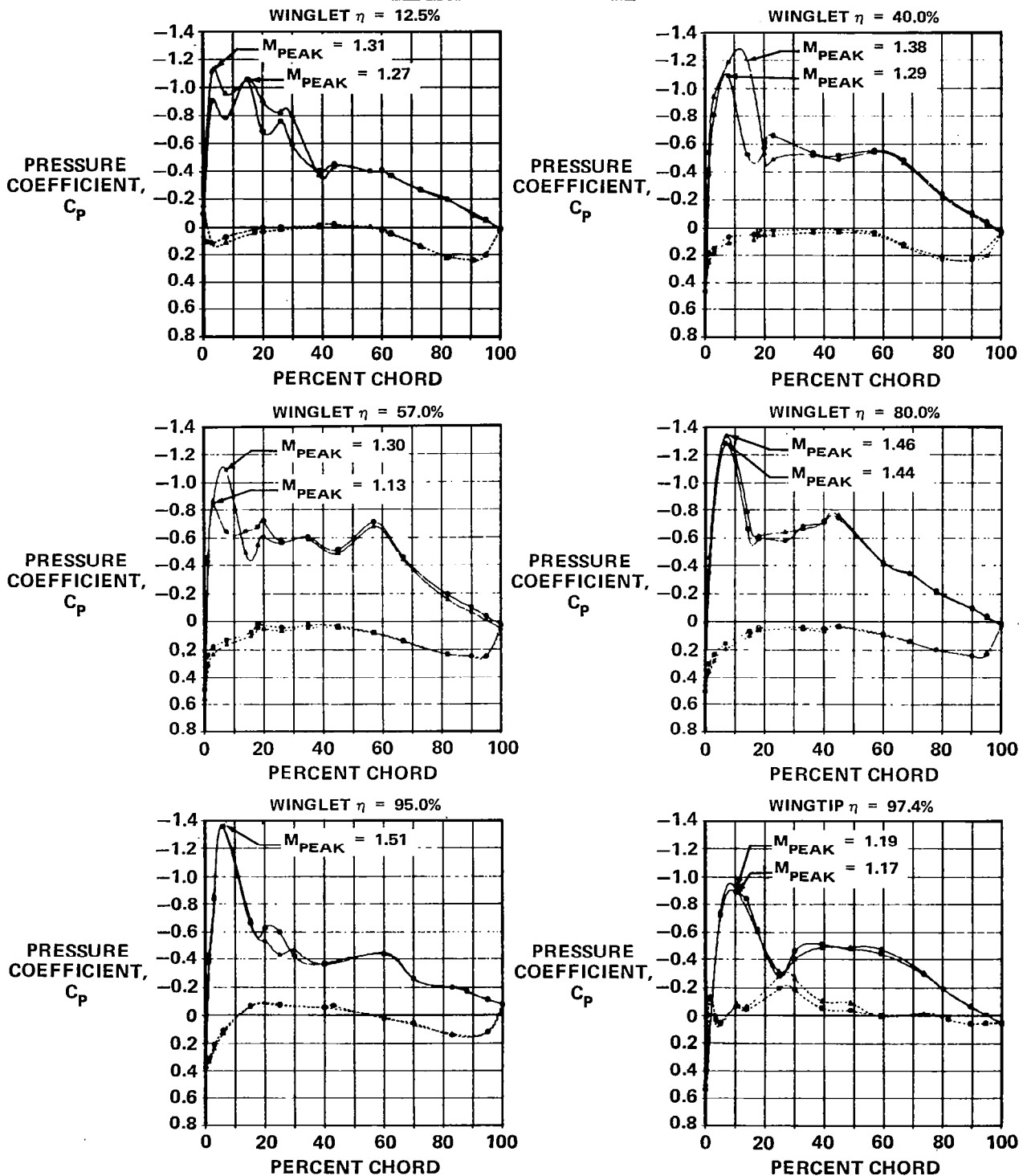


FIGURE 70. EFFECT OF LOWER WINGLET ON BASIC UPPER WINGLET/WINGTIP PRESSURE DISTRIBUTION AT CRUISE

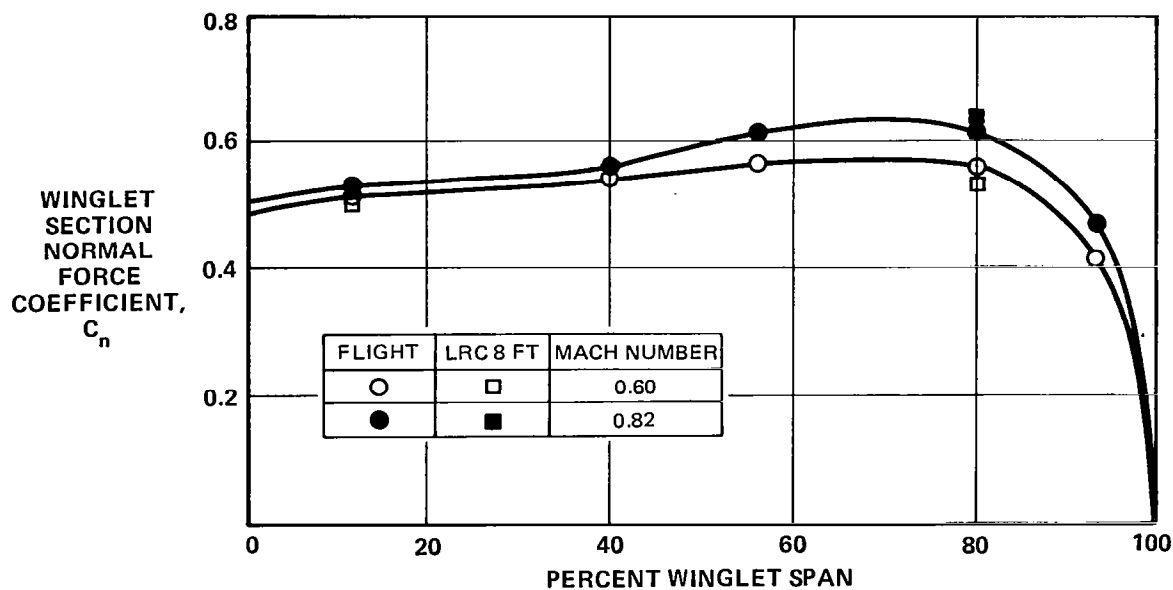


FIGURE 71. BASIC WINGLET SPAN LOAD AT CRUISE

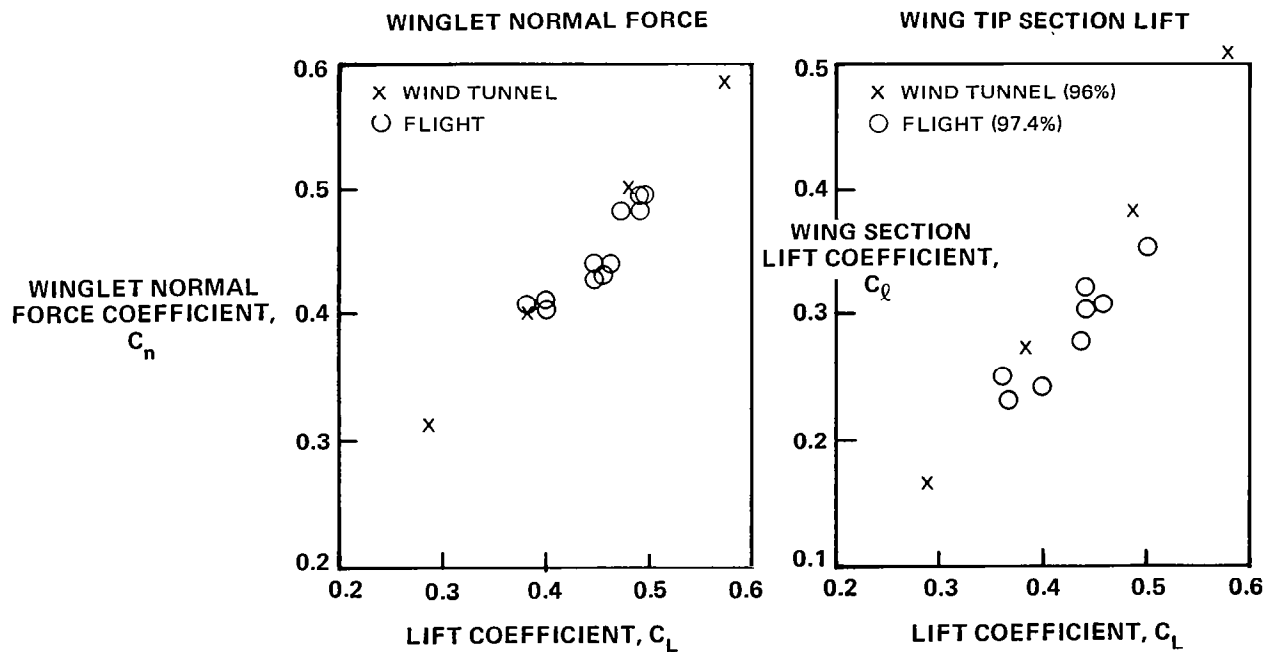


FIGURE 72. BASIC WINGLET AND WINGTIP LOADING AT CRUISE

Figure 73 compares the flight and wind tunnel measurements of wing-tip section load. As before, excellent agreement is seen with the wind tunnel-measured values.

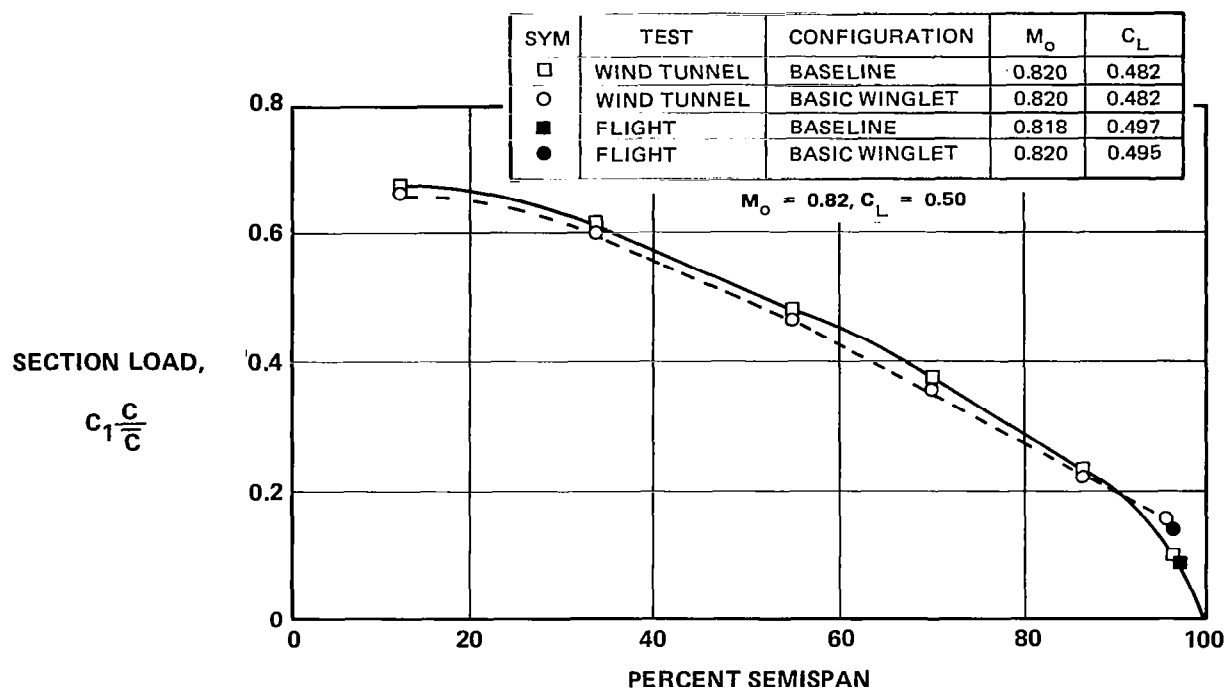


FIGURE 73. EFFECT OF BASIC WINGLET ON WING SPAN LOAD – FLIGHT AND WIND TUNNEL

In summary, analysis of the cruise data for the basic winglet indicate that at typical cruise conditions the demonstrated performance benefit was about 75 percent of the improvement predicted analytically and from wind tunnel results. Analysis of the data does not provide a clear insight for the shortfall, although some of it may be related to compressibility effects on the winglet.

Cruise Buffet – For the DC-10, the buffet boundary is defined by an intensity of 0.2g peak-to-peak normal acceleration at the airplane center of gravity. For Ship 101, normal accelerations were measured during wind-up turns to establish the buffet intensity. These were measured over a Mach number range of from 0.75 to 0.83 for both the baseline aircraft and BWL Configuration 1. The results of these tests are summarized in Figure 74 as incremental buffet lift coefficients from the baseline airplane for peak-to-peak accelerations of 0.1, 0.15, and 0.2g.

The winglet results fell within the scatterband of the baseline aircraft and it was concluded that the winglet has little or no effect on the buffet boundary. In fact, for the 0.2g peak-to-peak level (the value used for FAA certification), the data would indicate a slight improvement with the winglet although there are not enough data to substantiate this. These results are in agree-

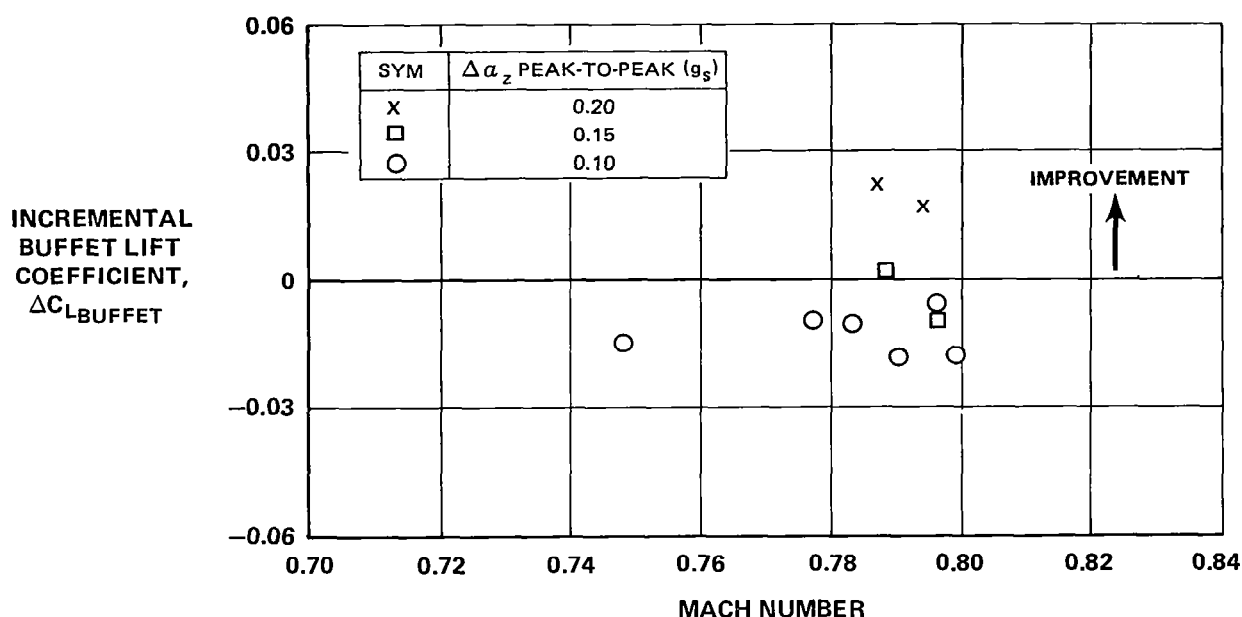


FIGURE 74. EFFECT OF BASIC WINGLET ON HIGH-SPEED BUFFET BOUNDARY

ment with the wind tunnel results (Reference 4). The wind tunnel data showed that high-speed buffet onset is controlled by flow separation on the wing which was not changed by the presence of the winglets. Pressure measurements and flow visualization indicated that the winglet flow was still attached at buffet conditions where the wing outer panel was experiencing flow separation. The flight results, showing essentially no winglet effect, tend to confirm these findings.

Since the BWL had no significant effect on the high-speed buffet boundary, it was concluded that the smaller RSWL would also have no effect. Therefore, no more buffet boundary tests were conducted in the program.

Longitudinal Static Stability — Longitudinal static stability tests were conducted in the clean configuration (Number 9). The tests included cruise conditions at 4 572 m (15,000 ft) at V_{MO} and at 10 668 m (35,000 ft) at $M = 0.85$, and a climb condition at 3 048 m (10,000 ft) at 648 km/h (350 kt), all flown at an aft center of gravity.

Figure 75 presents control column force as a function of Mach number for the cruise condition, trimmed at 10 688 m (35,000 ft) and $M = 0.85$, and as a function of equivalent airspeed for the climb condition, trimmed at 3 048 m (10,000 ft) and an airspeed of 648 km/h (350 kt). Shown are both the winglet flight data and calculated results for the baseline DC-10 Series 10 with no winglets. For both the cruise and climb cases, the data show that, with winglets on, a higher con-

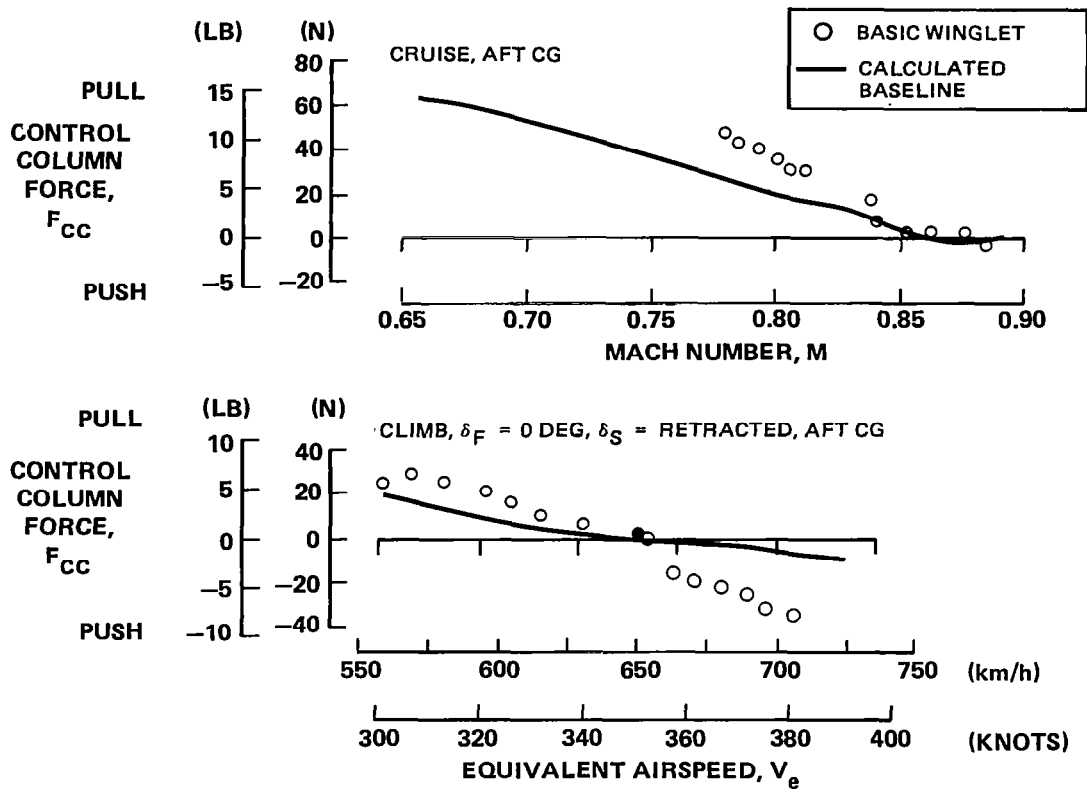


FIGURE 75. EFFECT OF BASIC WINGLET ON LONGITUDINAL STATIC STABILITY

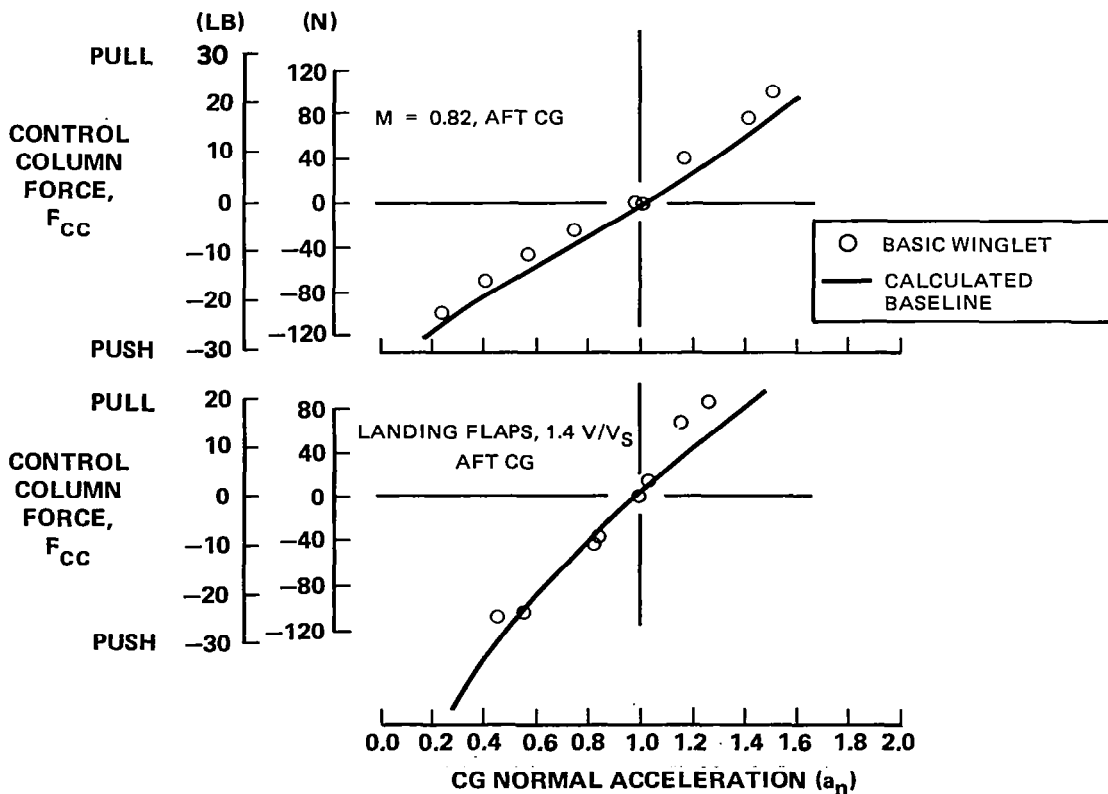


FIGURE 76. EFFECT OF BASIC WINGLET ON LONGITUDINAL MANEUVERING STABILITY

trol pull was required to reduce either the Mach number or equivalent airspeed (that is, to increase angle of attack) than with winglets off. This indicates a higher level of static longitudinal stability with winglets on. This increased stability was to be expected because the additional lift produced near the wing tip by the winglets acts aft of the cg and provides an airplane-nose-down moment.

Figure 75 also shows longitudinal static stability for a climb condition. The winglet flight test data are compared with a calculated case for the baseline, and the winglet data again show a higher level of static stability.

Longitudinal Maneuvering Stability — Longitudinal maneuvering stability tests were conducted in the cruise configuration at 11 247 m (36,900 ft) and $M = 0.82$, and in the landing configuration at $1.4 V_{MIN}$, both at aft centers of gravity. The results are presented in Figure 76.

The high-altitude cruise case shows good agreement between the flight test data and the calculated case for the baseline DC-10 Series 10 without winglets. The control column position data do not agree with the calculated curve, but the shape of the curve looks correct and the error probably is the result of an instrumentation problem. The low-speed landing-configuration longitudinal-maneuvering-stability case shows excellent agreement between the flight test data and the calculated case for the baseline DC-10 Series 10.

For the flight tests, the cruise load factor was restricted to 1.6 and the landing load factor to 1.3. The maximum load factors attained in the tests were 1.46 and 1.26, respectively.

Longitudinal Trim Characteristics — Figure 77 shows the stabilizer incidence required to trim the aircraft in cruise at 7 620 m (25,000 ft) for center of gravity locations from 10.5 to 30.7 percent of the mean aerodynamic chord. The two sets of symbols identify the baseline and winglet flight data obtained with the center of gravity at 24.5 percent. The correlation between the estimated values and the flight test results is very good, and the winglet data show no significant change from the baseline trim levels.

Static Directional Stability — The flight test results were in good agreement with calculated values and showed that the winglets had no effect on static directional stability.

The static directional stability data for the three test configurations — baseline, basic winglet, and reduced-span winglet — are compared in Figures 78 and 79, which show the amount of rudder and aileron control wheel deflection needed to maintain a steady aircraft heading at a given sideslip angle. The symbols represent the flight data and the lines the values predicted from previous DC-10 Series 10 data. The flight tests were made in a takeoff configuration ($\delta_F = 0/TO$) and a landing configuration ($\delta_F = 50/LND$), at $1.2 V_{MIN}$ and $1.4 V_{MIN}$ for each configuration. The results shown are for the $1.4 V_{MIN}$ condition. Although the variation of con-

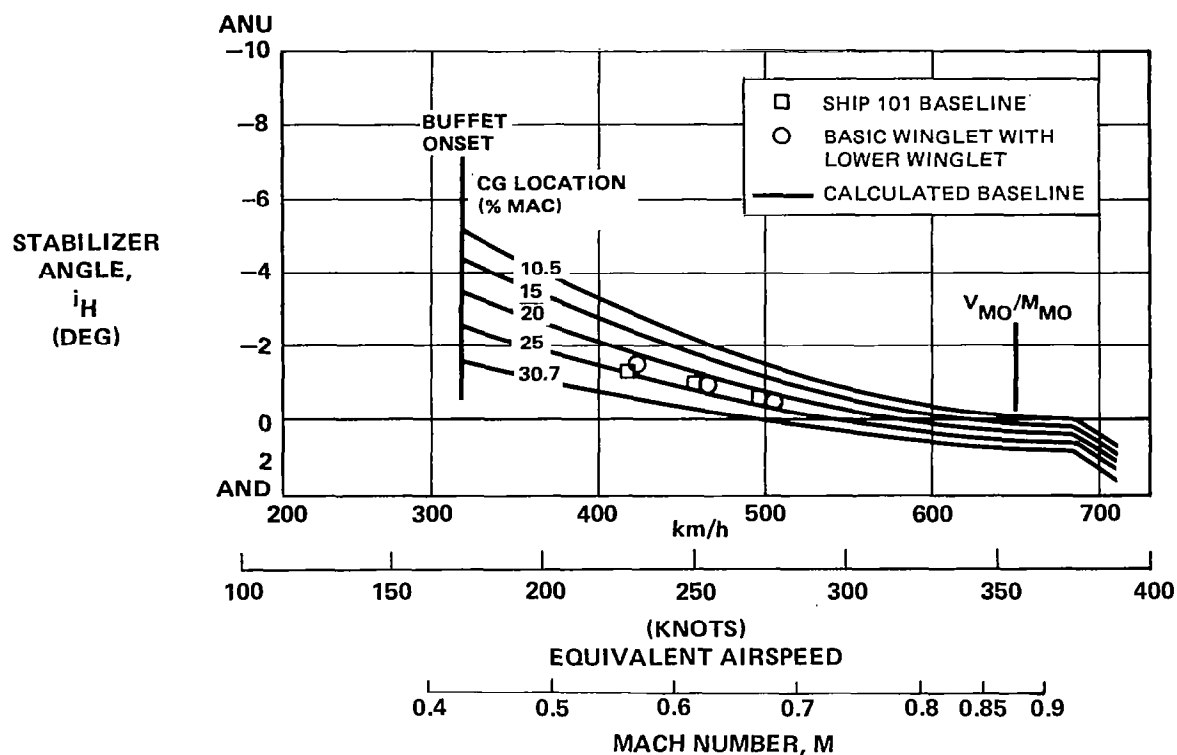


FIGURE 77. EFFECT OF BASIC WINGLET ON CRUISE LONGITUDINAL TRIM CHARACTERISTICS

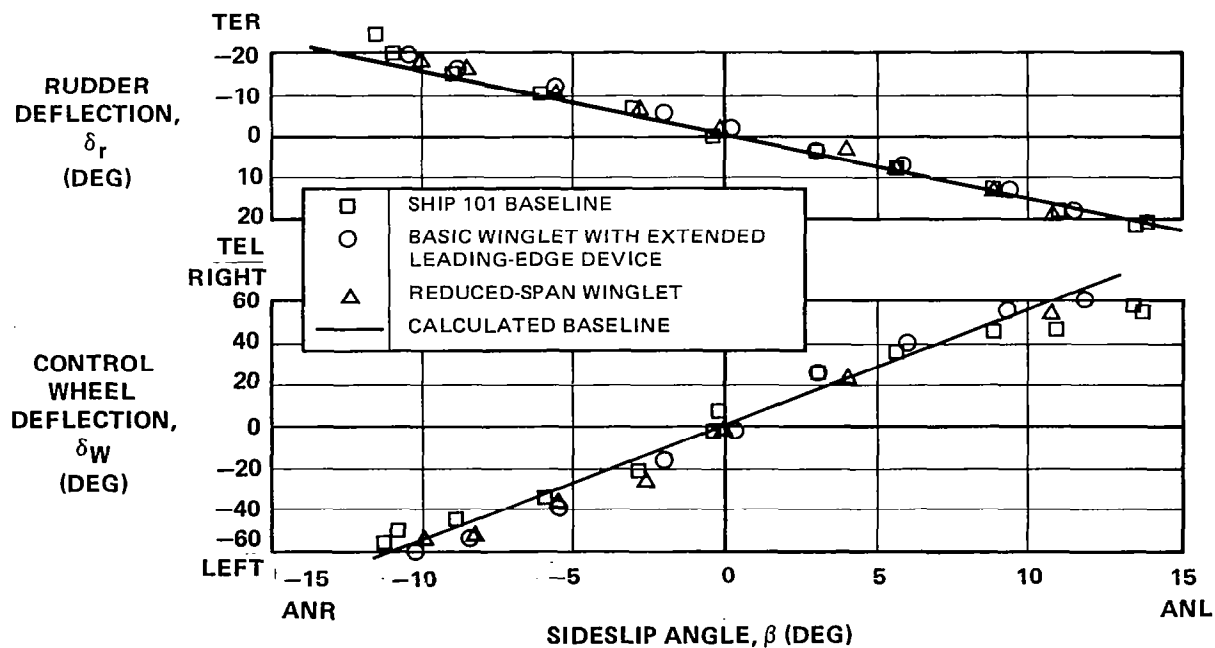


FIGURE 78. EFFECT OF BASIC AND REDUCED-SPAN WINGLETS ON TAKEOFF STATIC DIRECTIONAL STABILITY

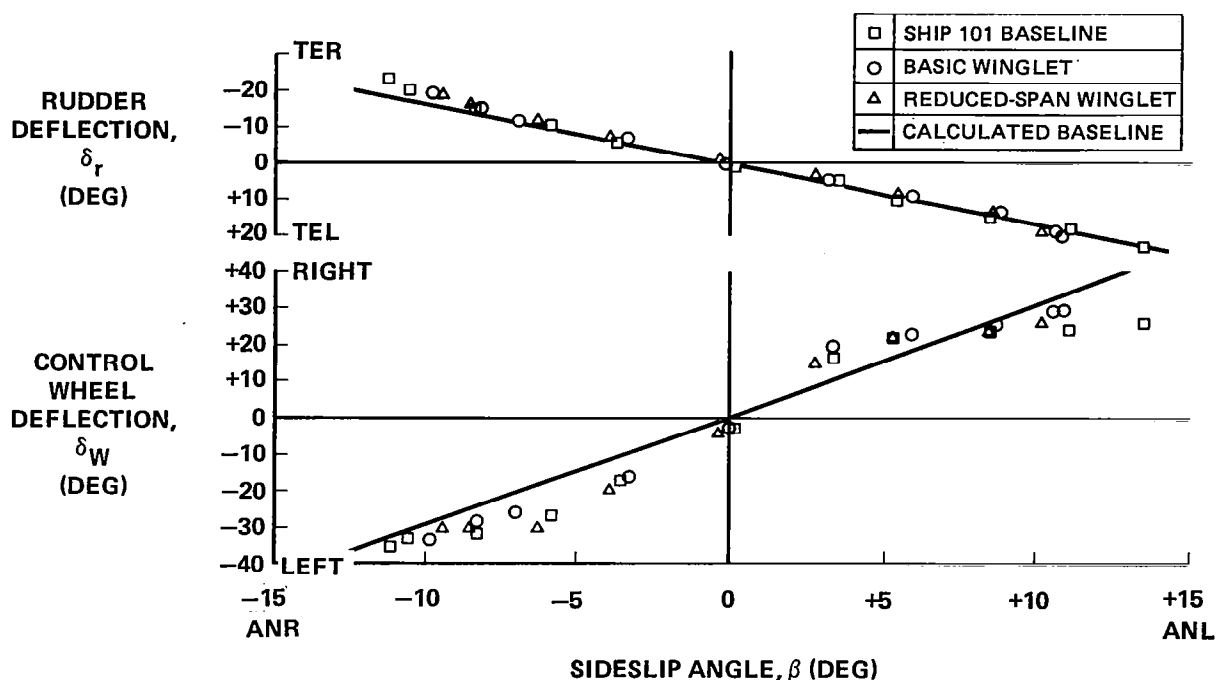


FIGURE 79. EFFECT OF BASIC AND REDUCED-SPAN WINGLETS ON LANDING STATIC DIRECTIONAL STABILITY

control wheel deflection, particularly for the landing case, is not as linear as had been predicted, the correlation with the predicted values was good. The winglets are seen to have no noticeable effect on static direction stability.

Dynamic Lateral Stability (Dutch Roll) — Investigations were conducted at three cruise conditions: $M = 0.70$ at 6 096 m (20,000 ft), $M = 0.80$ at 9 144 m (30,000 ft), and $M = 0.82$ at 10 668 m (35,000 ft). In each case, with the yaw dampers off the time to damp to half amplitude was less than the calculated value for the basic DC-10 Series 10, indicating that the dutch roll damping was greater than for the basic aircraft.

Dutch roll tests were also conducted in the landing configuration ($\delta_F \approx 50/\text{LND}$) at $1.2 V_{\text{MIN}}$ and $1.4 V_{\text{MIN}}$. The time to damp to half amplitude was greater than the calculated basic DC-10 Series 10 values, indicating that the dutch roll damping was less than the calculated basic DC-10 Series 10 values.

Loads Measurement — The results indicated that:

- The measured winglet normal force levels were approximately at the expected levels.
- The variation of winglet normal force coefficient with aircraft angle of attack was in agreement with prediction.

- The effects of aeroelasticity were clearly evident. The 1.6g maneuvers produced lower normal force coefficients (for a given angle of attack) than 1g level flight. Also, the rate of change with angle of attack was less at the higher g level. This aeroelastic effect was accounted for in the loads analysis.
- Comparison of the uncalibrated wing strain gauge data with baseline data confirms the general levels of incremental bending associated with the addition of winglets. The horizontal bending effect resulting from the inboard acting winglet load and wing sweepback is also evident.
- For most flights the instrumented outboard aileron was rigged as received from the airline, approximately 1.75 degrees trailing edge up from the nominal (zero-degree) position. As a result, the loads measured at the outboard hinge support bracket were substantially lower than predicted. However, for one flight of the later RSWL phase, in which the ailerons were rigged 3 degrees trailing edge down, the loads measured were closer to the predicted levels.

Reduced-Span Winglet Phase

Flight Test Program — The planned objectives for the RSWL phase were met. Adjustments to the test details were made, considering the effects of the insertion into the test program of the development activities and the good quality of the data in the BWL phase.

The following deletions were made:

- The flutter envelope expansion, since the BWL tests provided a sound foundation for understanding flutter characteristics.
- The cruise matrix was reduced from 25 to 19 points.

The following contingency tests were not performed since no significant winglet influence was detected during the BWL tests:

- Stall speeds and characteristics
- Buffet boundary

Added to the original test plan was the cruise and low-speed buffet investigation conducted during the final flight where symmetrically drooped (3 degrees trailing edge down) outboard ailerons were employed to investigate the effect of an increase in the wing tip/winglet loading on cruise performance.

All the configurations tested are described in Figure 80. As in the BWL phase, a leading device was tested at low speed. However, configurations without a leading edge device were tested both in the low-speed and high-speed regimes. The features of the configurations of the figure, which are also illustrated by the photographs of Figure 81, are as follows:

- Configuration 13: Upper Krueger flap extended root to tip, no lower winglet. The extent of this flap is shown in Figure 82, together with features of the later Configuration 17.
- Configuration 14: Upper winglet only
- Configuration 15: Configuration 14 with lower winglet
- Configuration 16: Configuration 13 with lower winglet
- Configuration 17: Configuration 13 with modified (extended chord) lower winglet. This winglet had a chord extension of 80 percent of the local chord of the basic original lower winglet. The leading edge shape of the original lower winglet was maintained forward of the front spar. Aft of the front spar, the airfoil shapes were composed of straight line segments. The resulting airfoil physical thickness was the same as the original lower winglet. The modified winglet was also fitted with a simple sealed Krueger flap that was constructed of sheet metal and which had a tapered circular cross section attached to its leading edge. This flap, together with the extended-chord lower winglet, is shown in Figure 82. The flap was 15 percent of the basic (unextended) lower winglet chord in length and the radius of the leading edge bulb was 5 percent of the basic winglet chord.
- Configuration 18: Configuration 17 without leading edge devices.
- Configuration 19: Configuration 18 with the outboard ailerons drooped 3 degrees (measured in the streamwise direction) from the basic rigged position.

During the description of the BWL development configurations, it was noted that the evolution of a satisfactory winglet should balance or resolve the apparently opposing requirements for and against the lower winglet. On the one hand, the lower winglet improved cruise performance; on the other, it adversely contributed to the low-speed buffet. An attempt to resolve this opposition led to the extended-chord lower winglet, whose design was aided by NASA Langley investigators. It was reasoned that such a chord extension would reduce the local section lift coefficients on the lower winglet and thus delay flow separation on the lower winglet to a higher level of airplane lift coefficient. However, there was concern over the potential degradation of cruise performance since during the wind tunnel tests (Reference 2), overlap of the lower and upper winglet was identified as a potential problem area. Therefore, a number of tests were made with this configuration in various forms.




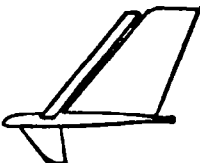
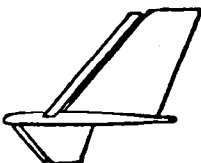
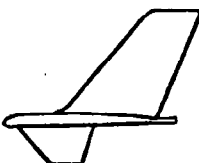
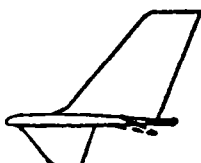
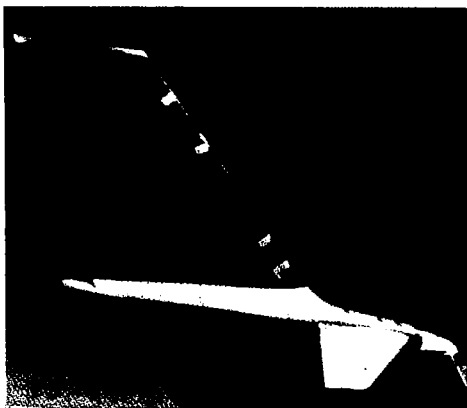
CONFIGURATION NUMBER	13	14	15	16	17	18	19
PHYSICAL APPEARANCE							
DESCRIPTION	REDUCED-SPAN WINGLET WITH KRUEGER FLAP INSTALLED WITH EXTENSION TO WING TIP. KRUEGER FLAP DEFLECTION WAS 40 DEGREES	REDUCED-SPAN UPPER WINGLET WITHOUT LOWER WINGLET	REDUCED-SPAN UPPER WINGLET WITH BASIC LOWER WINGLET INSTALLED	CONFIGURATION NUMBER 13 WITH BASIC LOWER WINGLET INSTALLED	CONFIGURATION NUMBER 13 WITH 80-PERCENT EXTENDED CHORD LOWER WINGLET INSTALLED. LOWER WINGLET HAD SEALED KRUEGER FLAP INSTALLED	REDUCED-SPAN UPPER WINGLET WITH 80-PERCENT EXTENDED CHORD LOWER WINGLET INSTALLED. (NO LEADING EDGE DEVICES ON UPPER OR LOWER WINGLET)	CONFIGURATION NUMBER 18 WITH OUTBOARD AILERONS DROOPED 3.0 DEGREES
FLIGHTS WHICH EMPLOYED CONFIGURATION	A50	A51-A53	A54-A56	A57	A58	A59-A60	A61

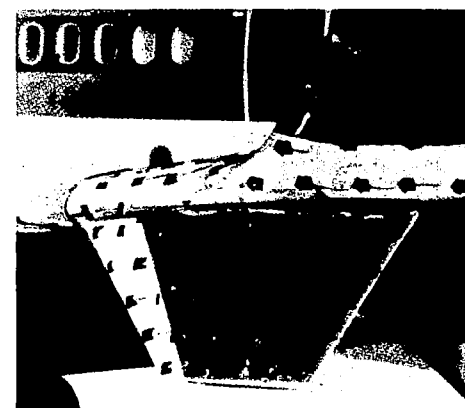
FIGURE 80. CONFIGURATION IDENTIFICATION FOR REDUCED-SPAN WINGLET FLIGHT PROGRAM



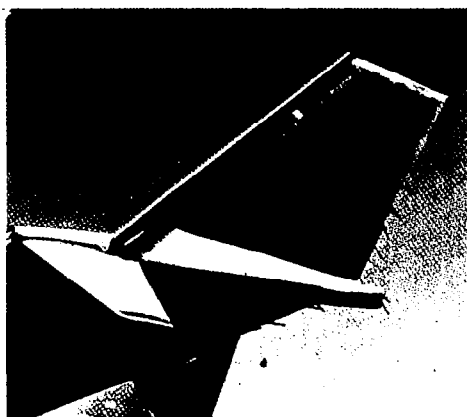
**REDUCED-SPAN UPPER WINGLET
AND LOWER WINGLET**



**REDUCED-SPAN UPPER WINGLET WITHOUT
LOWER WINGLET**



**REDUCED-SPAN UPPER WINGLET AND
80-PERCENT EXTENDED CHORD
LOWER WINGLET**



UPPER WINGLET KRUEGER FLAP



LOWER WINGLET KRUEGER FLAP



LOWER WINGLET KRUEGER FLAP

FIGURE 81. REDUCED-SPAN WINGLET CONFIGURATIONS

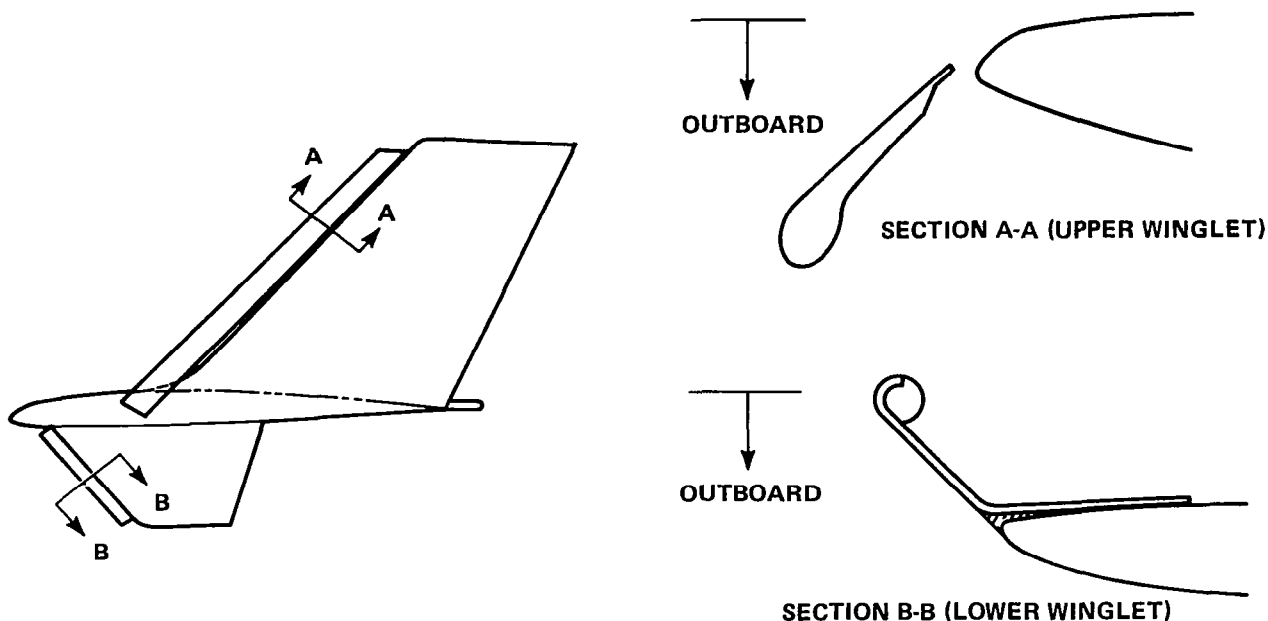


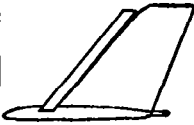
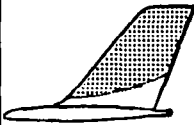

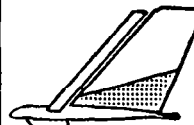

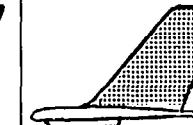

FIGURE 82. LEADING-EDGE KRUEGER FLAP GEOMETRY FOR REDUCED-SPAN UPPER WINGLET AND EXTENDED-CHORD LOWER WINGLET

Low-Speed Buffet — Figure 83 summarizes the low-speed buffet evaluation for the RSWL. Configuration 13, the first tested, was directly related to the most promising configuration from the BWL low-speed buffet and performance evaluation. The Krueger flap covering the whole span was installed on the upper winglet, and the lower winglet was removed. Like the BWL, this configuration exhibited acceptable buffet characteristics.

Since removing the Krueger flap on the BWL resulted in buffet characteristics which were also acceptable even though there was extensive flow separation, a similar configuration (Number 14) was next tested. Acceptable buffet characteristics were achieved, but again the flow on the winglet was about 75-percent separated, which would adversely affect the drag improvement. At this point it was decided to obtain a low-speed drag polar on this configuration in order to determine the performance penalty associated with the rather significant area of flow separation.

During the flight in which cruise data were gathered for the configuration with the upper and lower winglets installed (Configuration 15), the low-speed buffet was also evaluated. Detailed analysis of the data for this configuration indicated that it had acceptable buffet characteristics.

$\delta_F = 15$ DEGREES $\delta_S =$ TAKEOFF

CONFIGURATION NUMBER	13	14	15	16	17	18	19
CONFIGURATION DESCRIPTION	UPPER WL AND FCK EXT	UPPER WL	UPPER WL WITH LOWER WL	UPPER WL WITH FCK EXT AND LOWER WL	UPPER WL WITH FCK EXT AND LOWER EXT WL WITH FCK	UPPER WL AND LOWER EXT WL	UPPER WL AND LOWER EXT WL AND DROOPED AILERON
FLIGHT	A-50	A-52	A-54	A-57	A-58	A-59	A-61
BUFFET AT $1.35 V_{MIN}$	NONE	NONE	PERCEPTIBLE	LIGHT	NONE	VERY LIGHT	PERCEPTIBLE
BUFFET AT $1.20 V_{MIN}$	PERCEPTIBLE	LIGHT	LIGHT	MODERATE	BARELY PERCEPTIBLE	LIGHT	LIGHT
VERTICAL BOUNCE AT $1.20 V_{MIN}$	NO	NO	NO	NO	NO	NO	NO
WING FLOW VISUALIZATION	ATTACHED	ATTACHED	NO FLOW VISUALIZATION	ATTACHED	ATTACHED	SEPARATED	NO FLOW VISUALIZATION
WINGLET FLOW VISUALIZATION AT $1.20 V_{MIN}$				 NO CHASE			
PILOT SEAT ACCELERATION AT $V = 1.20 V_{MIN}$ (PEAK-TO-PEAK)	0.03	0.04	0.04	0.07	0.04	0.05	0.06

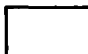

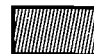
 ATTACHED STREAMWISE FLOW
  SEPARATED FLOW
  SPANWISE FLOW
 FLOW VISUALIZATION SHOWN ON THE INBOARD SURFACE OF UPPER WINGLET AND OUTBOARD SURFACE OF LOWER WINGLET

FIGURE 83. SUMMARY OF LOW-SPEED BUFFET CHARACTERISTICS – REDUCED-SPAN WINGLET

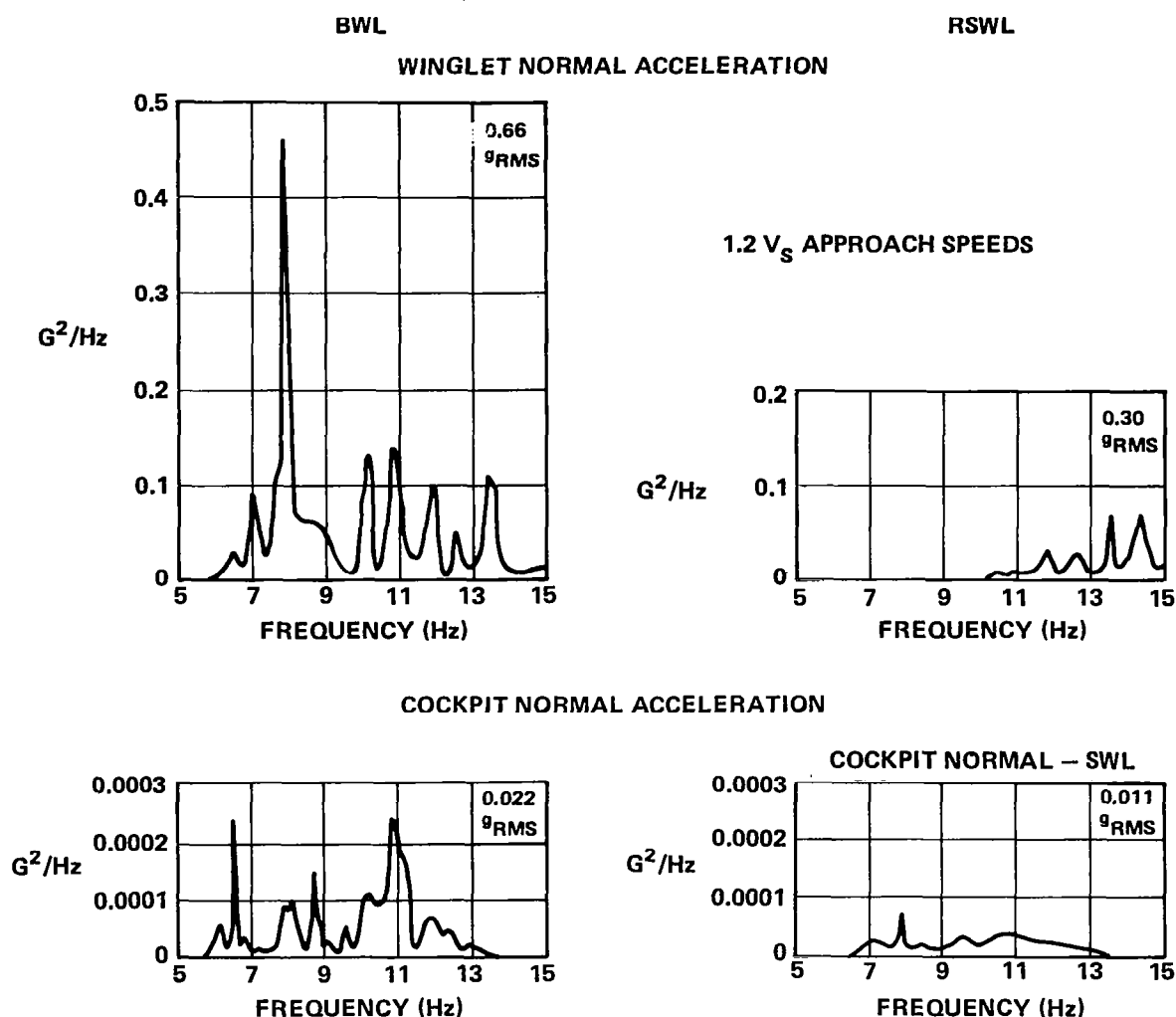


FIGURE 84. BUFFET RESPONSE ACCELERATION POWER SPECTRA

At this point it was clear that the lower aspect ratio of the RSWL or its structural response to the separated flow was having a significantly favorable effect on low-speed buffet characteristics.

Structural responses during buffet were measured with the accelerometers located at selected stations on the aircraft. These data were used to generate power spectral densities (PSDs) showing vibratory power as a function of the buffet frequency.

Figure 84 presents a comparison of buffet response data for the BWL and RSWL configurations. Acceleration power spectra and RMS values are shown for winglet-normal and cockpit-normal response parameters. These data show that the PSD levels with the RSWL are significantly lower than those with the BWL. The winglet and cockpit RMS values for the RSWL are approximately half those for the BWL.

The winglet-normal PSD data for the BWL shows a dominant peak at 8 Hz, the first bending frequency of the winglet. The corresponding cockpit PSD data show a small peak at 8 Hz with higher peaks at several other frequencies. This indicates that the cockpit response is the result of several structural modes being excited, most probably by the aerodynamic forcing function due to flow separation. However, no correlation appears obvious between the shape of the acceleration power spectrum and the size of the winglet or the degree of separation.

The remaining configurations evaluated (15 through 19) were aimed at finding the best overall configuration from the standpoints of buffet, low-speed drag improvement, and cruise drag improvement. All except Configuration 16 were acceptable from a buffet standpoint.

Configuration 17 was a modification of Configuration 16 employing an extended-chord lower winglet with a Krueger flap leading edge device. The leading edge device did not prevent flow separation on the lower winglet at V_2 conditions; however, the flow on the leading edge device itself stayed attached thus providing significant leading edge suction. In addition, the flow mechanism was different from the configuration without the lower winglet leading edge device in that the wake from the separated flow did not go over the wing.

The performance aspects of these configurations will be discussed in subsequent sections.

Low-Speed Drag — Data were obtained for Configuration 13 (extended upper leading edge devices, no lower winglet), Configuration 14 (Configuration 13 with no leading edge devices), and Configuration 17 (Configuration 13 with extended-chord lower winglet and leading edge devices on both winglets).

The low-speed drag improvement is shown in Figure 85 for all three configurations at the 15-degree flap setting. The left side of this figure indicates the drag improvement for the RSWL without the lower winglets installed, and provides comparison with the BWL performance. The RSWL drag improvement (with leading edge device) is approximately 80 percent of the BWL (with leading edge device). The figure also shows that the removal of the upper winglet leading edge device resulted in more than a 50-percent loss in performance improvement (from 4.4 percent to 2.1 percent) at V_2 conditions. The reason for this performance loss is the significant amount of flow separation observed during the flow visualization flight on the inboard surface of the upper winglet. Wind tunnel results have also indicated a loss in performance improvement when the winglet inner surface has significant amounts of flow separation. The right side of Figure 85 indicates that the lower winglet has favorable impact on low-speed drag improvement particularly at the higher lift coefficients. It shows an additional 1.5-percent improvement at V_2 conditions, even though the lower winglet was completely separated for this condition. The resulting low-speed drag improvement at V_2 for the RSWL with the lower winglet is 5.9 percent. This more than equals the value of 5.7 percent obtained for the BWL without the lower winglet. While no BWL configuration had acceptable buffet characteristics with the lower winglet in-

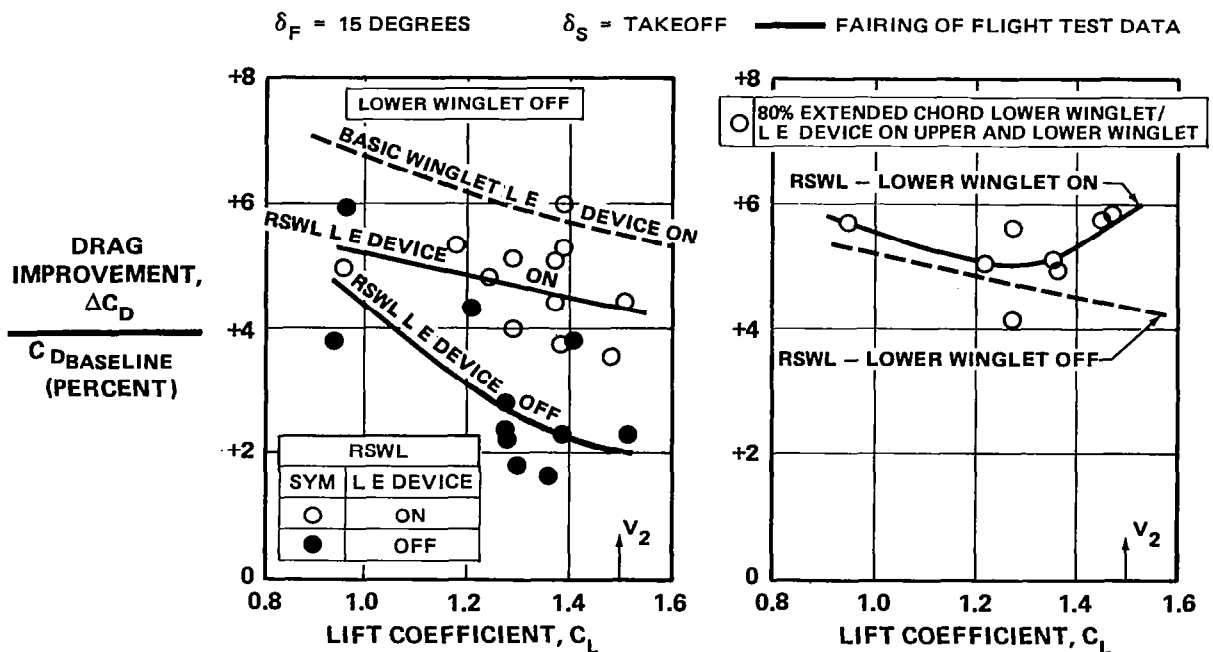


FIGURE 85. LOW SPEED DRAG IMPROVEMENT – REDUCED-SPAN WINGLET

stalled, it can probably be concluded that a leading edge device on the lower winglet would have provided acceptable buffet characteristics and similar performance improvements as was measured on the RSWL.

Cruise Performance — Figure 86 shows the cruise drag improvements for the RSWL, with and without the lower winglet installed (Configurations 15 and 14 respectively). While scatter in the flight test data is greater than in the BWL data, the characteristics of the performance benefits are similar. With the lower winglet installed, the incompressible and compressible data collapse to show the same improvement. At $C_L = 0.47$, the improvement is about 2 percent. This is only 0.5 percent less than the BWL while the predicted difference was 1 percent. Since the RSWL was not wind tunnel-tested for high-speed characteristics, the dashed predicted line shown on the curve was determined by incrementing the BWL wind tunnel data (Reference 3) by a vortex lattice calculation using the computer code of Reference 6. The slope of the flight measured improvement with lift coefficient is closer to the prediction than that for the BWL.

The RSWL pressure distributions in Figure 87 show that reducing the span of the winglet effectively eliminated the very high suction peaks ($M_{\text{peak}} \approx 1.5$) that were occurring on the outer span of the BWL (see Figure 69), while essentially not affecting the area where the suction peaks were lower ($M_{\text{peak}} \approx 1.3$). Clearly, these results would indicate that the high suction peaks on the

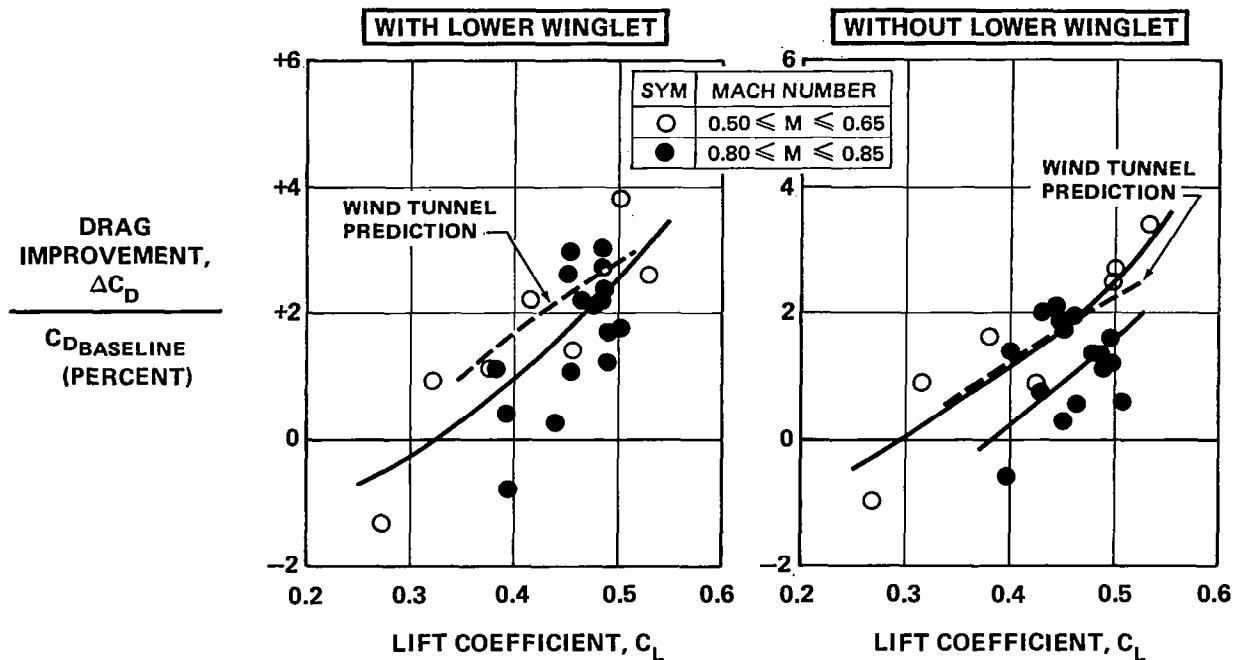


FIGURE 86. CRUISE DRAG IMPROVEMENT – REDUCED-SPAN WINGLET

outer span of the BWL are contributing to the failure to meet the full predicted performance benefit. This further suggests that the BWL performance could probably be improved by redesign.

Figure 86 also shows a detrimental compressible effect due to removal of the lower winglet, an effect very similar to that obtained with the BWL ($\cong 0.9$ percent penalty). The removal of the lower winglet resulted in increased upper winglet loading and increased suction peaks, as was observed for the BWL (see Figure 70). It should also be pointed out that the spanwise extent of increased loading for the BWL was about the same physical length as the full span of the RSWL.

During the design of the extended chord lower winglet that was tested at low speed (Configuration 17), there was some concern (from some of the data in Reference 3) that the overlap between lower and upper winglets could adversely affect the cruise performance. The cruise version of the configuration (Number 18) was therefore tested, and the results are summarized in Figure 88.

The test points shown in the left-hand plot of Figure 88 give the deviation from the faired data for the basic-chord lower winglet (Configuration 15). An average of the test points indicates a slight penalty for the extended-chord lower winglet, although it is very difficult to discern small differences of this magnitude. There was no evidence of flow separation at cruise conditions on the lower winglet from the tuft survey.

$M = 0.82$
 $C_L = 0.50$
FLIGHT 54
CONFIGURATION 15

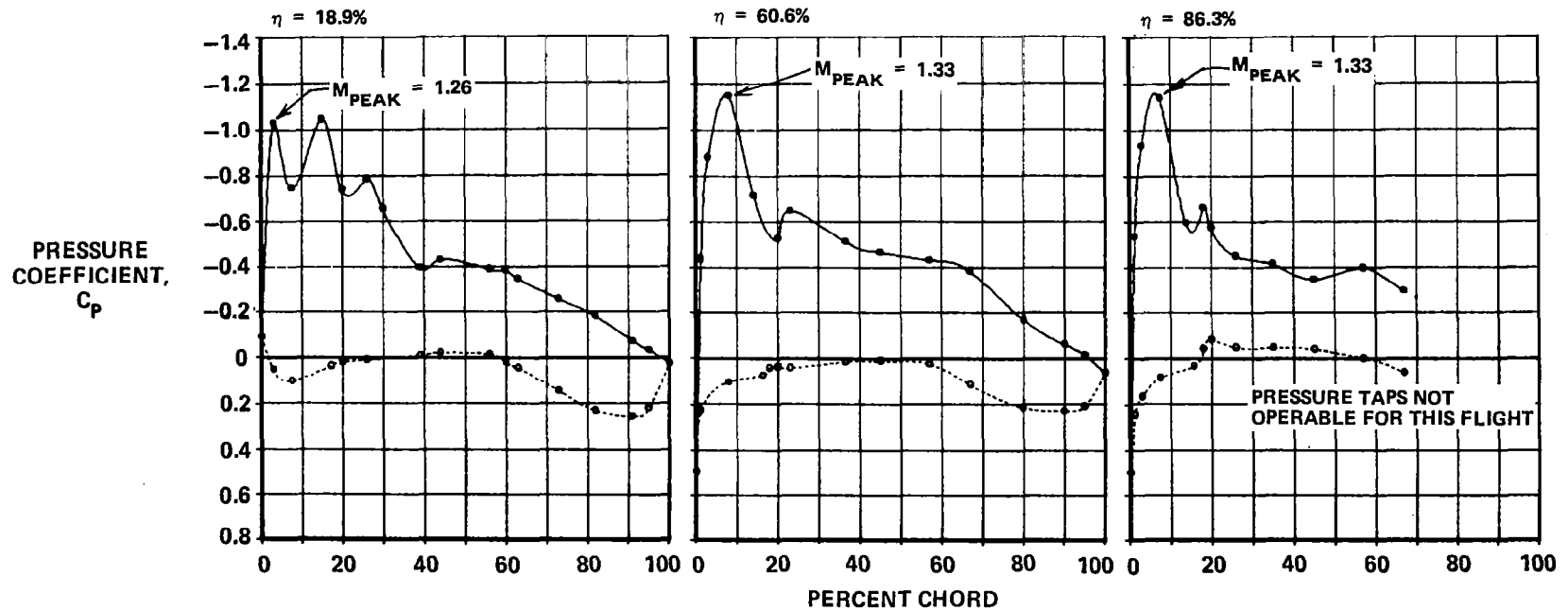


FIGURE 87. REDUCED-SPAN WINGLET PRESSURE DISTRIBUTION AT CRUISE

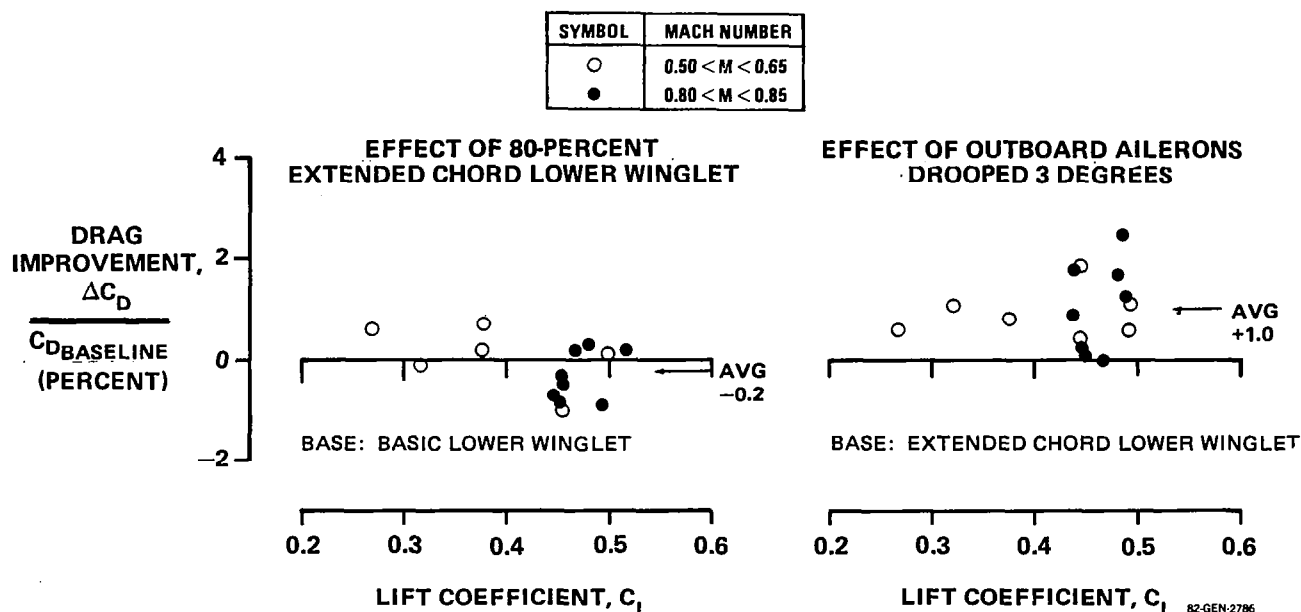


FIGURE 88. EFFECT OF CONFIGURATION VARIABLES ON CRUISE DRAG IMPROVEMENT – REDUCED-SPAN WINGLET

Analytical calculations using a vortex lattice computer code (Reference 6) had indicated that drooping of the outboard ailerons to load the outer wing and winglet could offer additional drag improvement of as much as 1 percent. On the last flight of the program, cruise performance was gathered for the extended-chord lower winglet configuration with the outboard ailerons drooped 3 degrees (Configuration 19). The right side of Figure 89 shows the incremental drag improvement relative to the same configuration without the ailerons drooped. An average of the data show a 1-percent improvement which is in very good agreement with the analytical estimate.

Configuration 19 was the best for improving cruise drag. At $C_L = 0.47$, the measured drag improvement was 2.8 percent. If the extended-chord lower winglet, which showed a small penalty by itself, was replaced with the original lower winglet, a cruise speed configuration with a nominal improvement of about 3 percent would be expected.

Figure 89 shows the effect of the aileron droop on the winglet and wing-tip pressure distributions. The pressures show that both the winglet and the wing tip are loaded higher with the aileron droop than without. The benefit is therefore due jointly to the additional winglet loading and wing span loading. The additional benefit is in good agreement with preflight estimates.

$M = 0.82, C_L = 0.2$

LOWER WINGLET ON

- AILERONS UNDROOPED
- △ 3° OUTBOARD AILERON DROOP

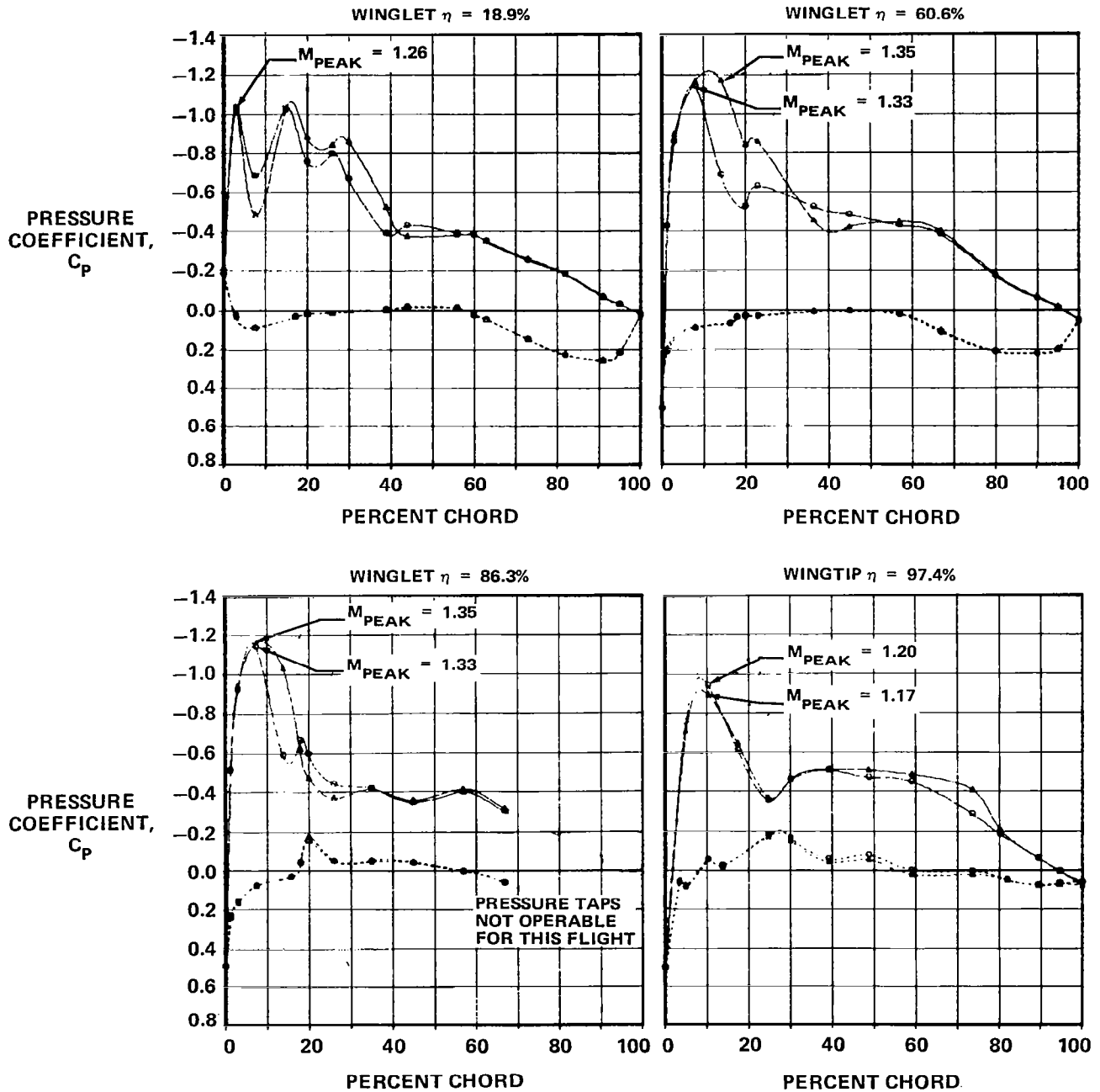


FIGURE 89. EFFECT OF OUTBOARD AILERON DROOP ON REDUCED-SPAN WINGLET/WINGTIP PRESSURE DISTRIBUTION AT CRUISE

IMPACT OF FLIGHT EVALUATION RESULTS ON OPERATIONAL PERFORMANCE

The data obtained during the flight evaluation were used to estimate the configuration and performance effects on a derivative version of the existing DC-10 Series 10 transport. Only those configuration changes resulting directly from winglet test requirements were considered.

The baseline DC-10 Series 10 selected for this evaluation features a 297-passenger interior (26 943-kg payload with maximum passenger and baggage load), has a maximum takeoff gross weight of 195 045 kg (430,000 lb), and is powered by three General Electric CF6-6D engines each rated at 117.9 kN (40,000 lb) sea level static thrust.

The basic lower winglet shape, without chord extension, was employed. All winglet configurations had upper plus lower winglets with winglet leading edge devices deployed for takeoff and landing. The winglets used in the estimation were:

- The basic winglet
- The reduced-span winglet
- The reduced-span winglet with aileron droop

The flight-measured loads were used to determine the increase in operator empty weight (Δ OEW) for the production installation of the winglets. These are summarized in Figure 90.

The cruise and low-speed drag improvements were input into the aircraft performance computer codes as a function of lift coefficient. This allowed the aircraft performance to be re-optimized at a new lift coefficient for cruise and a new flap setting for takeoff. Where a single drag improvement value is quoted (as summarized in Figure 90), it should be noted that this is an average value at a typical operating condition.

	Δ OEW \approx kg (LB)					
	BASIC WINGLET		REDUCED-SPAN WINGLET		REDUCED-SPAN WINGLET WITH AILERON DROOP	
WINGLET	382	(842)	321	(708)	321	(708)
WING						
BOX (BENDING)	207	(457)	83	(183)	135	(298)
BOX (SHEAR)	10	(22)	1	(2)	2	(4)
SLATS, FLAPS, AILERON	72	(159)	58	(128)	92	(203)
FLUTTER	635	(1,400)	136	(300)	136	(300)
SYSTEMS	34	(75)	34	(75)	59	(130)
TOTAL	1,340	(2,955)	633	(1,396)	745	(1,643)

FIGURE 90. INCREASES IN OPERATOR'S EMPTY WEIGHT

The impact of the three winglet configurations on key operating conditions is summarized in Figure 91, with further details given in subsequent figures. At a range of 3 704 km (2,000 n mi), representative of typical Series 10 operation, the best winglet configuration results in a 2.7-percent fuel burn improvement. (This increases to 3 percent at maximum range.) At the maximum takeoff gross weight, the range is increased 113 km (61 n mi) and the field length is reduced 162 m (530 ft).

DRAG AND WEIGHT CHANGES	BASIC WINGLET	REDUCED-SPAN WINGLET	REDUCED-SPAN WINGLET PLUS AILERON DROOP
CRUISE DRAG IMPROVEMENT = PERCENT	2.5	2.0	3.0
OPERATOR EMPTY WEIGHT = kg (LB)	1,340 (2,955)	633 (1,396)	745 (1,643)
LOW SPEED DRAG IMPROVEMENT = PERCENT	6.8	5.8	5.8
AIRCRAFT PERFORMANCE CHANGES			
FUEL BURNED = PERCENT			
AT 3,704 km (2,000 N MI)	-1.8	-1.7	-2.7
AT 6,112 km (3,300 N MI)	-2.1	-2.0	-3.0
RANGE = km (N MI)	-9 (-5)	+59 (+32)	+113 (+61)
TAKEOFF FIELD LENGTH = m (FT) AT MTOGW	-198 (-650)	-162 (-530)	-162 (-530)

FIGURE 91. EFFECT OF WINGLETS ON DC-10 SERIES 10 PERFORMANCE CHARACTERISTICS

Figure 92 shows the payload range capability. The effect on range of the winglets is relatively small, varying from a loss of 9 km (5 n mi) for the basic winglet to a gain of 113 km (61 n mi) for the reduced-span winglet with drooped ailerons, at maximum passenger and baggage payload. It can be seen that the OEW increase for the basic winglet more than offsets the drag improvement, resulting in a slight loss in range, whereas the reduced-span winglets require about half the OEW increase of the basic winglet and therefore effect a range improvement.

Figure 93 shows the takeoff field length envelope at sea level temperature of 29°C. At the maximum takeoff gross weight of 195 045 kg (430,000 lb), significant field length improvements are shown for both winglet configurations. Note that since the aircraft is engine-out climb limited (2.7% climb gradient required) at this condition, the improved lift-to-drag ratio at a given flap setting allows a higher flap setting while still meeting the required climb gradient. The flap setting increases from 9 degrees to 15 degrees, thus effecting a lower V_2 speed and a lower field length.

NOTES 1. STANDARD DAY
2. DOMESTIC OPERATION
3. CRUISE AT M = 0.82

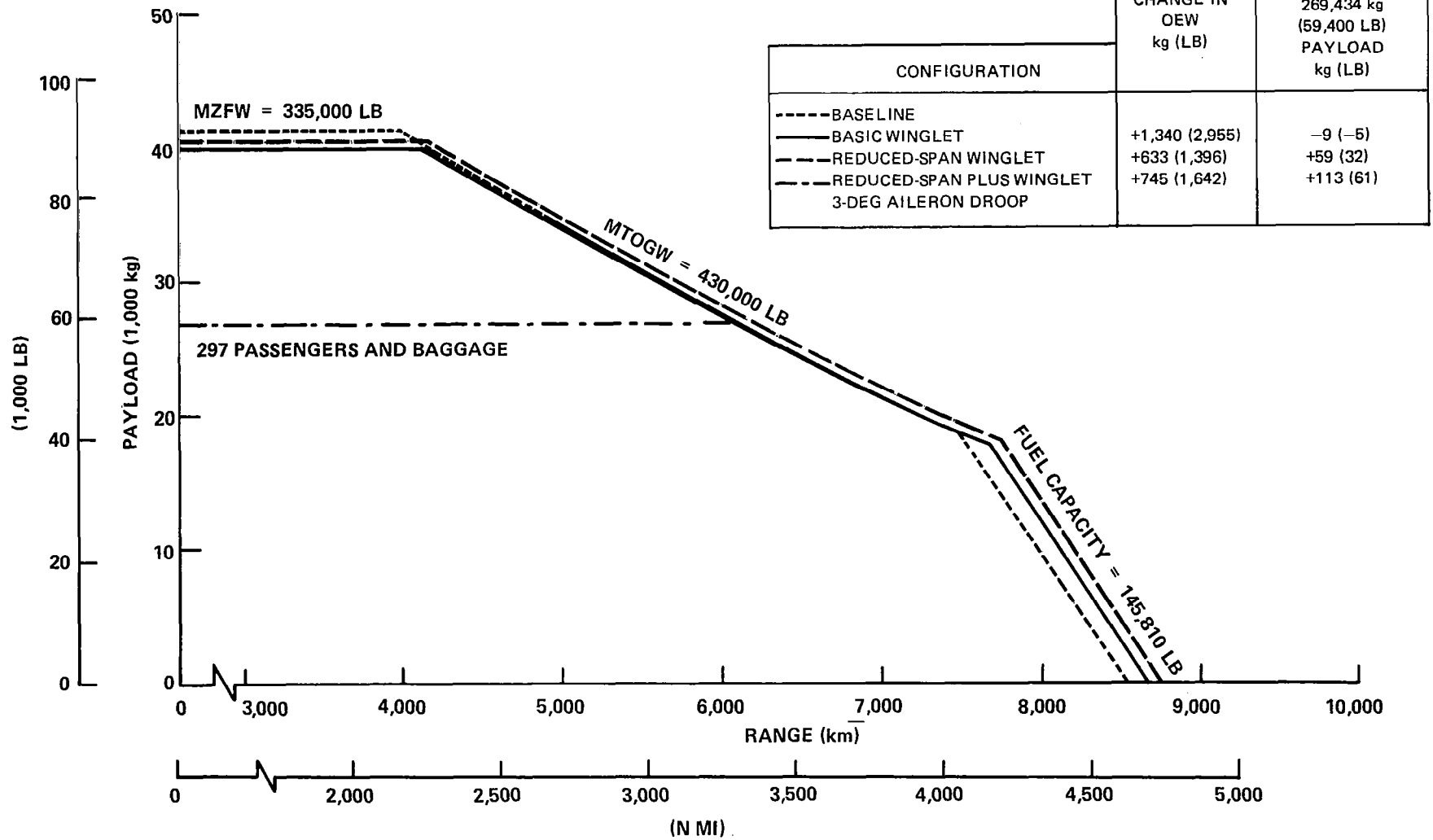


FIGURE 92. EFFECT OF WINGLET CONFIGURATIONS ON PAYLOAD RANGE

Fuel burn improvement versus range is shown in Figure 94. The basic and reduced-span winglets show about the same improvement, nearly 2 percent. While the basic winglet drag improvement is higher than that for the reduced-span winglet, the higher Δ OEW almost negates the added drag benefit. For only a small weight penalty, the drooped ailerons provided an additional 1-percent reduction in fuel burned.

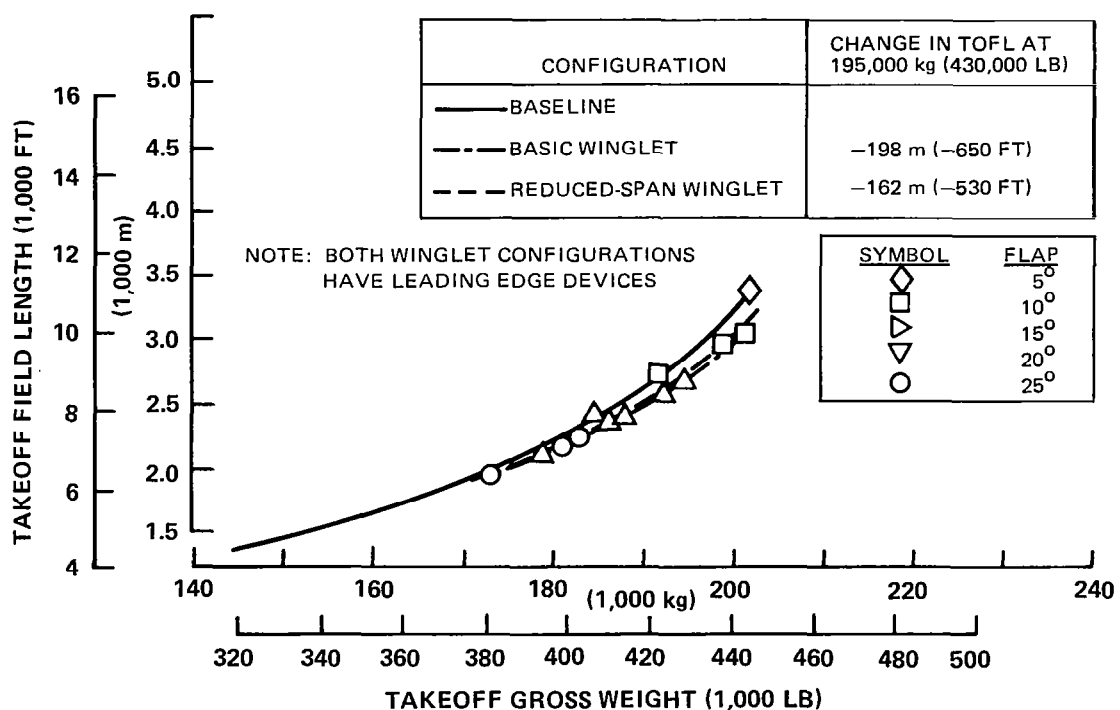


FIGURE 93. EFFECT OF WINGLET CONFIGURATIONS ON TAKEOFF FIELD LENGTH

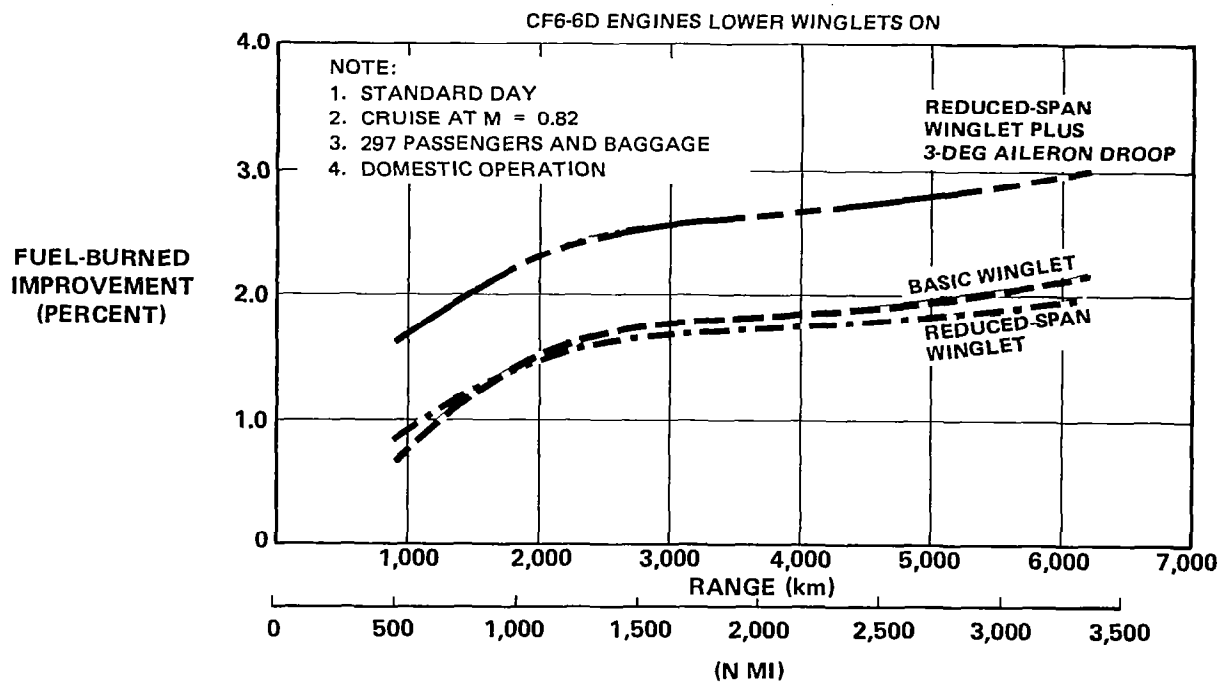


FIGURE 94. EFFECT OF WINGLET CONFIGURATIONS ON FUEL BURNED

CONCLUSIONS

A flight evaluation program was performed to determine the effects of winglets on a DC-10 aircraft. Two winglet spans (3.22 m and 2.13 m) were evaluated over the low-speed and high-speed flight envelope. Results derived from the comparison of the winglet and baseline (no winglet) phases of the flight test program lead to the following conclusions:

1. At typical cruise operating conditions the drag reduction was 2.5 percent for the basic winglet and 2.0 percent for the reduced-span winglet. This was about three-fourths of the predicted level derived from the wind tunnel tests.
2. Removal of the lower winglet significantly detracted from the cruise performance benefit, reducing the benefit by about 1 percent.
3. Drooping the outboard ailerons 3 degrees resulted in an additional cruise drag reduction of 1 percent (only tested on the reduced-span winglet).
4. Flow separation was experienced on the winglets in the low-speed high-lift configuration resulting in aircraft buffet for some configurations. A winglet leading edge device eliminated the flow separation.
5. For the basic winglet configurations evaluated, acceptable low-speed buffet/performance characteristics were achieved with a leading edge device on the upper winglet and the lower winglet removed. The low-speed-drag reduction for this configuration was in excess of 5 percent, which was better than expected.
6. For the reduced-span winglet, acceptable low-speed buffet characteristics were achieved with or without the winglet leading edge devices and with or without the lower winglet. The low-speed drag improvement was nearly 6 percent with the leading edge devices installed.
7. Removal of the leading edge devices and the lower winglet reduced the low-speed-drag improvement to 2 percent.
8. Stability and control characteristics, minimum stall speeds, and the high-speed buffet boundary were basically unchanged by the winglets.
9. Loads measurements were in good agreement with preflight estimates.
10. The flutter test did not reveal any unforeseen behavior, and the data showed good agreement with the ground vibration test and analysis data.

11. Application of the reduced-span winglet with aileron droop to a production DC-10 Series 10 is estimated to yield the following at maximum range:

- 3-percent reduction in fuel burned
- 113 km (61 n mi) increase in range
- 162 m (530 ft) reduction in takeoff field length

REFERENCES

1. Whitcomb, R. T.: A Design Approach and Selected Wind-Tunnel Results at High Subsonic Speeds for Wing-Tip-Mounted Winglets. NASA TN D-8260, July 1976.
2. Gilkey, R. D.: Design and Wind Tunnel Tests of Winglets on a DC-10 Wing. NASA CR-3119, April 1979.
3. Shollenberger, C. A.; Humphreys, J. W.; Heiberger, F. S.; and Pearson, R. M.: Results of Winglet Development Studies for DC-10 Derivatives. NASA CR-3677, March 1983.
4. Skopinski, T. H.; Aiken, W. S. Jr.; and Huston, W. B.: Calibration of Strain-Gauge Installations in Aircraft Structures for Measurement of Flight Loads. NACA Report 1178, 1954.

APPENDIX A
FLIGHT TEST MEASUREMENT INDEX

MEAS NUMBER	MEAS	MEASUREMENT DESCRIPTION		MEAS RANGE	MEAS RESOLUT	MEAS UNIT
210402	PRESS	CABIN PRESSURE		3,15	0.015/CT	SUB PSIA
221008	POSIT	LHIB ELEVATOR RAM PISTON POSITION		+28DEG	.06DEG/CT	PRI DEG
221012	RATE	PITCH RATE DERIVED (AFCS 1A)		+20DPS	.09DPS/CT	SUB DPS
221045	POSIT	LHOB FLAP POSITION (AFCS-1)		0-50	.05DEG/CT	PRI DEG
221059	POSIT	LHIB AILERON RAM PISTON POSITION	AFCS R/C-1	+20DEG	.04DEG/CT	PRI DEG
221062	RATE	ROLL RATE (AFCS 1A)		+20DPS	.09DPS/CT	SUB DPS
221100	RATE	YAW RATE (AFCS 1A)		+20DPS	.07DPS/CT	SUB DPS
221104	POSIT	LOWER RUDDER RAM PISTON POSITION		+24DEG	.05DEG/CT	PRI DEG
221361	POSIT	HORIZONTAL STABILIZER POSITION AT/SC		-5+15	.02DEG/CT	PRI DEG
222059	POSIT	RHOB AILERON RAM PISTON POSITION		+20DEG	.04DEG/CT	PRI DEG
223008	POSIT	RHIB ELEVATOR RAM PISTON POSITION		+28DEG	.06DEG/CT	PRI DEG
223059	POSIT	RHIB AILERON RAM PISTON POSITION	AFCS R/C-2	+20DEG	.04DEG/CT	PRI DEG
224059	POSIT	LHOB AILERON RAM PISTON POSITION		+20DEG	.04DEG/CT	PRI DEG
270102	POSN	AILERON WHEEL POSITION		+120	0.25/CT	PRI DEG
270104	FORCE	AILERON WHEEL FORCE		+50	0.1 LB/CT	PRI LBS
270301	POSN	ELEVATOR COLUMN POSITION		+20	0.04/CT	PRI DEG
270303	FORCE	ELEVATOR COLUMN FORCE		+100	0.21B/CT	PRI LBS
270352	DISCR	PILOT'S STICK SHAKER		ON/OFF		
270451	POSIT	HORIZONTAL STABILIZER POSITION		-2,15	.02DEG/CT	SUB DEG
270600	POSIT	LHOB SPOILER POSITION L5		60/0	.1DEG/CT	SUB
270602	POSIT	LHOB SPOILER POSITION L3		60/0	.1DEG/CT	SUB
270607	POSIT	RHOB SPOILER POSITION R3		60/0	.1DEG/CT	SUB
270609	POSIT	RHOB SPOILER POSITION R5		60/0	.1DEG/CT	SUB
270801	DISCR	SLATS EXTENDED TAKEOFF POSITION		ON-OFF		

MEAS NUMBER	MEAS	MEASUREMENT DESCRIPTION	MEAS RANGE	MEAS RESOLUT	MEAS UNIT
270803	DISCR	SLATS EXTENDED LANDING POSITION	ON-OFF		
271355	ANGLE	ANGLE OF ATTACK LOCAL LH (PROD)	-10,50	.06DEG/CT	PRI DEG
272355	ANGLE	ANGLE OF ATTACK LOCAL RH (PROD)	-10,50	.06DEG/CT	PRI DEG
340021	PRESS	AUX PITOT TOTAL PRESSURE	0,40	0.001	PRI INHG
340451	SPEED	INS GROUND SPEED - INS	0,600	0.1/CT	PRI KNOT
340452	SPEED	INS WIND SPEED - INS	0,200	0.1	SUB KNOT
340453	ANGLE	INS WIND DIRECTION - INS	0,360	0.1	SUB DEG
340455	SPEED	INS NORTH/SOUGHT VELOCITY - INS	-600,600	0.1	PRI KNOT
340456	SPEED	INS EAST/WEST VELOCITY - INS	-600,600	0.1	PRI KNOT
341005	PRESS	CAPTAIN'S STATIC PRESSURE	0,30	0.0005	PRI INHG
341006	PRESS	CAPTAIN'S PITOT TOTAL PRESSURE	0,40	0.001	PRI INHG
341150	TEMP	CAPTAIN'S TOTAL AIR TEMPERATURE - PROD ADC 1	-60,60	0.125/CT	SUB DEGC
341151	TEMP	CAPTAIN'S STATIC AIR TEMPERATURE	-60,60	0.125/CT	SUB DEGC
341161	MACH	CAPTAIN'S MACH NUMBER	0/1	.001	PRI MACH
341164	ALTDE	CAPT'S ALTITUDE	0,50000	1.0/CT	PRI FEET
341166	ARSPD	CAPT'S AIRSPEED	0,450	0.1/CT	PRI KNOT
341430	ATTIT	INS PITCH ATTITUDE - INS	+40,-25	0.1	PRI DEG
341431	ATTIT	INS ROLL ATTITUDE - INS	-40,40	0.1	PRI DEG
341432	ANGLE	INS TRUE HEADING - INS	0,360	0.1	SUB DEG
342005	PRESS	FIRST OFFICER'S STATIC PRESSURE	0,30	0.0005	PRI INHG
342006	PRESS	FIRST OFFICER'S PITOT TOTAL PRESSURE	0,40	0.001	PRI INHG
342151	TEMP	FIRST OFFICER'S STATIC AIR TEMPERATURE	-60,60	0.125/CT	SUB DEGC
342164	ALTDE	FIRST OFFICER'S ALTITUDE	0,50000	1.0/CT	PRI INHG
342166	ARSPD	FIRST OFFICER'S AIRSPEED	0,450	0.1/CT	PRI INHG

MEAS NUMBER	MEAS	MEASUREMENT DESCRIPTION	MEAS RANGE	MEAS RESOLUT	MEAS UNIT
349011	PRESS	AUX PITOT VS T/C STATIC CALIBRATE PRESSURE			
349012	PRESS	AUX PITOT VS T/C STATIC CALIBRATE PRESSURE			
349013	PRESS	AUX PITOT VS T/C STATIC CALIBRATE PRESSURE			
349021	PRESS	AUX PITOT VS T/C STATIC CALIBRATE PRESSURE			
349022	PRESS	AUX PITOT VS T/C STATIC CALIBRATE PRESSURE			
349023	PRESS	AUX PITOT VS T/C STATIC CALIBRATE PRESSURE			
349031	PRESS	AUX PITOT VS T/C STATIC CALIBRATE PRESSURE			
349032	PRESS	AUX PITOT VS T/C STATIC CALIBRATE PRESSURE			
349033	PRESS	AUX PITOT VS T/C STATIC CALIBRATE PRESSURE			
349041	PRESS	AUX PITOT VS T/C STATIC CALIBRATE PRESSURE			
349042	PRESS	AUX PITOT VS T/C STATIC CALIBRATE PRESSURE			
349043	PRESS	AUX PITOT VS T/C STATIC CALIBRATE PRESSURE			
349921	PRESS	AUX TOTAL PRESSURE MEASURED IN WINGLET	5/40	.001/CT	SUB INHG
543000	ACCEL	NO3 ENGINE FWD NORMAL ACCEL	+18G	.04G'S	PRI
543001	ACCEL	NO3 ENGINE FWD LATERAL ACCEL	+3G	.04G'S	PRI
551099	ACCEL	LH HORIZONTAL STABILIZER TIP NORMAL ACCEL FRONT SPAR	+25G	.05G	PRI
551104	ACCEL	LH OB ELEVATOR BALANCE WEIGHT NORMAL ACCEL	+35G	.07G	PRI
552099	ACCEL	RH HORIZONTAL STABILIZER TIP NORMAL ACCEL FRONT SPAR	+25G	.05G	PRI
552104	ACCEL	RH OB ELEVATOR BALANCE WEIGHT NORMAL ACCEL	+35G	.07G	PRI
556113	ACCEL	VERTICAL STABILIZER TIP LATERAL ACCEL	+15G	.03G	PRI
571001	ACCEL	LH WING TIP FRONT SPAR NORMAL ACCEL	+18G	.04G'S	PRI
572001	ACCEL	RH WING TIP FRONT SPAR NORMAL ACCEL	+18G	.04G'S	PRI
572004	ACCEL	RH WING TIP REAR SPAR NORMAL ACCEL	+18G	.04G'S	PRI
572379	LOAD	RH OTBD AIL HINGE NO4 BRACKET STRAIN GAGE UPPER LEG-PRIMARY	+25KSI	.03KSI/CT	PRI KSI

MEAS NUMBER	MEAS	MEASUREMENT DESCRIPTION	MEAS RANGE	MEAS RESOLUT	MEAS UNIT
572380	LOAD	RH OTBD AIL HINGE NO4 BRACKET STRAIN GAGE UPPER LEG-SPARE	+25KSI	.03KSI/CT	SUB KSI
572381	LOAD	RH OTBD AIL HINGE NO4 BRACKET STRAIN GAGE LOWER LEG-PRIMARY	+25KSI	.03KSI/CT	PRI KSI
572382	LOAD	RH OTBBD AIL HINGE NO4 BRACKET STRAIN GAGE LOWER LEG-SPARE	+25KSI	.03KSI/CT	SUB KSI
572383	LOAD	RH OTBD AIL ACTIVATOR PISTON AXIAL LOAD PRIMARY	+15000LB	30LBS/CT	PRI LBS
572384	LOAD	RH OTBD AIL ACTIVATOR PISTON AXIAL LOAD SPARE	+15000LB	30LBS/CT	SUB LBS
576000	PRESS	PRESSURE ORIFICE WING LE 97.4PCT SEMISPAN 0PCT CHORD			
576001	PRESS	PRESSURE ORIFICE WING TOP 97.4PCT SEMISPAN 1.25PCT CHORD			
576002	PRESS	PRESSURE ORIFICE WING TOP 97.4PCT SEMISPAN 3.50PCT CHORD			
576003	PRESS	PRESSURE ORIFICE WING TOP 97.4PCT SEMISPAN 5.00PCT CHORD			
576004	PRESS	PRESSURE ORIFICE WING TOP 97.4PCT SEMISPAN 10.4PCT CHORD			
576005	PRESS	PRESSURE ORIFICE WING TOP 97.4PCT SEMISPAN 13.8PCT CHORD			
576006	PRESS	PRESSURE ORIFICE WING TOP 97.4PCT SEMISPAN 17.5PCT CHORD			
576007	PRESS	PRESSURE ORIFICE WING TOP 97.4PCT SEMISPAN 24.8PCT CHORD			
576008	PRESS	PRESSURE ORIFICE WING TOP 97.4PCT SEMISPAN 30.2PCT CHORD			
576009	PRESS	PRESSURE ORIFICE WING TOP 97.4PCT SEMISPAN 39.3PCT CHORD			
576010	PRESS	PRESSURE ORIFICE WING TOP 97.4PCT SEMISPAN 48.8PCT CHORD			
576011	PRESS	PRESSURE ORIFICE WING TOP 97.4PCT SEMISPAN 59.1PCT CHORD			
576012	PRESS	PRESSURE ORIFICE WING TOP 97.4PCT SEMISPAN 73.6PCT CHORD			
576013	PRESS	PRESSURE ORIFICE WING TOP 97.4PCT SEMISPAN 82.0PCT CHORD			
576014	PRESS	PRESSURE ORIFICE WING TOP 97.4PCT SEMISPAN 89.5PCT CHORD			
576015	PRESS	PRESSURE ORIFICE WING TOP 97.4PCT SEMISPAN 94.6PCT CHORD			
576016	PRESS	PRESSURE ORIFICE WING TE 97.4PCT SEMISPAN 100PCT CHORD			
576017	PRESS	PRESSURE ORIFICE WING BOT 97.4PCT SEMISPAN 1.25PCT CHORD			
576018	PRESS	PRESSURE ORIFICE WING BOT 97.4PCT SEMISPAN 3.50PCT CHORD			

MEAS NUMBER	MEAS	MEASUREMENT DESCRIPTION	MEAS RANGE	MEAS RESOLUT	MEAS UNIT
576019	PRESS	PRESSURE ORIFICE WING BOT 97.4PCT SEMISPAN 5.00PCT CHORD			
576020	PRESS	PRESSURE ORIFICE WING BOT 97.4PCT SEMISPAN 10.4PCT CHORD			
576021	PRESS	PRESSURE ORIFICE WING BOT 97.4PCT SEMISPAN 13.8PCT CHORD			
576022	PRESS	PRESSURE ORIFICE WING BOT 97.4PCT SEMISPAN 24.8PCT CHORD			
576023	PRESS	PRESSURE ORIFICE WING BOT 97.4PCT SEMISPAN 30.2PCT CHORD			
576024	PRESS	PRESSURE ORIFICE WING BOT 97.4PCT SEMISPAN 39.3PCT CHORD			
576025	PRESS	PRESSURE ORIFICE WING BOT 97.4PCT SEMISPAN 48.8PCT CHORD			
576026	PRESS	PRESSURE ORIFICE WING BOT 97.4PCT SEMISPAN 59.1PCT CHORD			
576027	PRESS	PRESSURE ORIFICE WING BOT 97.4PCT SEMISPAN 73.6PCT CHORD			
576028	PRESS	PRESSURE ORIFICE WING BOT 97.4PCT SEMISPAN 82.0PCT CHORD			
576029	PRESS	PRESSURE ORIFICE WING BOT 97.4PCT SEMISPAN 89.5PCT CHORD			
576030	PRESS	PRESSURE ORIFICE WING BOT 97.4PCT SEMISPAN 94.6PCT CHORD			
576031	PRESS	PRESSURE ORIFICE WINGLET LE 12.5PCT SPAN 0PCT CHORD			
576032	PRESS	PRESSURE ORIFICE WINGLET INBRD 12.5PCT SPAN 1.25PCT CHORD			
576033	PRESS	PRESSURE ORIFICE WINGLET INBRD 12.5PCT SPAN 3.00PCT CHORD			
576034	PRESS	PRESSURE ORIFICE WINGLET INBRD 12.5PCT SPAN 7.60PCT CHORD			
576035	PRESS	PRESSURE ORIFICE WINGLET INBRD 12.5PCT SPAN 14.8PCT CHORD			
576036	PRESS	PRESSURE ORIFICE WINGLET INBRD 12.5PCT SPAN 20.0PCT CHORD			
576037	PRESS	PRESSURE ORIFICE WINGLET INBRD 12.5PCT SPAN 26.0PCT CHORD			
576038	PRESS	PRESSURE ORIFICE WINGLET INBRD 12.5PCT SPAN 30.0PCT CHORD			
576039	PRESS	PRESSURE ORIFICE WINGLET INBRD 12.5PCT SPAN 39.0PCT CHORD			
576040	PRESS	PRESSURE ORIFICE WINGLET INBRD 12.5PCT SPAN 44.0PCT CHORD			
576041	PRESS	PRESSURE ORIFICE WINGLET INBRD 12.5PCT SPAN 56.0PCT CHORD			
576042	PRESS	PRESSURE ORIFICE WINGLET INBRD 12.5PCT SPAN 60.0PCT CHORD			

MEAS NUMBER	MEAS	MEASUREMENT DESCRIPTION	MEAS RANGE	MEAS RESOLUT	MEAS UNIT
576043	PRESS	PRESSURE ORIFICE WINGLET INBRD 12.5PCT SPAN 63.0PCT CHORD			
576044	PRESS	PRESSURE ORIFICE WINGLET INBRD 12.5PCT SPAN 73.0PCT CHORD			
576045	PRESS	PRESSURE ORIFICE WINGLET INBRD 12.5PCT SPAN 82.0PCT CHORD			
576046	PRESS	PRESSURE ORIFICE WINGLET INBRD 12.5PCT SPAN 91.0PCT CHORD			
576047	PRESS	PRESSURE ORIFICE WINGLET INBRD 12.5PCT SPAN 95.0PCT CHORD			
576048	PRESS	PRESSURE ORIFICE WINGLET TE 12.5PCT SPAN 100PCT CHORD			
576049	PRESS	PRESSURE ORIFICE WINGLET OUTBRD 12.5PCT SPAN 1.25PCT CHORD			
576050	PRESS	PRESSURE ORIFICE WINGLET OUTBRD 12.5PCT SPAN 3.00PCT CHORD			
576051	PRESS	PRESSURE ORIFICE WINGLET OUTBRD 12.5PCT SPAN 7.60PCT CHORD			
576052	PRESS	PRESSURE ORIFICE WINGLET OUTBRD 12.5PCT SPAN 17.2PCT CHORD			
576053	PRESS	PRESSURE ORIFICE WINGLET OUTBRD 12.5PCT SPAN 20.0PCT CHORD			
576054	PRESS	PRESSURE ORIFICE WINGLET OUTBRD 12.5PCT SPAN 26.0PCT CHORD			
576055	PRESS	PRESSURE ORIFICE WINGLET OUTBRD 12.5PCT SPAN 30.0PCT CHORD			
576056	PRESS	PRESSURE ORIFICE WINGLET OUTBRD 12.5PCT SPAN 39.0PCT CHORD			
576057	PRESS	PRESSURE ORIFICE WINGLET OUTBRD 12.5PCT SPAN 44.0PCT CHORD			
576058	PRESS	PRESSURE ORIFICE WINGLET OUTBRD 12.5PCT SPAN 56.0PCT CHORD			
576059	PRESS	PRESSURE ORIFICE WINGLET OUTBRD 12.5PCT SPAN 60.0PCT CHORD			
576060	PRESS	PRESSURE ORIFICE WINGLET OUTBRD 12.5PCT SPAN 63.0PCT CHORD			
576061	PRESS	PRESSURE ORIFICE WINGLET OUTBRD 12.5PCT SPAN 73.0PCT CHORD			
576062	PRESS	PRESSURE ORIFICE WINGLET OUTBRD 12.5PCT SPAN 82.0PCT CHORD			
576063	PRESS	PRESSURE ORIFICE WINGLET OUTBRD 12.5PCT SPAN 91.0PCT CHORD			
576064	PRESS	PRESSURE ORIFICE WINGLET OUTBRD 12.5PCT SPAN 95.0PCT CHORD			
576065	PRESS	PRESSURE ORIFICE WINGLET TE 25PCT SPAN 100PCT CHORD			
576066	PRESS	PRESSURE ORIFICE WINGLET LE 40PCT SPAN 0PCT CHORD			

MEAS NUMBER	MEAS	MEASUREMENT DESCRIPTION	MEAS RANGE	MEAS RESOLUT	MEAS UNIT
576067	PRESS	PRESSURE ORIFICE WINGLET INBRD 40PCT SPAN 1.25PCT CHORD			
576068	PRESS	PRESSURE ORIFICE WINGLET INBRD 40PCT SPAN 3.00PCT CHORD			
576069	PRESS	PRESSURE ORIFICE WINGLET INBRD 40PCT SPAN 8.00PCT CHORD			
576070	PRESS	PRESSURE ORIFICE WINGLET INBRD 40PCT SPAN 14.3PCT CHORD			
576071	PRESS	PRESSURE ORIFICE WINGLET INBRD 40PCT SPAN 18.0PCT CHORD			
576072	PRESS	PRESSURE ORIFICE WINGLET INBRD 40PCT SPAN 20.0PCT CHORD			
576073	PRESS	PRESSURE ORIFICE WINGLET INBRD 40PCT SPAN 23.0PCT CHORD			
576074	PRESS	PRESSURE ORIFICE WINGLET INBRD 40PCT SPAN 36.5PCT CHORD			
576075	PRESS	PRESSURE ORIFICE WINGLET INBRD 40PCT SPAN 45.0PCT CHORD			
576076	PRESS	PRESSURE ORIFICE WINGLET INBRD 40PCT SPAN 57.0PCT CHORD			
576077	PRESS	PRESSURE ORIFICE WINGLET INBRD 40PCT SPAN 67.0PCT CHORD			
576078	PRESS	PRESSURE ORIFICE WINGLET INBRD 40PCT SPAN 80.0PCT CHORD			
576079	PRESS	PRESSURE ORIFICE WINGLET INBRD 40PCT SPAN 90.0PCT CHORD			
576080	PRESS	PRESSURE ORIFICE WINGLET INBRD 40PCT SPAN 95.0PCT CHORD			
576081	PRESS	PRESSURE ORIFICE WINGLET TE 40PCT SPAN 100PCT CHORD			
576082	PRESS	PRESSURE ORIFICE WINGLET OUTBRD 40PCT SPAN 1.25PCT CHORD			
576083	PRESS	PRESSURE ORIFICE WINGLET OUTBRD 40PCT SPAN 3.00PCT CHORD			
576084	PRESS	PRESSURE ORIFICE WINGLET OUTBRD 40PCT SPAN 8.00PCT CHORD			
576085	PRESS	PRESSURE ORIFICE WINGLET OUTBRD 40PCT SPAN 16.4PCT CHORD			
576086	PRESS	PRESSURE ORIFICE WINGLET OUTBRD 40PCT SPAN 18.0PCT CHORD			
576087	PRESS	PRESSURE ORIFICE WINGLET OUTBRD 40PCT SPAN 20.0PCT CHORD			
576088	PRESS	PRESSURE ORIFICE WINGLET OUTBRD 40PCT SPAN 23.0PCT CHORD			
576089	PRESS	PRESSURE ORIFICE WINGLET OUTBRD 40PCT SPAN 36.5PCT CHORD			
576090	PRESS	PRESSURE ORIFICE WINGLET OUTBRD 40PCT SPAN 45.0PCT CHORD			

MEAS NUMBER	MEAS	MEASUREMENT DESCRIPTION	MEAS RANGE	MEAS RESOLUT	MEAS UNIT
576091	PRESS	PRESSURE ORIFICE WINGLET OUTBRD 40PCT SPAN 57.0PCT CHORD			
576092	PRESS	PRESSURE ORIFICE WINGLET CUTBRD 40PCT SPAN 67.0PCT CHORD			
576093	PRESS	PRESSURE ORIFICE WINGLET OUTBRD 40PCT SPAN 80.0PCT CHORD			
576094	PRESS	PRESSURE ORIFICE WINGLET OUTBRD 40PCT SPAN 90.0PCT CHORD			
576095	PRESS	PRESSURE ORIFICE WINGLET CUTBRD 40PCT SPAN 95.0PCT CHORD			
576096	PRESS	PRESSURE ORIFICE WINGLET TE 48PCT SPAN 100PCT CHORD			
576100	PRESS	PRESSURE ORIFICE WINGLET LE 57PCT SPAN 0PCT CHORD			
576101	PRESS	PRESSURE ORIFICE WINGLET INBRD 57PCT SPAN 1.25PCT CHORD			
576102	PRESS	PRESSURE ORIFICE WINGLET INBRD 57PCT SPAN 3.00PCT CHORD			
576103	PRESS	PRESSURE ORIFICE WINGLET INBRD 57PCT SPAN 7.50PCT CHORD			
576104	PRESS	PRESSURE ORIFICE WINGLET INBRD 57PCT SPAN 13.9PCT CHORD			
576105	PRESS	PRESSURE ORIFICE WINGLET INBRD 57PCT SPAN 18.0PCT CHORD			
576106	PRESS	PRESSURE ORIFICE WINGLET INBRD 57PCT SPAN 20.0PCT CHORD			
576107	PRESS	PRESSURE ORIFICE WINGLET INBRD 57PCT SPAN 26.0PCT CHORD			
576108	PRESS	PRESSURE ORIFICE WINGLET INBRD 57PCT SPAN 35.0PCT CHORD			
576109	PRESS	PRESSURE ORIFICE WINGLET INBRD 57PCT SPAN 45.0PCT CHORD			
576110	PRESS	PRESSURE ORIFICE WINGLET INBRD 57PCT SPAN 57.0PCT CHORD			
576111	PRESS	PRESSURE ORIFICE WINGLET INBRD 57PCT SPAN 67.0PCT CHORD			
576112	PRESS	PRESSURE CRIFICE WINGLET INBRD 57PCT SPAN 82.0PCT CHORD			
576113	PRESS	PRESSURE ORIFICE WINGLET INBRD 57PCT SPAN 90.0PCT CHORD			
576114	PRESS	PRESSURE ORIFICE WINGLET INBRD 57PCT SPAN 95.0PCT CHORD			
576115	PRESS	PRESSURE ORIFICE WINGLET TE 57PCT SPAN 100PCT CHORD			
576116	PRESS	PRESSURE ORIFICE WINGLET CUTBRD 57PCT SPAN 1.25PCT CHORD			
576117	PRESS	PRESSURE ORIFICE WINGLET CUTBRD 57PCT SPAN 3.00PCT CHORD			

MEAS NUMBER	MEAS	MEASUREMENT DESCRIPTION	MEAS RANGE	MEAS RESOLUT	MEAS UNIT
576118	PRESS	PRESSURE ORIFICE WINGLET OUTBRD 57PCT SPAN 7.50PCT CHORD			
576119	PRESS	PRESSURE ORIFICE WINGLET OUTBRD 57PCT SPAN 15.7PCT CHORD			
576120	PRESS	PRESSURE ORIFICE WINGLET OUTBRD 57PCT SPAN 18.0PCT CHORD			
576121	PRESS	PRESSURE ORIFICE WINGLET OUTBRD 57PCT SPAN 20.0PCT CHORD			
576122	PRESS	PRESSURE ORIFICE WINGLET OUTBRD 57PCT SPAN 26.0PCT CHORD			
576123	PRESS	PRESSURE ORIFICE WINGLET OUTBRD 57PCT SPAN 35.0PCT CHORD			
576124	PRESS	PRESSURE ORIFICE WINGLET OUTBRD 57PCT SPAN 45.0PCT CHORD			
576125	PRESS	PRESSURE ORIFICE WINGLET OUTBRD 57PCT SPAN 57.0PCT CHORD			
576126	PRESS	PRESSURE ORIFICE WINGLET OUTBRD 57PCT SPAN 67.0PCT CHORD			
576127	PRESS	PRESSURE ORIFICE WINGLET OUTBRD 57PCT SPAN 82.0PCT CHORD			
576128	PRESS	PRESSURE ORIFICE WINGLET OUTBRD 57PCT SPAN 90.0PCT CHORD			
576129	PRESS	PRESSURE ORIFICE WINGLET OUTBRD 57PCT SPAN 95.0PCT CHORD			
576130	PRESS	PRESSURE ORIFICE WINGLET LE 80PCT SPAN 0PCT CHORD			
576131	PRESS	PRESSURE ORIFICE WINGLET INBRD 80PCT SPAN 1.25PCT CHORD			
576132	PRESS	PRESSURE ORIFICE WINGLET INBRD 80PCT SPAN 3.00PCT CHORD			
576133	PRESS	PRESSURE ORIFICE WINGLET INBRD 80PCT SPAN 6.80PCT CHORD			
576134	PRESS	PRESSURE ORIFICE WINGLET INBRD 80PCT SPAN 14.3PCT CHORD			
576135	PRESS	PRESSURE ORIFICE WINGLET INBRD 80PCT SPAN 18.0PCT CHORD			
576136	PRESS	PRESSURE ORIFICE WINGLET INBRD 80PCT SPAN 27.0PCT CHORD			
576137	PRESS	PRESSURE ORIFICE WINGLET INBRD 80PCT SPAN 33.0PCT CHORD			
576138	PRESS	PRESSURE ORIFICE WINGLET INBRD 80PCT SPAN 40.0PCT CHORD			
576139	PRESS	PRESSURE ORIFICE WINGLET INBRD 80PCT SPAN 45.0PCT CHORD			
576140	PRESS	PRESSURE ORIFICE WINGLET INBRD 80PCT SPAN 60.0PCT CHORD			
576141	PRESS	PRESSURE ORIFICE WINGLET INBRD 80PCT SPAN 69.0PCT CHORD			

MEAS NUMBER	MEAS	MEASUREMENT DESCRIPTION	MEAS RANGE	MEAS RESOLUT	MEAS UNIT
576142	PRESS	PRESSURE ORIFICE WINGLET INBRD 80PCT SPAN 78.0PCT CHORD			
576143	PRESS	PRESSURE ORIFICE WINGLET INBRD 80PCT SPAN 90.0PCT CHORD			
576144	PRESS	PRESSURE ORIFICE WINGLET INBRD 80PCT SPAN 95.0PCT CHORD			
576145	PRESS	PRESSURE ORIFICE WINGLET TE 80PCT SPAN 100PCT CHORD			
576146	PRESS	PRESSURE ORIFICE WINGLET OUTBRD 80PCT SPAN 1.25PCT CHORD			
576147	PRESS	PRESSURE ORIFICE WINGLET OUTBRD 80PCT SPAN 3.00PCT CHORD			
576148	PRESS	PRESSURE ORIFICE WINGLET OUTBRD 80PCT SPAN 6.00PCT CHORD			
576149	PRESS	PRESSURE ORIFICE WINGLET OUTBRD 80PCT SPAN 14.9PCT CHORD			
576150	PRESS	PRESSURE ORIFICE WINGLET OUTBRD 80PCT SPAN 18.0PCT CHORD			
576151	PRESS	PRESSURE ORIFICE WINGLET OUTBRD 80PCT SPAN 27.0PCT CHORD			
576152	PRESS	PRESSURE ORIFICE WINGLET OUTBRD 80PCT SPAN 33.0PCT CHORD			
576153	PRESS	PRESSURE ORIFICE WINGLET OUTBRD 80PCT SPAN 40.0PCT CHORD			
576154	PRESS	PRESSURE ORIFICE WINGLET OUTBRD 80PCT SPAN 45.0PCT CHORD			
576155	PRESS	PRESSURE ORIFICE WINGLET OUTBRD 80PCT SPAN 60.0PCT CHORD			
576156	PRESS	PRESSURE ORIFICE WINGLET OUTBRD 80PCT SPAN 69.0PCT CHORD			
576157	PRESS	PRESSURE ORIFICE WINGLET OUTBRD 80PCT SPAN 78.0PCT CHORD			
576158	PRESS	PRESSURE ORIFICE WINGLET OUTBRD 80PCT SPAN 90.0PCT CHORD			
576159	PRESS	PRESSURE ORIFICE WINGLET OUTBRD 80PCT SPAN 95.0PCT CHORD			
576160	PRESS	PRESSURE ORIFICE WINGLET TE 70PCT SPAN 100PCT CHORD			
576161	PRESS	PRESSURE ORIFICE WINGLET LE 95PCT SPAN 0PCT CHORD			
576162	PRESS	PRESSURE ORIFICE WINGLET INBRD 95PCT SPAN 1.25PCT CHORD			
576163	PRESS	PRESSURE ORIFICE WINGLET INBRD 95PCT SPAN 3.00PCT CHORD			
576164	PRESS	PRESSURE ORIFICE WINGLET INBRD 95PCT SPAN 6.00PCT CHORD			
576165	PRESS	PRESSURE ORIFICE WINGLET INBRD 95PCT SPAN 15.1PCT CHORD			

MEAS NUMBER	MEAS	MEASUREMENT DESCRIPTION	MEAS RANGE	MEAS RESOLUT	MEAS UNIT
576166	PRESS	PRESSURE ORIFICE WINGLET INBRD 95PCT SPAN 20.0PCT CHORD			
576167	PRESS	PRESSURE ORIFICE WINGLET INBRD 95PCT SPAN 25.0PCT CHORD			
576168	PRESS	PRESSURE ORIFICE WINGLET INBRD 95PCT SPAN 30.0PCT CHORD			
576169	PRESS	PRESSURE ORIFICE WINGLET INBRD 95PCT SPAN 40.0PCT CHORD			
576170	PRESS	PRESSURE ORIFICE WINGLET INBRD 95PCT SPAN 43.0PCT CHORD			
576171	PRESS	PRESSURE ORIFICE WINGLET INBRD 95PCT SPAN 60.0PCT CHORD			
576172	PRESS	PRESSURE ORIFICE WINGLET INBRD 95PCT SPAN 70.0PCT CHORD			
576173	PRESS	PRESSURE ORIFICE WINGLET INBRD 95PCT SPAN 83.0PCT CHORD			
576174	PRESS	PRESSURE ORIFICE WINGLET INBRD 95PCT SPAN 88.0PCT CHORD			
576175	PRESS	PRESSURE ORIFICE WINGLET INBRD 95PCT SPAN 95.0PCT CHORD			
576176	PRESS	PRESSURE ORIFICE WINGLET TE 95PCT SPAN 100PCT CHORD			
576177	PRESS	PRESSURE ORIFICE WINGLET OUTBRD 95PCT SPAN 1.25PCT CHORD			
576178	PRESS	PRESSURE ORIFICE WINGLET OUTBRD 95PCT SPAN 3.00PCT CHORD			
576179	PRESS	PRESSURE ORIFICE WINGLET OUTBRD 95PCT SPAN 6.00PCT CHORD			
576180	PRESS	PRESSURE ORIFICE WINGLET OUTBRD 95PCT SPAN 15.5PCT CHORD			
576181	PRESS	PRESSURE ORIFICE WINGLET OUTBRD 95PCT SPAN 20.0PCT CHORD			
576182	PRESS	PRESSURE ORIFICE WINGLET OUTBRD 95PCT SPAN 25.0PCT CHORD			
576183	PRESS	PRESSURE ORIFICE WINGLET OUTBRD 95PCT SPAN 30.0PCT CHORD			
576184	PRESS	PRESSURE ORIFICE WINGLET OUTBRD 95PCT SPAN 40.0PCT CHORD			
576185	PRESS	PRESSURE ORIFICE WINGLET OUTBRD 95PCT SPAN 43.0PCT CHORD			
576186	PRESS	PRESSURE ORIFICE WINGLET OUTBRD 95PCT SPAN 60.0PCT CHORD			
576187	PRESS	PRESSURE ORIFICE WINGLET OUTBRD 95PCT SPAN 70.0PCT CHORD			
576188	PRESS	PRESSURE ORIFICE WINGLET OUTBRD 95PCT SPAN 83.0PCT CHORD			
576189	PRESS	PRESSURE ORIFICE WINGLET OUTBRD 95PCT SPAN 88.0PCT CHORD			

MEAS NUMBER	MEAS	MEASUREMENT DESCRIPTION	MEAS RANGE	MEAS RESOLUT	MEAS UNIT
576 190	PRESS	PRESSURE ORIFICE WINGLET OUTBRD 95PCT SPAN 95.0PCT CHORD			
576 191	PRESS	PRESSURE ORIFICE WING/WINGLET INNR JUNC 70PCT WINGLET CHORD			
576 192	PRESS	PRESSURE ORIFICE WING/WINGLET INNR JUNC 75PCT WINGLET CHORD			
576 193	PRESS	PRESSURE ORIFICE WING/WINGLET INNR JUNC 82.5PCT WINGLET CHORD			
576 194	PRESS	PRESSURE ORIFICE WING/WINGLET INNR JUNC 86PCT WINGLET CHORD			
576 195	PRESS	PRESSURE ORIFICE WING/WINGLET INNR JUNC 90PCT WINGLET CHORD			
576 196	PRESS	PRESSURE ORIFICE WING/WINGLET INNR JUNC 95PCT WINGLET CHORD			
576 197	PRESS	PRESSURE ORIFICE WING/WINGLET INNR JUNC 100PCT WINGLET CHORD			
576 200	PRESS	SCANIVALVE MODULE 1 HEAD 1 PRESSURES	+ -2.5 PSI		.005/CT
576 201	PRESS	SCANIVALVE MODULE 1 HEAD 2 PRESSURES	+ -2.5 PSI		.005/CT
576 202	PRESS	SCANIVALVE MODULE 1 HEAD 3 PRESSURES	+ -2.5 PSI		.005/CT
576 203	PRESS	SCANIVALVE MODULE 2 HEAD 1 PRESSURES	+ -2.5 PSI		.005/CT
576 204	PRESS	SCANIVALVE MODULE 2 HEAD 2 PRESSURES	+ -2.5 PSI		.005/CT
576 205	PRESS	SCANIVALVE MODULE 2 HEAD 3 PRESSURES	+ -2.5 PSI		.005/CT
576 206	PRESS	SCANIVALVE MODULE 3 HEAD 1 PRESSURES	+ -2.5 PSI		.005/CT
576 207	PRESS	SCANIVALVE MODULE 3 HEAD 2 PRESSURES	+ -2.5 PSI		.005/CT
576 208	PRESS	SCANIVALVE MODULE 3 HEAD 3 PRESSURES	+ -2.5 PSI		.005/CT
576 209	PRESS	SCANIVALVE MODULE 4 HEAD 1 PRESSURES	+ -2.5 PSI		.005/CT
576 210	PRESS	SCANIVALVE MODULE 4 HEAD 2 PRESSURES	+ -2.5 PSI		.005/CT
576 211	PRESS	SCANIVALVE MODULE 4 HEAD 3 PRESSURES	+ -2.5 PSI		.005/CT
576 212	INDEX	SCANIVALVE MODULE 1 PCRT COUNTER	1-24		1/CT
576 213	INDEX	SCANIVALVE MODULE 2 PORT COUNTER	1-24		1/CT
576 214	INDEX	SCANIVALVE MODULE 3 PCRT COUNTER	1-24		1/CT
576 215	INDEX	SCANIVALVE MODULE 4 PCRT COUNTER	1-24		1/CT

MEAS NUMBER	MEAS	MEASUREMENT DESCRIPTION	MEAS RANGE	MEAS RESOLUT	MEAS UNIT
576216	TEMP	SCANIVALVE MODULE 1 TEMPERATURE	0-300		1DEGF/CT
576217	TEMP	SCANIVALVE MODULE 2 TEMPERATURE	0-300		1DEGF/CT
576218	TEMP	SCANIVALVE MODULE 3 TEMPERATURE	0-300		1DEGF/CT
576219	TEMP	SCANIVALVE MODULE 4 TEMPERATURE	0-300		1DEGF/CT
576220	PRESS	PRESSURE ORIFICE AILERON TOP 82 PCT SEMISPAN 75.0 PCT WNG CRD			
576221	PRESS	PRESSURE ORIFICE AILERON TOP 82 PCT SEMISPAN 77.5 PCT WNG CRD			
576222	PRESS	PRESSURE ORIFICE AILERON TOP 82 PCT SEMISPAN 82.0 PCT WNG CRD			
576223	PRESS	PRESSURE ORIFICE AILERON TOP 82 PCT SEMISPAN 90.0 PCT WNG CRD			
576224	PRESS	PRESSURE ORIFICE AILERON TE 82 PCT SEMISPAN 100.0 PCT WNG CRD			
576225	PRESS	PRESSURE ORIFICE AILERON BOT 82 PCT SEMISPAN 75.0 PCT WNG CRD			
576226	PRESS	PRESSURE ORIFICE AILERON BOT 82 PCT SEMISPAN 77.5 PCT WNG CRD			
576227	PRESS	PRESSURE ORIFICE AILERON BOT 82 PCT SEMISPAN 82.0 PCT WNG CRD			
576228	PRESS	PRESSURE ORIFICE AILERON BOT 82 PCT SEMISPAN 90.0 PCT WNG CRD			
576229	PRESS	PRESSURE ORIFICE AILERON TOP 90 PCT SEMISPAN 75.0 PCT WNG CRD			
576230	PRESS	PRESSURE ORIFICE AILERON TOP 90 PCT SEMISPAN 77.5 PCT WNG CRD			
576231	PRESS	PRESSURE ORIFICE AILERON TOP 90 PCT SEMISPAN 82.0 PCT WNG CRD			
576232	PRESS	PRESSURE ORIFICE AILERON TOP 90 PCT SEMISPAN 90.0 PCT WNG CRD			
576233	PRESS	PRESSURE ORIFICE AILERON TE 90 PCT SEMISPAN 100.0 PCT WNG CRD			
576234	PRESS	PRESSURE ORIFICE AILERON BOT 90 PCT SEMISPAN 75.0 PCT WNG CRD			
576235	PRESS	PRESSURE ORIFICE AILERON BOT 90 PCT SEMISPAN 77.5 PCT WNG CRD			
576236	PRESS	PRESSURE ORIFICE AILERON BOT 90 PCT SEMISPAN 82.0 PCT WNG CRD			
576237	PRESS	PRESSURE ORIFICE AILERON BOT 90 PCT SEMISPAN 90.0 PCT WNG CRD			
576238	PRESS	PRESSURE ORIFICE UPPER AILERON WELL 90 PCT SEMISPAN			
576239	PRESS	PRESSURE ORIFICE LOWER AILERON WELL 90 PCT SEMISPAN			

MEAS NUMBER	MEAS	MEASUREMENT DESCRIPTION	MEAS RANGE	MEAS RESOLUT	MEAS UNIT
576301	LOAD	RH WINGLET FRNT SPAR AFT CAP ZRSWLU=6.0 BENDING GAGE 1	+2500mi/i4.7/ct		PRI
576303	LOAD	RH WINGLET FRNT SPAR AFT CAP ZRSWLU=6.0 BENDING GAGE 2	+2500mi/i4.7/ct		PRI
576305	LOAD	RH WINGLET FRNT SPAR AFT CAP ZRSWLU=6.0 BENDING GAGE 3	+2500mi/i4.7/ct		PRI
576307	LOAD	RH WINGLET FRNT SPAR AFT WEB ZRSWLU=6.0 SHEAR GAGE 1	+1000mi/i2/ct		PRI
576309	LOAD	RH WINGLET FRNT SPAR AFT WEB ZRSWLU=6.0 SHEAR GAGE 2	+1000mi/i2/ct		PRI
576311	LOAD	RH WINGLET FRNT SPAR AFT WEB ZRSWLU=6.0 SHEAR GAGE 3	+1000mi/i2/ct		PRI
576313	LOAD	RH WINGLET REAR SPAR FWD CAP ZRSWLU=6.0 BENDING GAGE 1	+2500mi/i4.7/ct		PRI
576315	LOAD	RH WINGLET REAR SPAR FWD CAP ZRSWLU=6.0 BENDING GAGE 2	+2500mi/i4.7/ct		PRI
576317	LOAD	RH WINGLET REAR SPAR FWD CAP ZRSWLU=6.0 BENDING GAGE 3	+2500mi/i4.7/ct		PRI
576319	LOAD	RH WINGLET REAR SPAR FWD WEB ZRSWLU=6.0 SHEAR GAGE 1	+1000mi/i2/ct		PRI
576321	LOAD	RH WINGLET REAR SPAR FWD WEB ZRSWLU=6.0 SHEAR GAGE 2	+1000mi/i2/ct		PRI
576323	LOAD	RH WINGLET REAR SPAR FWD WEB ZRSWLU=6.0 SHEAR GAGE 3	+1000mi/i2/ct		PRI
576327	STRES	RH WING XORS 522 FRNT SPAR UPPR OUTR CAP AXIAL	+20KSI	.04/CT	PRI KSI
576328	STRES	RH WING XORS 522 FRNT SPAR UPPR OUTR CAP AXIAL SP	+20KSI	.04/CT	PRI KSI
576329	STRES	RH WING XORS 522 FRNT SPAR LOWR OUTR CAP AXIAL	+20KSI	.04/CT	PRI KSI
576330	STRES	RH WING XORS 522 FRNT SPAR LOWR OUTR CAP AXIAL SP	+20KSI	.04/CT	PRI KSI
576331	STRES	RH WING XORS 522 REAR SPAR UPPR OUTR CAP AXIAL	+20KSI	.04/CT	PRI KSI
576332	STRES	RH WING XORS 522 REAR SPAR UPPR OUTR CAP AXIAL SP	+20KSI	.04/CT	PRI KSI
576333	STRES	RH WING XORS 522 REAR SPAR LOWR OUTR CAP AXIAL	+20KSI	.04/CT	PRI KSI
576334	STRES	RH WING XORS 522 REAR SPAR LOWR OUTR CAP AXIAL SP	+20KSI	.04/CT	PRI KSI
576335	STRES	RH WING XORS 522 NO9 UPPR STRINGER OUTR SKN AXIAL	+20KSI	.04/CT	PRI KSI
576336	STRES	RH WING XORS 522 NO9 UPPR STRINGER OUTR SKN AXIAL SP	+20KSI	.04/CT	PRI KSI
576337	STRES	RH WING XORS 522 NO36 LOWR STRINGER OUTR SKN AXIAL	+20KSI	.04/CT	PRI KSI
576338	STRES	RH WING XORS 522 NO36 LOWR STRINGER OUTR SKN AXIAL SP	+20KSI	.04/CT	PRI KSI

MEAS NUMBER	MEAS	MEASUREMENT DESCRIPTION	MEAS RANGE	MEAS RESOLUT	MEAS UNIT
576339	STRES	RH WING XORS 522 FRNT SPAR WEB OUTR SURF SHEAR	+20KSI	.04/CT	PRI KSI
576340	STRES	RH WING XORS 522 FRNT SPAR WEB OUTR SURF SHEAR SP	+20KSI	.04/CT	PRI KSI
576341	STRES	RH WING XORS 522 REAR SPAR WEB OUTR SURF SHEAR	+5KSI	.02/CT	PRI KSI
576342	STRES	RH WING XORS 522 REAR SPAR WEB OUTR SURF SHEAR SP	+5KSI	.02/CT	PRI KSI
576343	STRES	RH WING XORS 815 FRNT SPAR UPPR OUTR CAP AXIAL	+24KSI	.048/CT	PRI KSI
576344	STRES	RH WING XORS 815 FRNT SPAR UPPR OUTR CAP AXIAL SP	+24KSI	.048/CT	PRI KSI
576345	STRES	RH WING XORS 815 TRNT SPAR LOWR OUTR CAP AXIAL	+30KSI	.097/CT	PRI KSI
576346	STRES	RH WING XORS 815 FRNT SPAR LOWR OUTR CAP AXIAL SP	+30KSI	.097/CT	PRI KSI
576347	STRES	RH WING XORS 815 REAR SPAR UPPR OUTR CAP AXIAL	+30KSI	.097/CT	PRI KSI
576348	STRES	RH WING XORS 815 REAR SPAR UPPR OUTR CAP AXIAL SP	+30KSI	.097/CT	PRI KSI
576349	STRES	RH WING XORS 815 REAR SPAR LOWR OUTR CAP AXIAL	+20KSI	.04/CT	PRI KSI
576350	STRES	RH WING XORS 815 REAR SPAR LOWR OUTR CAP AXIAL SP	+20KSI	.04/CT	PRI KSI
576351	STRES	RH WING XORS 815 NO5 UPPR STRINGER OUTR SKN AXIAL	+35KSI	.099/CT	PRI KSI
576352	STRES	RH WING XORS 815 NO5 UPPR STRINGER OUTR SKN AXIAL SP	+35KSI	.099/CT	PRI KSI
576353	STRES	RH WING XORS 815 NO34 LOWR STRINGER OUTR SKN AXIAL	+30KSI	.097/CT	PRI KSI
576354	STRES	RH WING XORS 815 NO34 LOWR STRINGER OUTR SKN AXIAL SP	+30KSI	.097/CT	PRI KSI
576355	STRES	RH WING XORS 815 FRNT SPAR WEB OUTR SURF SHEAR	+20KSI	.04/CT	PRI KSI
576356	STRES	RH WING XORS 815 FRNT SPAR WEB OUTR SURF SHEAR SP	+20KSI	.04/CT	PRI KSI
576357	STRES	RH WING XORS 815 REAR SPAR WEB OUTR SURF SHEAR	+10KSI	.02/CT	PRI KSI
576358	STRES	RH WING XORS 815 REAR SPAR WEB OUTR SURF SHEAR SP	+10KSI	.02/CT	PRI KSI
576359	STRES	RH WING XORS 933 FRNT SPAR UPPR OUTR CAP AXIAL	+25KSI	.05/CT	PRI KSI
576360	STRES	RH WING XORS 933 FRNT SPAR UPPR OUTR CAP AXIAL SP	+25KSI	.05/CT	PRI KSI
576361	STRES	RH WING XORS 933 FRNT SPAR LOWR OUTR CAP AXIAL	+25KSI	.05/CT	PRI KSI
576362	STRES	RH WING XORS 933 FRNT SPAR LOWR OUTR CAP AXIAL SP	+25KSI	.05/CT	PRI KSI

MEAS NUMBER	MEAS	MEASUREMENT DESCRIPTION	MEAS RANGE	MEAS RESOLUT	MEAS UNIT
900062	ARSPD	KEIL PITOT VS VFT T/C AIRSPEED	0,450	0.1/CT	PRI KNOT
900064	MACH	KIEL TOTAL VS TRAIL CONE STATIC MACH NUMBER	0/1	.001	PRI MACH
900075	ARSPD	AUX PITOT VS VFT T/C AIRSPEED	0,450	0.1/CT	PRI KNOT
900301	ACCEL	C.G NORMAL ACCEL	+4-2G	.01G	PRI G
900302	ACCEL	C.G LATERAL ACCEL	+2G	.01G	PRI G
900303	ACCEL	C.G LONGITUDINAL ACCEL	+2G	.01G	PRI G
900401	VOLTS	160A ENCLOSURE 5VDC REFERENCE PSA1	-5/+5VOLT	.01 VOLT	SUB
900402	VOLTS	160B ENCLOSURE 5VDC REFERENCE PSB1	-5/+5VOLT	.01 VOLT	SUB
900601	ANGLE	ANGLE OF ATTACK F/T LOCAL	-5,55	0.2DEG/CT	PRI DEG
900602	ANGLE	ANGLE OF SIDESLIP F/T LOCAL	-30,30	0.1DEG/CT	PRI DEG
900901	DISCR	FLIGHT TEST ENGR CORRELATION	0-28 VOLT	ON-OFF	PRI
900903	DISCR	CABIN OBSERVERS WALKAROUND CORRELATION	ON/OFF		PRI
900904	DISCR	TAPE SPEED INDEX 50	VOLT	ON-OFF	PRI
900905	DISCR	TAPE SPEED INDEX 51	VOLT		PRI
900906	DISCR	TAPE SPEED INDEX 52	VOLT		PRI
900907	DISCR	CALIBRATION CYCLE R CAL ON	VOLT		PRI
900908	DISCR	CALIBRATION CYCLE Z	VOLT		PRI
901311	ACCEL	PILOTS SEAT NORMAL ACCEL	+4-2G	.01G	PRI G
901312	ACCEL	PILOTS SEAT LATERAL ACCEL	+2G	.01G	PRI G
902800	LOAD	R. H. WINGLET CALIBRATION LOAD CELL	+4000LBS	4LBS/CNT	SUB
902801	LOAD	R. H. OUTBOARD AILERON CALIBRATION LOAD CELL	+1200LBS	1.2LB/CNT	SUB
909011	PRFSS	T/C STATIC VS T/C STATIC ZERO REFERENCE PRESSURE			
909012	PRESS	T/C STATIC VS T/C STATIC ZERO REFERENCE PRESSURE			
909013	PRESS	T/C STATIC VS T/C STATIC ZERO REFERENCE PRESSURE			

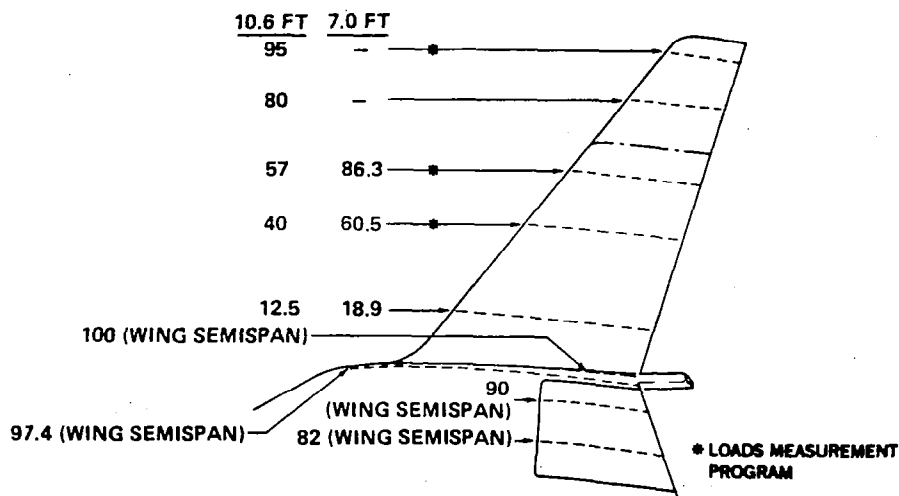
MEAS NUMBER	MEAS	MEASUREMENT DESCRIPTION	MEAS RANGE	MEAS RESOLUT	MEAS UNIT
909021	PRESS	T/C STATIC VS T/C STATIC ZERO REFERENCE PRESSURE			
909022	PRESS	T/C STATIC VS T/C STATIC ZERO REFERENCE PRESSURE			
909023	PRESS	T/C STATIC VS T/C STATIC ZERO REFERENCE PRESSURE			
909031	PRESS	T/C STATIC VS T/C STATIC ZERO REFERENCE PRESSURE			
909032	PRESS	T/C STATIC VS T/C STATIC ZERO REFERENCE PRESSURE			
909033	PRESS	T/C STATIC VS T/C STATIC ZERO REFERENCE PRESSURE			
909041	PRESS	T/C STATIC VS T/C STATIC ZERO REFERENCE PRESSURE			
909042	PRESS	T/C STATIC VS T/C STATIC ZERO REFERENCE PRESSURE			
909043	PRESS	T/C STATIC VS T/C STATIC ZERO REFERENCE PRESSURE			
909952	PRESS	VFT T/C STATIC PRESSURE MEASURED IN WINGLET	5/31	.0005/CT	SUB INHG

APPENDIX B

PRESSURE ORIFICE LOCATIONS

The pressure orifice locations on the winglet, wing, and aileron are defined on the accompanying illustration.

(PERCENT WINGLET SPAN)



	WINGLET					WING			
	12.5%	40.0%	57.0%	80.0%	95.0%	100.0%	97.4%	90.0%	82.0%
UPPER SURFACE x/c	0.00	0.00	0.00	0.00	0.00	0.700	0.00	0.750	0.775
	0.0125	0.0125	0.0125	0.0125	0.0125	0.750	0.0125	0.775	0.800
	0.030	0.030	0.030	0.030	0.030	0.825	0.035	0.820	0.840
	0.076	0.080	0.075	0.068	0.060	0.860	0.050	0.900	0.900
	0.148	0.143	0.139	0.143	0.151	0.900	0.104	1.000	1.000
	0.200	0.200	0.180	0.180	0.200	0.950	0.138		
	0.260	0.230	0.200	0.270	0.250	1.00	0.175		
	0.300	0.365	0.260	0.330	0.300		0.302		
	0.390	0.450	0.350	0.400	0.400		0.393		
	0.440	0.570	0.450	0.450	0.430		0.488		
	0.560	0.670	0.570	0.600	0.600		0.591		
	0.600	0.800	0.670	0.690	0.700		0.736		
	0.630	0.900	0.820	0.780	0.830		0.820		
	0.730	0.950	0.900	0.900	0.880		0.895		
	0.820	1.00	0.950	0.950	0.950		0.946		
LOWER SURFACE x/c	0.910		1.00	1.00	1.00		1.00		
	0.950								
	1.00								
	0.000	0.00	0.00	0.00	0.00		0.00	0.750	0.750
	0.0125	0.0125	0.0125	0.0125	0.0125		0.0125	0.775	0.775
	0.030	0.030	0.030	0.030	0.030		0.035	0.820	0.820
	0.076	0.080	0.075	0.068	0.060		0.050	0.900	0.900
	0.172	0.184	0.157	0.149	0.155		0.104	1.00	1.000
	0.200	0.180	0.180	0.180	0.200		0.138		
	0.260	0.200	0.200	0.270	0.250		0.248		
	0.300	0.230	0.260	0.330	0.300		0.302		
	0.390	0.365	0.350	0.400	0.400		0.393		
	0.440	0.450	0.450	0.450	0.430		0.488		
	0.560	0.570	0.570	0.600	0.600		0.591		
	0.600	0.670	0.670	0.690	0.700		0.736		
	0.630	0.800	0.820	0.780	0.830		0.820		
	0.730	0.900	0.900	0.900	0.880		0.895		
	0.820	0.950	0.950	0.950	0.950		0.946		
	0.910	1.000	1.00	1.00	1.00		1.00		
	0.950								
	1.000								

PRESSURE ORIFICE LOCATIONS